Lactoferrin Nanoparticles for Targeted Tumor Therapy: Implications in Glioblastoma and Melanoma Management

DOCTOR OF PHILOSOPHY

By

Sonali Kumari

11LTPH18

Department of Biotechnology & Bioinformatics

School of Life Sciences University of Hyderabad

Hyderabad - 500046. Telangana, India.

April 2017

Department of Biotechnology & Bioinformatics,
School of Life Sciences,
UNIVERSITY OF HYDERABAD,
Hyderabad-500046, Telangana, India

CERTIFICATE

This is to certify that thesis entitled "***Lactoferrin nanoparticles for targeted tumor therapy: implications in glioblastoma and melanoma management***" is a record of bonafide work done by Ms. Sonali Kumari, a research scholar for Ph.D. programme in the Department of Biotechnology and Bioinformatics, University of Hyderabad under my guidance and supervision. The thesis has not been submitted previously in part or full to this or any other University or Institution for the award of any degree or diploma. I recommend her thesis for submission towards the partial fulfilment of Doctor of Philosophy degree in Biotechnology.

(Signature of Supervisor)

(Head of the Department)

(Dean of the School)

Department of Biotechnology & Bioinformatics,
School of Life Sciences,
UNIVERSITY OF HYDERABAD,
Hyderabad-500046. Telangana, India.

CERTIFICATE

This is to certify that the thesis entitled "***Lactoferrin nanoparticles for targeted tumor therapy: implications in glioblastoma and melanoma management*** " submitted by **Ms. *Sonali Kumari*** bearing registration number **11LTPH18** for the partial fulfilment of the requirements for award of Doctor of Philosophy in the Department of Biotechnology and Bioinformatics, School of Life Sciences is a bonafide work carried out by her under my supervision and guidance. This thesis is free from plagiarism and has not been submitted previously in part or in full to this or any other University or Institution for award of any degree or diploma.

Part of this thesis has been:

A. Published in the following publication:

1. Kumari, S. & Kondapi, A. K. Lactoferrin nanoparticle mediated targeted delivery of 5-fluorouracil for enhanced therapeutic efficacy. International Journal of Biological Macromolecules 95, 232-237 (2017).

B. Presented in the following conferences:

1. Annual meeting of Society for neurochemistry India (SNCI), 2016.
2. Frontiers in life Sciences, 2016 (international)
3. Bio-quest, (2015)

C. Further, the student has successfully completed the following courses towards fulfilment of coursework requirement for PhD degree:

S.N	Course code	Name	Credits	Pass/Fail
1	AS801	Seminar 1	1	PASS
2	AS802	Research Ethics and management	2	PASS
3	AS803	Biostatistics	2	PASS
4	AS804	Analytical Techniques	3	PASS
5	AS805	Lab Work	4	PASS

Supervisor **Head of the Department** **Dean of the School**

Department of Biotechnology & Bioinformatics,
School of Life Sciences,
UNIVERSITY OF HYDERABAD,
Hyderabad-500046. Telangana, India

DECLARATION

I, Sonali Kumari, hereby declare that the work presented in this thesis, entitled as "***Lactoferrin nanoparticles for targeted tumor therapy: implications in glioblastoma and melanoma management***" has been carried out by me under the supervision of Prof. Anand K. Kondapi, Department of Biotechnology and Bioinformatics. To the best of my knowledge this work has not been submitted for the award of any degree or diploma at any other University or Institution. I hereby agree that my thesis can be deposited in Shodganga/INFLIBNET.

A report on plagiarism statistics from the University Librarian is enclosed.

Place: Hyderabad
Date:

Sonali Kumari
11LTPH18

Acknowledgements

This thesis would not have been possible without the care, support and guidance of many people who contributed directly or indirectly during my entire journey of Ph.D. I shall be highly indebted to all of you and now it is my opportunity to thank all of you.

First and foremost, I am highly thankful to almighty GOD for rewarding me health and wisdom to accomplish this work.

I would like to express my sincere gratitude to my supervisor Prof. Anand K. Kondapi for his continuous guidance during my Ph.D. I am thankful to him for his constructive and critical comments throughout my research tenure. His valuable suggestions, both personally and professionally, have directly or indirectly brought the best out of me. I owe him a lot of gratitude for providing me freedom of thoughts in designing my objectives and experiments which really helped me in becoming an independent researcher. I am also thankful to him for being kind hearted and patient throughout my tenure.

I am ever grateful to Dr. Madhusudhan Rao for making the final and yet the crucial leg of my research works possible by providing me CCMB facilities and his valuable mentorship, as part of the collaborative work. It was a great learning experience combined with a positive and constructive workplace that he has superlatively built. He has tried his best to provide me with all the necessary facilities and never ever doubted my abilities. Any note of thanks will be trivial for Dr. Madhu, who has always supported me through thick and thin of my times and has been very understanding, patient and supportive.

I am thankful to the present Dean, School of Life sciences Prof. P. Reddanna and former Deans Prof A. S. Raghavendra, Prof M. Ramanadham & Prof. R.P. Sharma for enabling necessary facilities to carry out my work.

I am also thankful to present Head of Department of Biotechnology & Bioinformatics - Prof. Anand K Kondapi and former Heads Dr. Niyaz Ahmed & Prof P. Prakash Babu for helping me with all the logistics & facilities needed for my research work.

I am also thankful to present director of CCMB Dr. Rakesh K.Mishra and former director Dr. Ch. Mohan Rao for granting the permission of this collaborative work in CCMB and also for maintaining state-of-the-art facilities.

My sincere gratitude to my doctoral committee members, Prof P. Prakash Babu and Dr. Sunanda Bhattacharya, for their valuable inputs and constructive comments during my PhD tenure.

I am thankful to Council of Scientific & Industrial Research (CSIR) for the financial support in the form of fellowship during the tenure of my PhD and funding agencies of Govt. of India (DST, DBT, CSIR and ICMR) for funding our laboratory and Departments.

I would like to thank my present and past lab mates at UoH - Dr. Farhan, Hari Kiran, Kiran, Dr. Satish, Dr. Prashant, Dr. Pankaj, Laxmi, Late Surujana, Kurumurthy, Akhila, Jagadeesh, Neha, Satayajit, Priya, Chuku, Kriti, Reena, Goden, Dr. Kishore Golla, Dr. Balakrishna, Dr. Bhaskar, Dr. Kannapiran, Dr. Priti, Dr. Upendra & Dr. Venkanna.

I would like to acknowledge the lab attendants at UoH- Chandra, Bhanu, and Sreenivas for the lab maintenance and document processing activities.

I would like to thank Dr. Sumana Chakaravarty from IICT & her student Dwaipayan Bhattacharya for helping me in glioma mice model generation.

My sincere thanks to all the CCMB staffs and faculty members for helping me as an when needed specially, Dr. Vijaya Gopal and Dr. Swasti Raychaudhuri for providing me some crucial antibodies on time, Dr. Nadini for confocal experiments, Harikrishna during TEM studies, Avinash sir for histology experiments, Dr. Krishna Kumari & Dr. Subbalakshmi for helping in HPLC experiments. The help provided by Dr. Mahesh and entire animal house staffs for mice experiments are highly acknowledged. I would also like to thank staff members of tissue culture facility for their support.

I would like to thank my former and present lab mates at CCMB - Gulzar, Erika, Durga, Mohammad, Tashneem, Harita, Dr. Vijaylaxmi, Venu ji, Dr. Bhanu, Dr. Laxmiprasanna, Tushar, Shankar and specially Priyanka and Pragya for last moment editing. I would also like to thank my friends Durgesh, Manoranjan, Shiwali, Prasanth and Dr. Saad in CCMB who had really helped me in dealing with challenges of the new work place and were always available for their support and advice.

My heartfelt thanks to my best friend Dr. Anjali for her unconditional care, support and all the fun times we had inside and outside the university. She is a true example of a friend in need is a friend indeed. I would also like to thank Dr. Saad for all his critical suggestions and out of the box ideas. A special note of thanks to him for helping me in the initial time of my stay in CCMB and then throughout.

I wish to express my gratefulness to my parents, in-laws and siblings for their trust, care and unconditional love.

I would like to thank my husband, for making this dream real. A note of thanks would be trivial for all his sacrifices and taking all the pains to look after our house responsibilities in my absence. It gives me a great joy in discussing my work with him. All his constructive and critical feedbacks have equally helped me throughout my work. Best thing about him is that he executes everything with a touch of perfection and after practicing the same I can see a great change in me. He has also played a significant role in the editing and formatting of this thesis. His constant support and patience during all my ups and downs is highly appreciated.

I express my deepest gratitude and reverence to my Late Father who had this dream and confidence in me. This confidence of his has been a major driving force which kept me focused and determined throughout these years. I wish he could be here today.

Sonali Kumari

"It is not the strongest of the species that survives, not the most intelligent that survives. It is the one that is the most adaptable to change" - Charles Darwin.

Human race rightly figures at the very top of food chain and have evolved over centuries to become the unchallenged species on earth. We now live in a world where our species is not only dominant, but also plays a major role in changing the biosphere.

However, this position does not render human being immune to afflictions of various kinds. Ranging from ancient diseases to new ailments, medical care still grapples with a wide variety of conditions. While the human body, over millions of years of evolution, is a finely tuned machine, there still remain multiple factors which can throw this machine off course.

The pace of man-made changes to the external and internal environment has intensified after the onset of the 20th century, a time-scale too short for evolution to work. This has aggravated the risk factors affecting human health. Some of these include rapid industrialization, leading both to a rise in population levels as well as drastic lifestyle changes over the years. This has in turn led to rapid depletion of natural resources and uncontrolled increases in pollution. Such environmental changes can lead to disastrous consequences in the functioning of our body, specifically our natural cell production systems as well as our immune systems.

One such deadly group of diseases that has plagued the mankind and become even more virulent is, CANCER! Researchers and scientists, across the globe, are working hard to find a definite cure but have had limited success till now. The severity of this ailment is underscored by the fact that cancer is the second leading cause of death globally (nearly 1 in 6 deaths), according to the WHO (World Health Organization).

But as is the ingenuity of human race, we survive because we adapt, we improvise, we change and most importantly - we fight! We fight to overcome all adversaries! As a species, we have consistently learnt and adapted, using the accumulated wisdom of the ages as well as the drive of innovation to solve seemingly impossible tasks.

My own work, over all these years, has been a small yet resilient effort to find a cure for this ominous disease that remains a threat, hitherto!!

"Resilience is all about being able to overcome the unexpected. Sustainability is about survival. The goal of resilience is to thrive" - Jamais Cascio

I dedicate this thesis to you "BABA"

Abbreviations

TMZ	Temozolomide
Lf	Lactoferrin
LfNP	Lactoferrin nanoparticle
TMZ-LfNP	Temozolomide loaded lactoferrin nanoparticle
5FU	5-flurouracil
5-FU-LfNP	5-flurouracil loaded lactoferrin nanoparticle
AKB	Arora Kinase B
AKB-LfNP	Arora Kinase B loaded lactoferrin nanoparticle
p35-LfNP	p53-plasmid loaded lactoferrin nanoparticle
I.V	Intravenous
I.C	Intracranial
S.C	Subcutaneous
B16F10	Mouse melanoma cell line
GL261	Mouse GBM cell line
HepG2	Human liver cancer cell line
A549	Human lung cancer cell line
AUC	Area under curve
Cmax	maximum concentration achieved after single dose
T1/2	Elimination half-life
MRT	Mean residence time
SGOT	Serum glutamic oxaloacetic transaminase
SGPT	Serum glutamic-pyruvic transaminase
BUN	Blood Urea Nitrogen
SEM	Scanning Electron Microscopy
TEM	Transmission Electron Microscopy
DLS	Dynamic light Scattering
FT-IR	Fourier transform infrared spectroscopy
HPLC	High-performance liquid chromatography
BBB	Blood Brain Barrier
GBM	Glioblastoma multiforme
EPR	Enhanced Permeability and Retention

Table of Contents

Chapter 1. Introduction

1.1 Cancer 1

1.1.1 Salient features of cancer 1

1.1.2 Malignant melanoma 2

1.1.3 Glioblastoma multiforme (GBM) 3

1.2 Cancer therapeutics 4

1.2.1 Surgery 4

1.2.2 Radiation therapy 5

1.2.3 Gene therapy 5

1.2.4 Chemotherapy 6

1.3 Targeted therapy 8

1.3.1 Antibody-drug conjugates 9

1.3.2 Nanomedicine based drug delivery systems 9

1.4 Targeting strategies 12

1.4.1 Passive targeting of nanoparticles 12

1.4.2 Active targeting of nanoparticles 13

1.4.3 Brain targeting 16

1.5 Lactoferrin nanoparticle based drug delivery 17

1.6 Rationale of the study 18

Chapter 2. Material and Methods

2.1 Materials 21

2.2 Methods 21

2.2.1 Preparation of 5-FU-LfNPs 21

2.2.2 Preparation of TMZ loaded Lf nanoparticles 22

2.2.3 Preparation of plasmid DNA loaded lactoferrin nanoparticles 22

2.2.4 Gel retardation and DNase protection assay of pDNA 22

2.2.5 Preparation of siRNA loaded lactoferrin nanoparticles 22

2.2.6 RNase protection and serum stability assay 22

2.2.7 Physico-chemical characterization of nanoparticles 23

2.2.8 Fourier transform infrared (FT-IR) spectroscopy 23

2.2.9 Determination of drug encapsulation efficiency and drug loading content 23

2.2.10 Entrapment efficiency calculations for siRNA 24
2.2.11 Determination of entrapment efficiency of pDNA 24
2.2.12 In vitro pH release studies 25
2.2.13 In vitro TMZ release studies 25
2.2.14 Cell culture 25
2.2.15 Competitive ligand binding assay 25
2.2.16 Cellular uptake assay 26
2.2.17 Cytotoxicity Assay 26
2.2.18 Receptor screening and receptor blocking assay 27
2.2.19 Estimation of intracellular TMZ 28
2.2.20 Wound-healing and migration assay 28
2.2.21 Cell based assays for siRNAs 28
2.2.22 Cell based assay for pDNA 30
2.2.23 Animal experiments 30

Chapter 3. Development of 5-fluorouracil loaded lactoferrin nanoparticle and their efficacy in mouse melanoma cells

3.1 Introduction 35
3.2 Result and Discussion 36
3.2.1 Physico-chemical characterization 36
3.2.2 Stability and biocompatibility of Lf nanoparticles 39
3.2.3 Receptor mediated endocytosis 40
3.2.4 5-FU release studies 41
3.2.5 Cellular uptake assay by HPLC 42
3.2.6 Cellular uptake by confocal microscopy 43
3.2.7 Enhanced antiproliferative activity of 5-FU-LfNPs 43
3.3 Conclusion 44

Chapter 4.Analysis of temozolomide-loaded lactoferrin nanoparticles & their therapeutic efficacy in orthotopic GBM model

4.1 Introduction 45
4.2 Results and Discussion 46
4.2.1 Characterization of TMZ-LfNPs 46
4.2.2 Receptor-mediated endocytosis of LfNPs 48
4.2.3 In vitro cytotoxicity of TMZ-LfNPs 51

4.2.4 Blood-brain barrier crossing capability of LfNPs in normal mice 53
4.2.5 Pharmacokinetic studies of TMZ-LfNPs 55
4.2.6 TMZ-LfNPs bio-distribution in GBM mice model 57
4.2.7 Tumor regression studies in glioma mice model 57
4.3 Conclusion 62

Chapter 5. Enhancing drug sensitivity in temozolomide resistant orthotopic GBM using aurora kinase b siRNA loaded lactoferrin nanoparticles

5.1 Introduction 63
5.2 Results and Discussions 65
5.2.1 Gel binding assay and nanoparticle characterization 65
5.2.2 Nuclease protection assay and serum stability 66
5.2.3 Comparative cellular uptake by Flow cytometry 67
5.2.4 Cellular uptake and endo-lysosomal escape 67
5.2.5 AKB-LfNPs mediated down-modulation of AKB expression in GBM cells 69
5.2.6 Potentiating cytotoxicity of TMZ and increased apoptosis using AKB-LfNPs in TMZ-resistant GL261 cells. 69
5.2.7 Animal studies 71
5.3 Conclusion 75

Chapter 6. Potentiating temozolomide activity by p53-loaded lactoferrin nanoparticles in subcutaneous GBM model

6.1 Introduction 76
6.2 Results and Discussion 77
6.2.1 Preparation and characterization of plasmid loaded LfNPs 77
6.2.2 Gel binding assay and nuclease protection 78
6.2.3 Stability studies of pDNA-LfNPs 79
6.2.4 Lf Receptor expression 81
6.2.5 Receptor mediated uptake and gene transfection abilities of LfNPs 81
6.2.6 Biocompatibility assay 83
6.2.7 Animal studies 84
6.3 Conclusions 85

Chapter 7. Summary and Future Directions

7.1 Summary 86

7.2 Future directions 87

Bibliography 88

Publications…….....100

Chapter 1

Introduction

1.1 Cancer

Broadly, CANCER is a class of diseases, characterized by uncontrolled growth of cells that eventually invades healthy tissues of the body (**Figure 1.1)**. When tumor is localized within the boundaries of the tissues, it is considered as benign. However in the later stages, when the cells metastasize, it spreads through blood and lymphatic system colonizing different organs, and is defined as malignant. Cancer differs widely in its causes, origin and biology.

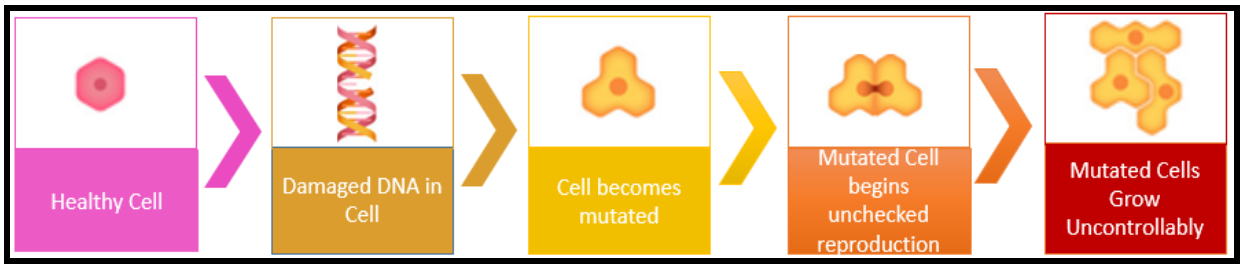

Figure 1.1: Stages of cancer development

All cells that undergo replication, may suffer from genetic errors caused by multiple mutations. In the absence of correction, errors survive, accumulate, get carried on to the daughter cells (if not controlled by cell signalling check points) and ultimately give rise to tumor development. The principal source of cancer is mutations in proto-oncogenes and tumor suppressor genes. Proto-oncogenes code for proteins which are responsible for the induction of cell proliferation and differentiation while tumor suppressor genes code for proteins which generate inhibitory signals for cell growth and/or stimulate cell death.

Typically, multiple genes undergo series of mutations for the transition of a normal cell into cancerous cells. These mutations are clonally selected to facilitate unusual and uncontrolled cell division. Additionally, absence of growth inhibition, evasion of the immune system, inhibition of apoptosis, transmission and accumulation of errors in genetic material leads to uncontrolled cell division [1-3].

1.1.1 Salient features of cancer

Described below are some of the abnormal traits associated with cancer cells that render them different from normal cells -

- Cancer cells grow and spread into several tissue types including hematopoietic, lymphatic systems and the bone marrow (Stein & Pardee, 2004).

- Cancer cells possess highly active metabolism and in order to sustain the unusual growth and uncontrolled cell proliferation, their growth demands are very high which in turn are fulfilled by over expression of specific receptors on cancer cells.
- Cancer cells secrete proteases during metastasis that facilitate them to invade nearby tissues through degradation of the extracellular matrix around the tissue boundaries and thus aid in their invasion.
- Unlike normal cell control mechanisms, cancer cells possess the ability to stimulate their own growth, resist against inhibitory signals, escape programmed cell death, inhibit shortening of telomere length despite repeated cell divisions, form new blood vessels to supply nutrients to tumor, invade surrounding tissues and spread to distant sites.

The focus of this thesis is to develop a targeted nanomedicine based therapy for the management of the two major lethal cancers *viz.* malignant melanoma and glioblastoma multiforme.

1.1.2 Malignant melanoma

Malignant melanoma (MM), the most lethal type of skin cancer, causes majority of skin cancer deaths. The past five decades have witnessed a steady and rapid rise in the incidence of MM in developed countries. As per the American Cancer Society's estimates around 87,110 new melanoma cases will be diagnosed in 2017 with a predictable mortality of 9730 people. Despite of increasing research on the risk factors along with the genetic and epigenetic causes of melanoma, the death rates of melanoma continue to rise faster than the death rates for most cancers. Common treatments for malignant melanoma involve combination of therapies which include surgery, chemotherapy and radiotherapy. The prognosis for patients with metastatic melanoma remains dismal. The 5 years survival rate is less than 6–8 months [5]. Accumulated genetic, functional and biochemical studies suggest that melanoma cells become “bullet proof ” against a number of chemotherapeutic agents by exploiting their inherent resistance to apoptosis and survival pathways during progression of melanoma. Till date, no agent has achieved a clinically meaningful prolongation of overall survival. Thus, novel therapeutic strategies for melanoma are still sought and there is a critical need for the development of therapeutic agents that can target abnormal survival pathways in metastatic melanoma to improve the clinical outcome of this disease.

1.1.3 Glioblastoma multiforme (GBM)

Glioma represents the most common cancer of primary brain tumors, accounting for about 46% of intracranial tumors [6]. Originated from glial cells, GBM include tumors of astrocytic, oligodendrial, ependymal or mixed type of cells [7, 8]. The primary causes of glioma have not yet been known accurately, but ecological factors such as the exposure to ionising radiation of higher intensity attributes to majority of the cases while genetic predisposition [8] is the reason behind 5-10 % of glioma cases.

According to the World Health Organisation (WHO), gliomas can be classified in four grades depending on the pathological diagnosis –

1. **Grade I** glioma is known to be least advanced, non-invasive and generally have better prognosis. Low grade gliomas are not benign but can be differentiated. Grade I glioma represents moderately increased cellular density and absence of mitotic activity.
2. **Grade II** gliomas can be treated using surgery, however chances of relapse are there as some of the microscopic cells may remain even after surgery. The treatment choices for this grade of glioma are chemotherapy and radiotherapy. This type of gliomas generally have good prognosis (survival rate of up to 5 years) but regular monitoring on the recurrence of symptoms is essential.
3. **Grade III** gliomas have tentacle like projections and are undifferentiated group of abnormal cells. The infiltrating tumor cells into the neighbouring tissues make it difficult to be treated by surgery. Increased cellular density, distinct nuclear atypia, absence of endothelial propagation and necrosis are its characteristic histological features [9]. Based on the tumor size and its location, treatment options can be evaluated.
4. **Grade IV** are high grade glioma and also identified as glioblastoma multiforme (GBM). GBM is the most malignant and fatal brain tumor among all. These correspond to approximately fifty percent of all primary brain tumors and about twenty percent of intracranial tumors with dismal clinical outcome [7]. GBM, commonly begin in the cerebral hemispheres and then infiltrates rapidly to other brain areas. Their aggressive growth causes increased brain pressure and further leads to the development of symptoms including headaches, seizures, loss of memory and behavioural changes. The extremely infiltrative properties are the characteristic features of GBM which make it very challenging to treat using standard therapies except for marginal increases in median survival time in patients [10]. Primarily,

GBM is categorized by mutation and amplification in epidermal growth factor receptor (EGFR) gene, mouse double minute 2 (MDM2) over expression and deletion of p16. In fact, 74% of GBMs analyzed harbour alterations in above three pathways. The three core pathways that are deregulated in most GBMs includes, receptor tyrosine kinase signalling pathway, TP53 pathway and RB tumor suppressor pathway (Cancer Genome Atlas Research Network 2008).

1.2 Cancer therapeutics

The choice of cancer therapy mainly depends on the type, location, grade, cancer stage and the patient's general health condition, as depicted below in **Figure 1.2**.

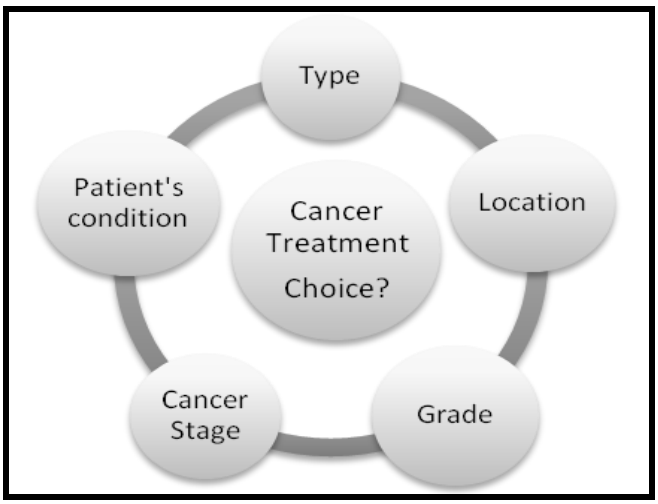

Figure 1.2: Cancer therapy selection matrix

In general, cancer confined within a particular region is removed surgically or destroyed by radiation therapy followed by chemotherapy thereafter. Once cancer cells spread to different tissues, chemotherapy is the only option as it can reach to the distant sites via systemic circulations.

Broadly, there are four treatment options including surgery, radiation therapy, gene therapy and chemotherapy that are used either alone or in conjunction to form the therapeutic regime. Different cancer therapeutics and their limitations are briefly discussed below.

1.2.1 Surgery

Localized tumor can be surgically excised either by the removal of tumor or the entire organ depending on the cancer grade. However, only few cancers have successful outcome after surgery such as prostatectomy for prostate cancer, mastectomy for breast cancer and lung cancer surgery for non-small cell lung cancer. The major limitation though is

the need for skilled surgeons as even a single cell left can re-grow into a new tumor. Additionally, it is an expensive procedure, requires prolonged duration of recovery and possesses high risk of vascular injuries.

1.2.2 Radiation therapy

Radiation therapy is the process of using ionizing radiations including gamma rays, x-rays and high energy particles to either shrink the tumor or to completely kill the cancer cells [11]. It is a localized treatment regime and only affects the specific part of the tissue. The major role of radiation therapy involves shrinkage of tumor prior to surgery, to impede the tumor relapse or to eradicate cancer cells in the neighbouring tissues. Nonetheless radiation therapy is also associated with some adverse effects, which includes mild skin reactions, fatigue, loose bowel movements and side effects on digestive system. Internal radiation therapy possibly causes infection, irritation or bleeding following implant removal.

1.2.3 Gene therapy

Gene therapy can be broadly defined as a transfer of genetic material for the treatment of a disease or at least for the better clinical status of a patient. It is an attractive approach to treat a disease either by silencing over-expressed genes, replacing defective genes or substituting missing genes. The advantage of using gene therapy is not only to replace a potentially mutated gene but essentially to manipulate the physiology and signal transduction in the cells by down-modulating or over-expressing single or multiple genes. Gene silencing can be achieved by either short antisense oligonucleotides (ODNs) or newly developed RNA interference technology where small interfering RNA (siRNA) down modulate the over expressed gene or restoration of mutated gene can be achieved by delivering the plasmid DNA (having the gene of interest under the influence of a promoter) into cells.

The delivery vehicles for nucleic acids (siRNA or plasmid DNA) are majorly categorized into two groups - viral and non-viral vectors. Viral vectors are used as genetic shuttles and have the benefit of using the host machinery for the production of viral proteins. Although viral vectors are potent gene-delivery platforms they are associated with several limitations in terms of safety and toxicity because of their immunogenicity and unwanted long term side effects. Besides that, viruses could also be transmitted to other individuals or the environment. Also being non-targeted, there is always a potential risk of insertion of the gene in the incorrect location in host genome that may cause non-desirable mutations and eventually lead to the development of cancer. There is significant body of research on non-viral methods of gene delivery demonstrating their advantages including

non-infectivity, the possibility of multi-dose administration, absence of immunogenicity and cost effectiveness. Several non-viral gene delivery vehicles, especially nanoparticle systems, have been developed so far using polymers such as PLGA [12] and polypropylenimine (PPI) [13].

However, the success rate associated with these non-viral gene delivery systems is moderate due to comparatively low transfection efficiency and the toxicity associated with the carrier materials. Among the non-viral vectors, PLGA is the only material approved for human application but is associated with the inherent disadvantage of incomplete DNA release at a very slow rate compared to the cell turnover rate [14, 15], consequently restricting the full use of the plasmid dose. Introduction of biodegradable delivery vehicle would add tremendous significance to the field of gene therapy.

1.2.4 Chemotherapy

Chemotherapy is the use of chemicals for the treatment of cancer. Different types of chemotherapeutic drug are being widely used to treat various types of cancers, either in combination or alone. Chemotherapeutic drugs can be categorized in different classes based on their chemical structure, origin and mechanism of action. Some of the chemotherapeutic drugs have broad spectrum activity while some are specific against a particular type of cancer.

Though chemotherapy is widely used, the clinical outcome of conventional chemotherapy is poor because of the following limitations associated with them –

1. **Poor aqueous solubility**– Majority of the chemotherapeutic drugs obtained either from plants or by chemical synthesis, are hydrophobic in nature and require excipients to enhance their aqueous solubility in systemic circulation. However, these excipients often cause detrimental long term side effects along with the drugs thereby diminishing the overall clinical outcome [16].
2. **Multi drug resistant (MDR) –** The excessive usage of chemotherapeutic drugs leads to resistance in most of the cancers. The mechanism that provides resistance to chemotherapeutic drug includes increased drug efflux pumps (Pgp glycoproteins) [17], reduced cellular drug uptake, intracellular drug inactivation or mutation, enhanced repair of DNA damage induced by chemotherapeutic agents. These mechanisms, increases the tolerance to DNA lesion resulting in resistant to drug induced apoptosis and provide survival benefits to the malignant cells [18].
3. **Lack of target specificity –** The side effects of chemotherapeutic drugs are primarily due to their inability to discriminate between cancerous and healthy cells. Being **c**ytotoxic in nature, they not only kill cancerous cells but also affect the

functionality of the normal cells leading to undesirable off-target effects in patients [19]. The clinical outcome of chemotherapeutic drugs depends on several factors such as patient's immunity status, drug type and dose frequency. The negative effects of chemotherapy can vary from minor symptoms e.g. fatigue, risk of infection, nausea, loss of appetite and diarrhoea to major life-threatening side effects such as bone marrow suppression, renal failure and hepatic abnormalities resulting in discontinuation of therapy. Additionally, drug instability in the biological fluids, shorter half-life, rapid metabolism and high binding affinity of certain drugs such as protease inhibitors [20], limit their diffusion across the organs.

The aim of the work described in this thesis was to improve the efficacy and bioavailability of two major chemotherapy drugs *viz.* 5-fluorouracil (5-FU) and Temozolomide (TMZ), used for the treatment of melanoma and glioblastoma multiforme (GBM) respectively as described below-

1.2.4.1 5-Fluorouracil

5-FU is a pyrimidine analogue **(Figure 1.3),** and a metabolic inhibitor of enzyme thymidylate synthase blocking the synthesis of DNA and RNA and can also get incorporated in the genomic DNA, resulting in DNA breakage [21].

5-FU is a clinically approved drug for the treatment of multiple cancers including melanoma, colorectal cancer and head and neck cancer. Its long term usage results in severe dose related toxicity such as myelosuppression, hepatotoxicity and nephrotoxicity [22]. In addition to that, 5-FU has poor water solubility, shorter half-life (8-20 mins) [23] and after long term uses melanoma cells develops resistance against 5-FU.

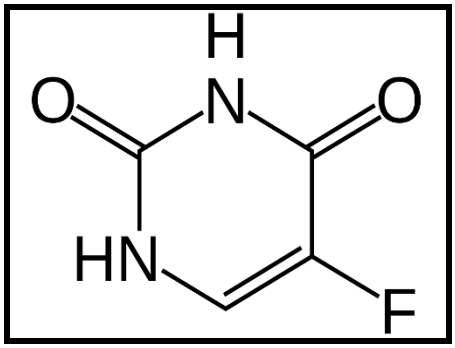

Figure 1.3: Structure of 5-FU

1.2.4.2 Temozolomide

Temozolomide (TMZ) is an alkylating agent which methylates purine bases of DNA at N-7 or O-6 positions of guanine and N-3 of adenine residues **(Figure 1.4).** Methylation of DNA creates cytotoxic lesions which lead to DNA damage and finally apoptosis [24]. Though TMZ is the approved first line treatment for glioma, it causes haematological toxicity [25], acute cardiomyopathy [26], hepatotoxicity [27] and pneumocystis pneumonia [28]. Additionally, TMZ has poor water solubility, shorter half-life (1.8 h) [24], limited access to blood brain barrier (BBB) and GBM develops resistance against TMZ. Primarily TMZ resistance is linked with up-regulation of methyl guanine methyl transferase (MGMT) and DNA mismatch repair system (MMR) pathways which eventually lead to poor treatment outcome [29].

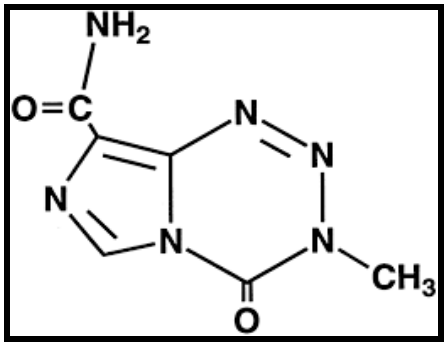

Figure 1.4 Structure of TMZ

Limitations of conventional chemotherapy are currently being addressed by different cutting edge researches globally in the different disciplines. Amongst them, most notable inventions have been in the field of targeted drug delivery for chemotherapy agents; which has been discussed explicitly in the next sections.

1.3 Targeted therapy

Targeted therapy has emerged as a fascinating field in cancer biology as it involves delivering a chemotherapeutic drug to its site of action without affecting other healthy organs. It increases the therapeutic dosage of the drug to the desired place while reducing side effects. Targeted therapy is vital for treatment of cancer as it requires effective and specific targeting. A number of efforts have been put forth for targeting drugs, either by conjugation with antibodies known as antibody-drug conjugates (ADCs) or encapsulation in colloidal drug delivery systems (CDDS).

1.3.1 Antibody-drug conjugates

Antibody–drug conjugates (ADCs) offer a strategy for developing targeted therapy by conjugating monoclonal antibodies to anti-cancer drugs. However, despite extensive efforts, application of monoclonal antibody technology has had modest success in improving the treatment outcome. In addition, early ADCs exhibit side-effect profiles similar to those of traditional chemotherapeutic agents and their performance in clinical trials of cancer patients has been generally poor.

1.3.2 Nanomedicine based drug delivery systems

Nanomedicine based systems are delivery vehicles in nanometre (nm) size range and exist either in vesicular or particulate form. A number of drug delivery systems have been investigated and identified for controlled release and targeting. They can effectively manage the bio-availability, pharmacokinetics and immunogenicity of chemotherapeutic drugs for superior clinical outcome. There are several advantages of nano-carriers viz. enhanced stability, sustained release, high drug loading efficiency, feasibility of incorporation of both hydrophilic and hydrophobic drugs and choice of multiple routes of administration - including oral, intravenous and pulmonary route. Nanomedicine based delivery systems majorly includes liposomes and nanoparticles.

1.3.2.1 Liposomes

Liposomes are spherical vesicles with lipid bi-layer, made up of phospholipids and used for delivery of pharmaceutical agents. The first liposomal formulation approved by FDA was Doxil (doxorubicin loaded liposomes) for the treatment of Kaposi's Sarcoma in 1995 [30]. Even though liposome based nanomedicine has improved the bioavailability and pharmacokinetics of doxorubicin, there are numerous bottlenecks associated with them which limits their wider application as drug delivery platforms. Some of them being - shorter shelf life, probability of oxidation of phospholipids, low drug loading efficiency and challenges in modulation of drug release.

1.3.2.2 Nanoparticles

Colloidal particles ranging in size between 10 and 1000 nm are known as nanoparticles. Nanoparticles are classified based on their matrix such as solid lipid nanoparticles, metallic nanoparticles, polymeric nanoparticles etc.

Solid Lipid Nanoparticles (SLN): SLNs are more attractive, new generation lipid particles compared to the existing traditional liposomal formulations. They are sub-micronic lipid emulsions where the liquid lipid is replaced by solid lipid. SLN offer great advantages like

small size, higher surface area and improved drug loading. However, this is limited by concerns such as the loading capacity, the polymeric state and structure of the lipid matrix [31].

Metallic nanoparticles: Metallic nanoparticles have emerged as a new dimension in the field of drug delivery because of their flexibility in synthesis and surface modification with functional groups which in turn allows them to bind drugs, antibodies and several ligands used for targeting purposes. Most commonly used metallic nanoparticles are gold, silver and iron; however, they are non-biodegradable and cause severe toxicity including hepatotoxicity, nephro-toxicity and haematological toxicity.

Protein nanoparticles: There has been a significant increase in polymeric nanoparticles in recent times due to their excellent bioavailability, better encapsulation, controlled release and minimal toxicity.

Table 1.1: Protein-based drug delivery systems

Sr. No.	Protein	Delivery System	Payload	Description	References
1.	Albumin	Nanoparticles	6-counmarin doxorubicin, Abraxane	• Most abundant plasma protein • versatile and stable in extreme conditions • affinity with many drugs • non-toxic and biodegradable	[33, 34]
2.	Casein	Microsphere	Progesterone	• easier incorporation of hydrophobic drug • tolerate robust conditions • degradable end products • no disulfide bridge	[35]
3.	Collagen	Microparticle	glucocorticosteroids, FITC-dextran, all-trans retinol	• low toxicity • structural protein rich in hydroxyproline, hydroxylysine and glycine, • comprises of secondary amino and carboxyl groups with	[36, 37]

Sr. No.	Protein	Delivery System	Payload	Description	References
				possible cross-linking	
4.	Gelatin	Microsphere, hydrogels, Nanoparticles	colchicines, thrombocidin	• biodegradable and biocompatible end products • denatured form of collagen • possess many carboxyl functional groups for cross-linking	[38, 39, 40]
5.	Heat shock protein	Protein cage	Doxorubicin fluorescein, RGD 4C peptide, anti-CD4 antibody	• homogeneous cage size with 6.5nm interior and 12nm exterior • big pores (3 nm) among interior and exterior for easy cargo exchange • capable of forming scaffold for chemical reactions and material synthesis	[41]
6.	Elastin/elastin like polypeptide (ELP)	ELPs-Dox	Doxorubicin plasmid DNA	• Thermally reversible protein • For therapeutic application, self-assembling into aggregate at phase transition • Molecular weight of ELP can be synthesized by recombinant technology as accurately as possible	[42, 43]
7.	Apo-Transferrin	Nanoparticle	Doxorubicin, Carboplatin	• Targeting abilities to tumor, brain	[44, 45]
8.	Lactoferrin	Nanoparticle	Fluorouracil, Carboplatin	• Anti-cancer, antimicrobial and anti-inflammatory effect	[46, 47]

Among polymeric nanoparticles, protein nanoparticles have several advantages over others. Firstly, they are biodegradable, non-antigenic and metabolizable. Secondly, surface modification and covalent attachment of drugs and ligands can be easily carried out because of the presence of various functional groups in the primary structure of the protein [32]. Thirdly, the biological properties of proteins can be exploited for cell specific targeting to mediate efficient drug delivery. Several protein-based delivery systems have been collated and presented in **table 1.1**.

Advantages of nanoparticles in drug delivery:

Nanoparticles have offered many advantages over conventional systems for drug delivery applications. These include

1. Targeting the drug to the site of action, thus increasing drug efficacy and reducing off-target effects.
2. Regulating drug delivery rates by changing polymer properties. The polymer matrix may be even tailored to respond to endogenous or external stimuli.
3. Packaging and protecting the drug from the surrounding environments and hence increasing the drug half-life.
4. Sustaining the drug release over prolonged periods of time, thereby reducing the dosage frequency.
5. Encapsulating multiple drugs simultaneously for different actions.
6. Modifying and/or conjugating the polymer matrix for specific features (like targeting, increasing circulation time, escaping phagocytosis etc.) without affecting the drug.
7. Protecting the drug from enzymatic degradation, hepatic inactivation and rapid clearance from the systems
8. Improving solubility of the drugs.
9. Provides opportunities for multiple route of administration.

1.4 Targeting strategies

Targeting strategies should be based on two crucial principles while designing the nanocarriers - firstly, there should be minimum loss of drug while carrying and secondly, it should selectively kill tumor cells sparing healthy cells. This can be achieved either by passive or active targeting [48].

1.4.1 Passive targeting of nanoparticles

Passive targeting takes advantage of the unique patho-physiology of tumor vessels, typically their highly disorganized and dilated blood vessels, attributed to the high demand of

nutrition and oxygen. This process of angiogenesis creates enlarged gap junctions between endothelial cells and compromised lymphatic drainage resulting into leaky vasculature with porosity of 100 nm to 2 μm based on tumor type. The phenomenon of 'leaky' vascularization, allow the permeation and entrapment of nanoparticles in the tumor region known as enhanced permeation and retention (EPR) effect [49]. Majorly nanoparticles with size less than 200 nm can be passively targeted to tumors because of EPR effect. In the beginning, conventional liposomes for drug delivery applications were based on passive targeting. Of late several other delivery systems, including micelles, polymeric and other types of nanoparticles were utilized for tumor localization using EPR effect [48]. However, this strategy suffers from several limitations such as certain tumors do not exhibit EPR effect and moreover the degree and porosity of tumor vascularisation vary among different tumors.

Additionally, cancer cells show reduced interactions with nanoparticles which further limit their internalization. Beside EPR effect, the microenvironment surrounding the tumor tissue also supports passive targeting. The elevated metabolism of rapidly dividing tumor cells, stimulate glycolysis to manage extra energy, resulting in an acidic environment [50]. To exploit the acidic tumor microenvironment, pH-sensitive liposomes have been designed with the purpose of releasing the drug at the acidic pH while maintaining their stability at physiological pH (7.4) [51]. However the random nature of the drug release might lead to drug expulsion and make cancer cells resistant towards a variety of drugs, a phenomenon called as multiple drug resistance (MDR) which inevitably reduces the therapeutic outcome [52].

1.4.2 Active targeting of nanoparticles

Active targeting of nanoparticles requires affinity ligands (antibodies, peptides, aptamers and small molecules) to facilitate the binding of nanoparticles to tumor antigens which are differentially or exclusively over-expressed on the tumor cells. The internalization of targeted nanoparticles may be facilitated by specific receptor mediated endocytic pathways (Figure 1.5), leading to endosomes formation and ultimately fusion with lysosome to deliver the drugs in the cytosol [53]. A number of cell surface receptors including folate receptor, transferrin receptor, lactoferrin receptor, epidermal growth factor receptor, integrins receptor and LDL receptor that are over expressed on the cancerous cells and have been utilized for targeting, are listed in **Table 1.2**.

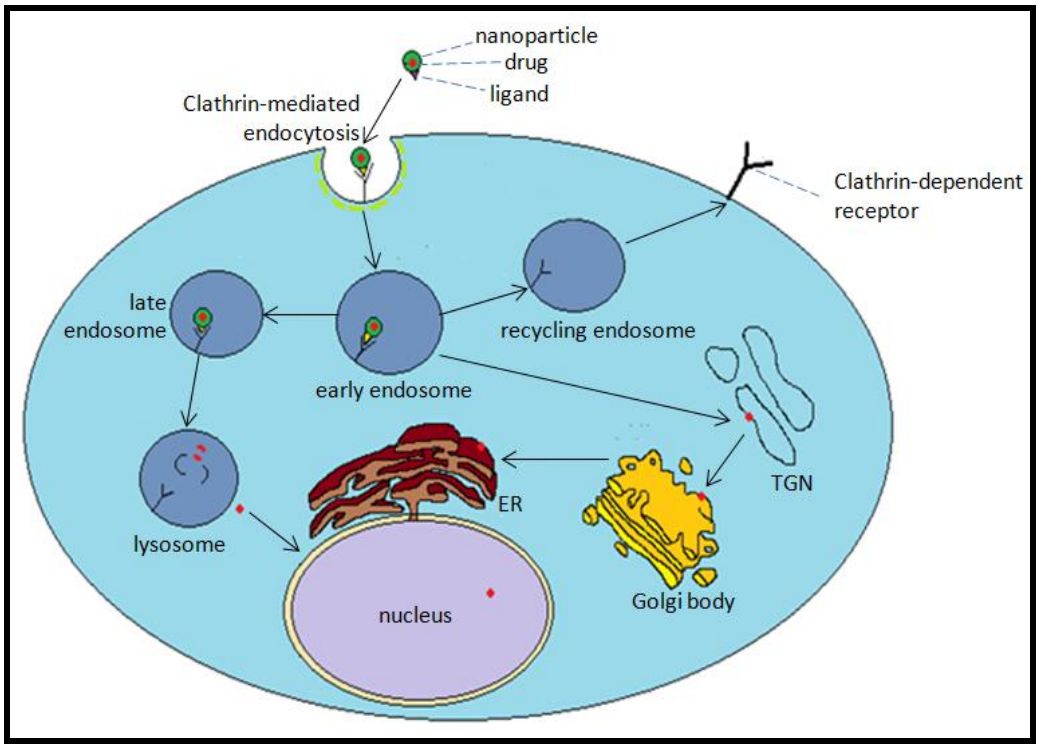

Figure 1.5: Active targeting using receptor mediated endocytosis by ligand decorated nanoparticles. Drug loaded nanoparticles are guided by the surface functionalized ligand to bind to their specific receptors on the cell surface and get internalized in the early endosomes through receptor mediated endocytosis. Post internalization, early endosomes mature to late endosomes and fuse with lysosome where the drug is released in the cytoplasm and eventually transported to the nucleus.

Although ligand-mediated targeting approaches have not yet made a considerable clinical impact on human health, it is not far when nanomedicine with high targeting ability and enhanced efficiency would be the treatment options for clinical applications, while avoiding nonspecific binding and the MDR efflux mechanism. **Table 1.3** lists a number of nanoparticle formulations that are approved or are under clinical trials.

Table 1.2: Receptor mediated active targeting of delivery vehicles

#	Receptor	Ligand	Matrix	Payload	Target	References
1.	Folate receptor	Folate	Liposomes	Ricin	KB cells	[54]
			Polymer	Paclitaxel	Ovarian cancer	[55]
			PEGylated Liposome	Doxorubicin	KB cells, SKOV-3, KB tumors	[30]
			Liposome	Imaging agents	KB cells	[56]
			Stealth Liposome	Doxorubicin	Hepatocellular carcinoma	[57]
2.	Transferrin Receptor	Transferrin	Liposomes	Doxorubicin	SBC-3/ADM	[58]
			Protein	Doxorubicin	Liver cancer	[45]
			PLGA	Paclitaxel	Prostate	[59]
		TfRscFv	PLA-PEG NP	Paclitaxel	BT4C rat glioma model	[60]
			Protein	Fluorouracil	B16F10 cells	[46]
3.	Lactoferrin Receptor	Lf	Protein	Gambogic acid	Oral delivery	[61]
			BSA	Doxorubicin	Brain glioma cells	[62]
			PAMAM	DNA	BCEC cells	[63]
			Gelatin nanoparticle	Cisplatin	A549 human lung adenocarcinoma	[64]
4.	EGF receptor	EGF	Iron oxide magnetic NPs		Glioblastoma multiforme (GBM)	[65]
		Antibody	Lipid carriers		Mouse melanoma tumour	[66]
		Antibody	Chitosan nanoparticle	siRNA	SKOV3ip1, HeyA8, and A2780 tumors	[67]
5.	Integrins Receptor	RGD sequence	Adenovirus	DNA	Recurrent gynaecologic solid tumor in Phase I clinical trial	[68]
			LDL nanoparticle	siRNA	HepG2 cell line	[69]
6.	LDL Receptor	LDL	Liposomes	Near-infrared dyes	Human hepatocellular carcinoma	[70]
				Doxorubicin	Prostate	[71]

Table 1.3: Nanoparticle based drugs that are approved or under clinical development.

#	Product	Drug encapsulated	Manufacturer	Indications	FDA approved [Year]
1.	Doxil	Doxorubicin	Jonson & Jonson	Kaposi sarcoma Ovarian cancer Multiple myeloma	1995 1999 2007
2.	DaunoXome	Daunorubicine	Galen	Kaposi sarcoma	1996
3.	Myocet	Doxorubicin	Cephalon	Breast cancer	2000
4.	Lipo-Dox	Doxorubicin	Sun Pharma	Ovarian cancer Breast cancer	2013
5.	Marquibo	Vincristine	Talon	Acute leukaemia	2012
6.	Abraxane	Albumin bound	Abraxis Paclitaxel nps	Various cancer	2005
7.	Abraxane	In combination with Gemcitabine	Celgene	Metastatic pancreatic cancer	2013

1.4.3 Brain targeting

Apart from tumor targeting, a number of ligands have been utilized for transport of drugs across the blood–brain barrier (BBB). BBB presents a formidable obstacle made up of endothelial layer and neuronal cells that largely limits the brain uptake of larger molecules and most of the hydrophilic agents. BBB presents a major hurdle for biologics following intravenous administration and limits their therapeutic efficacy. Receptor-mediated transcytosis (RMT) employing vesicular trafficking to transport ligands across the BBB can be a promising strategy to transport biologics to the brain. Modifications of drugs with appropriate targeting ligand can gain improved access to the brain via RMT. Various receptors present on the endothelial layer that have been utilized for drug delivery to the brain through RMT are discussed below-

1.4.3.1 Low Density Lipoprotein Receptor (LDLR)

The LDLR family includes lipoprotein receptor–related proteins 1 and 2 (LRP1 and LRP2). These proteins are expressed in brain endothelial cells and mediate the transport of lipoproteins across the BBB via RMT. Numerous studies have reported ApoB and ApoE as major protein ligands for LDLRs and hence are extensively used for brain targeting. Human serum albumin nanoparticles decorated with ApoE have been shown to cross the BBB [72, 73].

1.4.3.2 Transferrin Receptor (TfR)

TfRs are one of the very first studied receptors used for brain targeting. Typically TfRs are used for iron transport and are over-expressed in endothelial cells. There is a significant body of research on TfR being used as a carrier system for transportation of drugs across the brain to increase their therapeutic efficacy. Tf decorated liposomes have been used for brain delivery of DNA and imaging agents [74, 109]. However, the higher concentration of endogenous Tf competes with injected vector for TfR binding, leading to the administration of more dosage and thereby making it an incompatible system for brain targeting [75].

Lately, more advanced alternatives have been developed where antibodies to TfR (anti-TfR mAbs) have been decorated on the surface of nano-formulations. These guide them to bind to the epitopes present on the extracellular domain of TfR and thereby do not compete with endogenous Tf [76].

1.4.3.3 Lactoferrin Receptor (LfR)

In recent times, LfRs expressed on endothelial cells, have emerged as highly potential brain targeting receptors which are primarily used in transportation of Lactoferrin (Lf) across BBB. Lf has 300 times more affinity for LfR than transferrin. Endogenous Lf concentration is less and also the transportation of Lf is unilateral making it an ideal brain delivery ligand**.** Lactoferrin receptors are extensively exploited for the brain delivery of several drugs and nucleic acids [62, 63].

1.5 Lactoferrin nanoparticle based drug delivery

Lf an iron-binding glycoprotein is a member of the transferrin family having a molecular weight of 80 kDa. It is a water soluble, biodegradable, easily metabolizable protein and its surface modifications can be easily performed for interactions with drugs. It is a multifunctional protein and widely present in body fluids including nasal and bronchial secretions, bile, gastrointestinal fluids, urine [77], tears, saliva, vaginal fluids, semen, and most abundantly in milk, mainly in colostrum (7 g/L) [78]. It has several pleiotropic functions like antiviral, anti-cancer and immune modulation and thus can act as the first line of defence to inhibit inflammation and infection. Lf shows a wide spectrum of biological properties such as anti-bacterial, antifungal, anti-viral, anti-cancer, immunomodulatory and anti-inflammatory activities. Lactoferrin receptors (LfRs) are over expressed in certain epithelial and endothelial cells, for example intestinal and colon epithelial cells, Caco2 [79] and endothelial cells of brain capillary [80]. The over-expression of Lf receptors on the surface of glioma is a distinct

feature [81]. Moreover, Lf is reported for its ability to cross BBB by utilizing over expressed LfRs and has been extensively exploited as targeting ligands for the delivery of several drugs and genes [62, 63].

Our group has reported a unique sol-oil method for the preparation of Lf nanoparticles (LfNPs) [82]. The advantage of using Lf based nanoparticle formulations, is that the formulation has least number of components and derivatization steps. Such "as is" formulations may be more acceptable in federal regulatory demands. A classic example has been Abraxane®, an emulsion of paclitaxel with albumin, which has become the formulation of choice for most cancers [34].

The sol-oil method of preparation of LfNPs used in this study has several advantages. Firstly, the preparation of LfNPs does not involve any heating or cross linking of the protein to stabilize the nanoparticles. Compared to other methods of protein particle preparation, *viz.* coecervation, salt precipitation, heat denaturation etc., our method is non-disruptive and the protein is expected to remain close to its physiological state. In addition, Lf is a natural protein and present abundantly in human secretions. Our group has demonstrated excellent encapsulation efficiencies, bio-safety and enhanced therapeutic efficacy of several drugs including carboplatin, curcumin, doxorubicin, efavirenz and zidovudine both *in vitro* and *in vivo* [44, 47, 83]. Utilizing Lf as sole matrix of the particles and also for its ability to cross the BBB and specifically target tumor cells has clear advantages.

1.6 Rationale of the study

5-FU and TMZ are the first line treatment for melanoma and glioblastoma respectively but their clinical outcome is limited due to shorter half life, systemic toxicity, MDR, limited accessibility to BBB and sub therapeutic dosage achieved at the tumor site. Formulation providing a curative therapeutic dosage of TMZ or 5-FU at the tumor site by increasing their intracellular uptake, *in vivo* half-life and improved bioavailability and targeted delivery, would be beneficial in reducing the off-target effects of chemotherapeutic drugs and thereby improve the clinical outcomes.

Our group has developed Lf nanoparticles and demonstrated excellent encapsulation efficiencies, improved bioavailability and enhanced therapeutic efficacy of several drugs. Utilizing Lf for its ability to cross the BBB along with targeting Lf receptors over-expressed on tumor cells specifically in a nano-particulate form, is a practical and viable approach for delivery of chemotherapeutic drugs that are impermeable to BBB. Targeting BBB and brain tumor cells using a single ligand is further expected to enhance the therapeutic value of TMZ in terms of specificity and also in simplifying the design of the nanoparticles. Prepared from

natural and abundant protein with no modifications, Lf nanoparticles were shown to be very safe carriers of drugs.

TMZ resistance in glioblastoma is linked to mutation in p53 gene and up regulation of cell cycle protein Arora Kinase B (AKB). Drug-sensitization of cancer cells by restoration of wild type p53 and siRNA mediated down-modulation of AKB protein would potentiate TMZ efficacy in resistant GBM. Considering the unique properties of Lf nanoparticles, such as their ability to bind to nucleic acid and tumor targetibility, they were exploited for the delivery of plasmid p53 and AKB-siRNA. Chemotherapy combined with gene therapy for the treatment of complex diseases like cancer would likely improve the treatment outcome. Such combinatorial approach would be more advantageous compared to treatment based on single agent.

The present work explores a dual strategy of single component Lf nanoparticles - where Lf facilitates the transcytosis of therapeutic agents across the BBB along with tumor specific delivery by means of receptor mediated active targeting. In addition to that, the nanoparticulate form facilitates the preferential accumulation through EPR effect by passive targeting at the tumor site. With a simple synthesis procedure and the ability to exploit two hallmark features of tumor patho-physiology (over-expression of LfRs and low pH), the LfNPs demonstrated here may be considered as potential carrier for TMZ. Moreover, the proof-of-concept study provided here may be applied for other drugs as well.

The work has been addressed in the following objectives:

I. Development of 5-fluorouracil loaded lactoferrin nanoparticles and their efficacy in mouse melanoma cells

II. Analysis of temozolomide loaded lactoferrin nanoparticles and their therapeutic efficacy in orthotopic GBM model

III. Enhancing drug sensitivity in temozolomide resistant tumors using aurora kinase B-siRNA loaded lactoferrin nanoparticles in orthotopic GBM model

IV. Potentiating temozolomide activity by p53-DNA loaded lactoferrin nanoparticles in subcutaneous GBM model

Chapter 2

Materials and Methods

2.1 Materials

Lactoferrin and olive oil used for nanoparticles preparation were purchased from Symbiotic (USA) and Leonardo (Italy), respectively. 5-Fluorouracil, Rhodamine123 and Fluorescein (FL) were procured from Sigma (St. Louis, MO). MTT ((3-(4, 5-dimethylthiazol-2-yl)-2, 5-diphenyl tetrazoliumbromide) was purchased from Calbiochem (USA). Temozolomide (TMZ) was a gift from Celon Laboratories Pvt. Ltd (India). Mouse melanoma (B16 F10), Mouse glioma (GL261), Liver hepatocarcinoma (HepG2) and Lung carcinoma (A549) cell lines were obtained from ATCC. Anti-Lactoferrin (Anti-Lf) and anti-Lf receptor (Anti-LfR) antibodies were purchased from Pierce, Thermo Scientific (USA) and Biorbyt (UK), respectively. Anti-Caspase-III, anti-CD31 and goat anti-rabbit IgG antibodies were purchased from Abcam (UK). FITC Annexin V/dead cell apoptosis kit was purchased from Molecular Probes, Invitrogen (USA). Kits for biochemical analysis were purchased from Tulip Pvt. Ltd. (India). AKB siRNA was generously provided by Dr. Harinarayana Rao (Reliance Life Sciences, India). Cy3 and carboxyfluoroscein (FAM)-labelled siRNA were purchased from Eurogentic. Plasmid pGFPC1 (4.7 kb) encoding the green fluorescent protein and p53 plasmid were from addgene, SYBR Green I (Invitrogen). p53 antibody from Proteinase k and DNase I were purchased from Sigma–Aldrich. All other chemicals and reagents were of analytical grade.

2.2 Methods

2.2.1 Preparation of 5-FU-LfNPs

5-FU-LfNPs were prepared by a sol-oil method [46]. Briefly, 5-FU was mixed with Lf in a ratio of 1:2 (w/w) and incubated for 30 min on ice and then slowly added to 15 ml of olive oil at 4 °C with continuous dispersion by vortexing, followed by sonication (Ultrasonic homogenizer 300V/T, Biologics Inc., Manassas, Virginia, USA) at 4 °C. The resulting mixture was snap frozen and then thawed over ice. The particles were pelleted by centrifugation at 30,000x g for 20 min and the pellet was extensively washed thrice with diethyl ether followed by PBS to remove excess oil and free 5-FU. Finally the pellet was dispersed in phosphate buffered saline (PBS) and either stored at 4 ºC or lyophilized as per the experimental constraint.

For fluorescent labelling, blank lactoferrin nanoparticles (LfNPs) were prepared by similar procedure as stated above without the addition of 5-FU and then was incubated with 50µl of 20% rhodamine123 for overnight at 4 ºC to make Rhodamine123 tagged lactoferrin nanoparticles (LfNPs-Rh123).

2.2.2 Preparation of TMZ loaded Lf nanoparticles

Temozolomide loaded Lf nanoparticles (TMZ-LfNPs) were prepared using sol-oil method as in 2.2.1 except that TMZ is used in place of 5-FU. For fluorescence microscopy studies, fluorescein (FL) loaded Lf nanoparticles (FL-LfNPs) were prepared using the above mentioned method by replacing TMZ with FL.

2.2.3 Preparation of plasmid DNA loaded lactoferrin nanoparticles

For the preparation of plasmid DNA loaded Lf nanoparticles (pDNA-LfNPs) first a gel binding was carried out to investigate the affinity of Lf for plasmid DNA. Further NPs were prepared with some modification as described above. Briefly, the complex of Lf and pDNA in the desired ratio (10:1 W/W) was slowly added to 20 ml olive oil and processes similarly for nanoparticle formation.

2.2.4 Gel retardation and DNase protection assay of pDNA

The encapsulation of DNA in LfNPs was confirmed through gel retardation assay. pDNA-LfNPs were loaded on 1% agarose gel and run in the electrophoresis system (Bio-Rad, USA) at 80 V for 60 min with plasmid DNA as control. In another experiment stability of pDNA-LfNPs towards nuclease degradation was determined by incubating them with 1 µl of DNase I solution (0.1U/ml) at 37 ºC for 0.5 h followed with either phenol-chloroform isoamyl (PCI) extraction or directly DNA extraction from LfNPs and then resolved on 1% agarose gel and visualized by ethidium bromide staining. DNA alone digested with DNase I served as control.

2.2.5 Preparation of siRNA loaded lactoferrin nanoparticles

The ability of Lf protein to bind siRNA was assessed by agarose gel-based assays. The complex was prepared by incubating 20 pmol of siRNA with increasing amount of Lf protein in PBS buffer to obtain the desired mole ratios and incubated for 20 min prior to electrophoresis. For nanoparticles preparation the obtained ratio complex of siRNA and Lf was slowly added to 20 ml olive oil and processed further for nanoparticle preparation as described previously.

2.2.6 RNase protection and serum stability assay

The siRNA-LfNPs were incubated with RNaseA for 1 h at 37 °C. siRNA were then extracted by Proteinase K digestion of particles as described previously and resolved on a 2% agarose gel and visualized by ethidium bromide staining. siRNA alone and with RNase A,

loaded in separate lanes serve as controls. The serum stability of siRNA-LfNPs was assessed by monitoring their size over a period of 8-10 h at 37 ºC in 50 % serum using DLS.

2.2.7 Physico-chemical characterization of nanoparticles

Transmission Electron Microscopy (TEM) and scanning electron microscope (SEM) analysis was carried out to study the morphology and size of nanoparticles. For TEM analysis, LfNPs were placed on carbon coated copper 300 mesh grids, air dried and stained using 1% aqueous solution of uranyl acetate for 1 min. The samples were examined using Transmission Electron Microscope (JEM-2100, M/S Jeol Limited, Tachikawa, Tokyo, Japan). SEM analysis was carried out by coating nanoparticles onto the glass slides. Afterward slides were sputtered by silver paint. Particles were scanned in (PHILIPS Scanning electron microscope) and data was analyzed according to manufacturer's instruction.

The hydrodynamic diameter, poly dispersity index (PDI) and zeta potential were analyzed by nanoparticles analyzer system (Horiba Scientific, USA). For the in vitro storage stability studies, particles were prepared as described earlier, and stored in PBS at 4ºC and at physiological conditions (RT). At regular time intervals, aliquots were withdrawn and analyzed for their hydrodynamic diameter using a nanoparticle analyzer system (Horiba Scientific, USA) over a period of 5 weeks. Further particle stability is tested at physiological condition for several hours.

2.2.8 Fourier transform infrared (FT-IR) spectroscopy

The infra-red spectra of free Lf, LfNPs, free 5-FU and 5-FU-LfNPs, TMZ and TMZ-LfNPs were obtained at a resolution of 4 cm^{-1} in a FT-IR Spectrometer (Bruker Aplha T, Bruker Optik, Ettingen Germany), equipped with a single reflection diamond attenuated total reflectance accessory. A drop of nanoparticles was air dried on the surface of diamond crystal element by solvent evaporation followed with recording of 64 scans at 200 cm^{-1}/ min and averaged.

2.2.9 Determination of drug encapsulation efficiency and drug loading content

The encapsulation efficiency was determined by resuspending 0.5 mg of 5-FU-LfNPs in 1ml PBS (0.01 M, pH 5.0) and incubated for 4 h at 37 ºC on a rocker. Equal volume of acetonitrile was then added to precipitate the protein, followed by centrifugation at 30,000 × g for 15 min. The supernatant was collected and filtered through a 0.2 micron syringe filter and quantified using UV-Vis spectrophotometer (JASCO) at 254 nm. All experiments were performed in triplicates. Encapsulation efficiency and drug loading content was calculated by following formula -

$$Encapsulation\ efficiency\ (\%) = \frac{weight\ of\ drug\ in\ nanoparticles}{initial\ weight\ of\ drug\ used}\ X\ 100 \quad \ldots\ldots\ldots 1$$

$$Drug\ loading\ content\ (\%) = \frac{weight\ of\ drug\ in\ nanoparticles}{weight\ of\ the\ nanoparticles}\ X\ 100 \quad \ldots\ldots\ldots 2$$

TMZ entrapment efficiency in nanoparticles was determined by resuspending 0.5 mg TMZ-LfNPs in 1ml of PBS (pH 5.0) and incubated for 4 h at 37ºC on a rocker. 100 µl of 20 % AgNO3 was then added to precipitate the protein, followed by addition of 900 µl of mobile phase (a mixture of water: methanol: acetonitrile (45:45:10 v/v), pH adjusted to 3.0 with o-phophosphoric acid).The mixture was centrifuged at 30,000 x g for 15 min, supernatant was collected and filtered through a 0.2 µm syringe filter. The amount of TMZ released was quantified using an Agilent 1200 series reversed-phase high performance liquid chromatography (RP-HPLC) system. Separation was carried out by using a Zorbax 300 SB-C18 column (250 mm x 4.6 mm, 5 µm particle size, Flow rate - 0.5 ml min^{-1}, Injection volume - 200 µl and run time - 10 min). TMZ was estimated by its absorption at 340 nm. The limit of detection of TMZ by this method was found to be 10 ng ml^{-1}. All experiments were performed in triplicates. TMZ entrapment efficiency and drug loading content was calculated by using the formulae I and II.

2.2.10 Entrapment efficiency calculations for siRNA

Direct method was carried out to measure the encapsulation efficiency of siRNA. Freshly prepared siRNA-LfNPs were digested with proteinase k (100µg/ml) in Tris buffer (pH 8.0, 20 mM) for 60 min at 37°C followed by addition of Ribogreen (Invitrogen) according to the manufactures protocol. The fluorescence intensity measured at excitation 480 nm and 520 nm. Concentration of siRNA present in the particles was calculated by plotting standard graph with known concentration of ribosomal RNA standards provided with the kits. The encapsulation efficiency (EE) was calculated from the Equation.

EE = Amount of siRNA released from nanoparticle / Total amount of siRNA used for nanoparticle preparation X 100

2.2.11 Determination of entrapment efficiency of pDNA

Direct method was carried out to measure the encapsulation efficiency of DNA. Freshly prepared NPs were digested with proteinase k (100µg/ml) in Tris buffer (pH 8.0, 20 mM) for 60 min at 37°C followed by addition of SYBR Green I reagent. The fluorescence intensity measured at excitation 485 nm and 535 nm. Concentration of DNA present in the

particles was calculated by plotting standard graph with known concentration of DNA samples. The encapsulation efficiency (EE) was calculated from the equation:
EE = Amount of DNA released from nanoparticle/ Total amount of DNA used for nanoparticle preparation X 100

2.2.12 *In vitro* pH release studies

5-FU-LfNPs (0.5 mg) were resuspended in 1 ml of buffers (ranging from pH 1.0 to 9.0) and incubated for 4 h on rocker at 37 ºC. Individual samples were collected by centrifugation at 30,000 x g for 15 min. 5-FU released from the nanoparticles was quantified using UV–Vis spectrophotometer at 254 nm. All assays were done in triplicates.

2.2.13 *In vitro* TMZ release studies

TMZ-LfNPs (0.5 mg) were re-suspended in 1 ml of buffer (pH ranging from 1.0 to 9.0) and incubated for 4 h at 37°C on a rocker. Samples were collected by centrifugation at 30,000 x g for 15 min. TMZ released from the nanoparticles was quantified using HPLC as mentioned in section 2.2.9. All assays were done in triplicates.

To study the release kinetics of TMZ from TMZ-LfNPs, the nanoparticles (10 mg ml^{-1}) were re-suspended in PBS (pH 5.5 or 7.4) and placed in a dialysis tubing (MWCO 8 kDa to 12 kDa) and incubated in an incubator shaker at 37ºC. Samples were collected at various time intervals (0 to 72 h) and analyzed for TMZ using HPLC as mentioned.

2.2.14 Cell culture

Mouse melanoma (B16F10) cell line were maintained in a Dulbecco's modified Eagle's growth medium (DMEM, Invitrogen) supplemented with 10% fetal bovine serum (Invitrogen), 5 μg ml^{-1} penicillin, 6 μg ml^{-1} streptomycin, and 10 μg ml^{-1} kanamycin. All cells were grown and maintained in 5% CO_2, 95% humidity at 37 °C.

2.2.15 Competitive ligand binding assay

In order to investigate the receptor specificity of LfNPs, a competitive ligand binding assay with free Lf was performed. Briefly, cells (1×10^6) were incubated simultaneously with increasing amount of free Lf and LfNP-Rh123 (100 μg ml^{-1}) in serum-free medium for 2 h in a 12-well plate. After incubation, cells were harvested and analyzed using a FACSCaliber™ cell analyzer (BD Biosciences). Gating on forward and side scatter was done to exclude cell debris and 10,000 gated events were recorded. Data was analyzed using Cell Quest software (Becton Dickinson).

The effect of competitive ligand binding on 5-FU uptake when delivered through LfNPs was also investigated using spectrophotometer. Briefly, cells were incubated with 5-FU-LfNPs (equivalent to 60 μg of 5-FU) and simultaneously with free Lf in equal ratio of LfNPs**.** After 2 h incubation, cells were washed thrice with PBS and sonicated in PBST (PBS with 0.1 % triton X) for 30 s. The protein in the cell lysate was precipitated by adding equal volumes of 20% silver nitrate ($AgNO_3$) and then incubated overnight at 4 ºC. The precipitated protein was separated by centrifugation at 11000 × g for 15 min at 4 ºC and 5-FU was estimated using spectrophotometer as mentioned earlier**.**

2.2.16 Cellular uptake assay

2.2.16.1 Quantitative determination of intracellular 5-FU by HPLC

Cells were seeded in a 12-well plate and upon 70% confluence, free 5-FU and 5-FU-LfNPs (equivalent to 100 μg of 5-FU) were added. After 2 h cells were washed thrice with PBS and further incubated for indicated time points (30 min to 24 h). At the end of experiments, cells were harvested and equal number of cells was processed for 5-FU estimation using a UV–Vis spectrophotometer as described earlier.

2.2.16.2 Qualitative determination of cell uptake by confocal microscopy

Cells grown on cover slips to 70% confluence, were treated with 100 μg ml^{-1} of free rhodamine (Rh123) and equivalent amount of LfNPs-Rh123 for indicated time points (0.5, 1, 2 and 4 h). After indicated time points cells were washed thrice in PBS and fixed with 4% formaldehyde solution. Cells were counterstained with DAPI and mounted in VECTASHIELD mounting medium and analyzed by confocal laser scanning microscopy (Leica TCS-SP8) under 63X oil immersion objective lens.

2.2.17 Cytotoxicity Assay

The cytotoxicity of 5-FU-LfNPs in B16F10 cells, was measured by MTT assay and compared with free 5-FU. Briefly, cells were seeded in a 96-well plate at a density of 5000 cells per well and incubated at 37 ºC with 5 % CO_2 and 95 % humidity. After obtaining the desired confluency, cells were incubated with increasing concentrations of either free 5-FU or 5-FU-LfNPs (ranging from 5 to 50 μg ml^{-1}). Cells were then incubated for another 24 h and the % cell inhibition was calculated using the following formula.

$$\text{Inhibition (\%)} = \frac{\text{A570nm of control cells} - \text{A570nm of treated cells}}{\text{A570nm of control cells}} \text{ X 100}$$

The cellular toxicity of TMZ-LfNPs in GL261 cells was estimated similarly as mentioned above with increasing concentrations of either free TMZ or TMZ-LfNPs with an equivalent dose of TMZ (0 - 200 μg ml^{-1}) and further incubated for 24 h. The cell viability was calculated as above mentioned.

In order to determine the toxicity of the drug carrier (i.e. blank LfNPs without drug , cells were cultured in 12-well plate and incubated with increasing concentrations (5 to 1000 μg ml^{-1}) of blank LfNPs for 48 h. The cells were scraped, washed and fixed in 70% ethanol followed with addition of propidium iodide (PI) at a final concentration of 0.5 μg ml^{-1}. The samples were analyzed using flow cytometry as described in section 2.2.15.

2.2.18 Receptor screening and receptor blocking assay

Lf receptor (LfR) expression in GL261 cells was determined by western blot. Briefly, GL261 cells along with positive (HepG2) and negative control (A549) cells were homogenised in radio-immuno-precipitation assay buffer (RIPA : 50 mM Tris-Cl pH 8.0, 150 mM NaCl, 2 mM EDTA, 1% (w/v) NP-40, 0.5% (w/v) sodium deoxycholate, 0.1% (w/v) SDS containing protease inhibitor cocktail (G-Biosciences, India). The homogenate was subsequently centrifuged to remove insoluble debris and protein content of the lysate was estimated using Bradford's method. 20 μg of protein was then resolved using 12% SDS-PAGE and transferred to a nitrocellulose membrane. The membrane was subsequently blocked with 5% BSA and probed with primary anti-LfR antibody followed by secondary antibody conjugated with horse raddish peroxidase. The blot was developed by a Vilber-Lourmat Chemiluminescence Imaging System using the Chemi-Capt software, after adding the Pierce® ECL Western Blotting HRP substrate (Thermo Scientific).

To investigate the role of LfR in the cellular internalization of LfNPs, a receptor blocking experiment was performed. The uptake of LfNPs was assessed by pre-incubating cells with anti-LfR antibodies (1:300) in serum-free medium for 1 h. Subsequently FL-LfNPs (100 μg ml^{-1}) were added to the cells and further incubated for 2 h. After incubation, the cells were processed for confocal microscopy as mentioned previously. The effect of receptor blocking on TMZ delivery through LfNPs was investigated using HPLC. Briefly, GL261 cells (1 x 10^6) were incubated with anti-LfR antibody in serum-free media for 1 h followed by 2 h incubation with TMZ-LfNPs (100 μg ml^{-1}). After incubation, cells were washed thrice with PBS and sonicated in PBST for 30 s. Protein in the cell lysate was precipitated by adding equal volumes of 20% silver nitrate ($AgNO_3$) and incubated overnight at 4ºC. The precipitated protein was separated by centrifugation at 11000 x g for 15 min at 4ºC and TMZ was quantified using HPLC as mentioned previously.

2.2.19 Estimation of intracellular TMZ

The cellular uptake of TMZ was determined by treating cells with free TMZ and TMZ-LfNPs (equivalent to 60 μg TMZ) for a period of 2 h. The cells were washed with PBS and further incubated in fresh culture media. At indicated time points (0-24 h), cells were harvested. TMZ was estimated from fixed number of cells as described earlier.

2.2.20 Wound-healing and migration assay

Wound-healing migration assay was carried out according to the earlier reported method [84] with minor modifications. Briefly, GL261 cells were seeded in a 60 mm^3 tissue culture plates (Corning) and treated with PBS, free TMZ and TMZ-LfNPs (100 μg ml^{-1}). After 24 h, cells were scratched from the middle of the monolayer with a sterile plastic pipette tip, washed with PBS and the wound was allowed to heal. The extent of cell migration was calculated by imaging the cell boundary under Axiovert inverted microscope (Zeiss) at 37 °C and 5% CO_2 atmosphere. The wound area was measured using image analysis software (Image J).

2.2.21 Cell based assays for siRNAs

2.2.21.1 Cellular uptake of siRNA-LfNPs by flow cytometry and confocal microscopy.

The uptake of siRNA-FAM loaded LfNPs were determined using flow cytometry. GL261 cells were treated with 20 pmole of FAM-siRNA and equivalent amount of FAM-siRNA loaded LfNPs (FAM-siRNA-LfNPs). Lipofectamine complexed with similar amount of FAM-siRNA was used as a positive control. After 2 h of incubation, the cells were washed with PBS to remove the cell surface associated particles. The cells were detached by trypsinization and collected in 1.5 mL eppendorf tubes and were analyzed for fluorescence on a FACS Caliber with Cell Quest software (Becton Dickson) as described earlier.

For intracellular trafficking GL261 cells grown on cover slips to 70% confluence, were incubated with FAM-siRNA and equivalent amount of (FAM-siRNA-LfNPs-alexa-633) for indicated time points (4 and 6 h) at 37 °C. Cells were then fixed with 4% formaldehyde solution and processed for confocal microscopy as described earlier. For endo-lysosomal escape assay, cells were processed similarly and stained with LysoTracker red and visualized under confocal microscope as described earlier.

2.2.21.2 Quantitative RT-PCR and Immunoblotting

In order to assess the siRNA transfection abilities of LfNPs, GL261 cells seeded in a six well plate and upon 70% confluence, treated with siRNA specific to AKB at 50 nM

concentration either in AKB-LfNPs formulation or complexed with lipofectamine. siRNA alone was used as negative control. After 48 h of incubation total RNA was isolated by lysing the cells with Trizol reagent (Life technologies) and was reverse transcribed using SuperScriptTM III First Strand Synthesis system for RT-PCR (Life Technologies) and oligo dT, according to the manufacturer's guidelines. For quantitation of genes, 1µl of cDNA corresponding to 20ng of total RNA was used as a template in probe-based detection method, using Solaris quantitative PCR assay (Thermo Scientific) on ABI 7900 Real time PCR system (Applied Biosystem). The data was analyzed by comparative ΔΔCt method. The sequences of the primers are given below:

S.No	Name of primer	Sequence
1.	AKB fp	ACCCTTTGAGAGTGCATCAC
2.	AKB rp	GGAACTTTAGGTCCACCTTG
3.	GAPDH fp	GCCTCAAGATCATCAGCAATG
4.	GAPDH rp	CTTCCACGATACCAAAGTTGTC

For immunoblotting, GL261 cells treated with AKB-siRNA, lysed with RIPA buffer and processed as mentioned above. Later blots were probed with mouse monoclonal antibodies against AKB protein (Abcam) followed by incubation with goat anti-mouse IgG secondary antibody conjugated with peroxidase-conjugated secondary antibody (Thermo Fisher) and developed as describe earlier.

2.2.21.3 *In vitro* sensitization of TMZ resistant GL261 cells

The cellular toxicity of AKB-LfNPs and there degree of sensitization to TMZ was carried out by microscopic examination. Briefly, GL261 cells were treated with AKB-LfNPs for 48 h, followed by the addition of increasing concentrations of TMZ (0-500 µM). 24 h after the addition of TMZ (and 72 h after AKB-LfNPs treatment), cell death was visualized by bright field microscopy.

TMZ sensitization was further evaluated by assessing the degree of apoptosis in glioma cells as determined by the percent of cells in the sub-G1 population of the cell cycle. GL261 cells in 12 well plate were treated with AKB-LfNPs for 48 h, after which the cells were treated with increasing amounts of TMZ (0-500 µm). 24 h after the addition of TMZ, the cells and supernatant media were collected, fixed in cold ethanol (70% vol/vol) and stained with PI. The amount of apoptosis was assessed using flow cytometer as described earlier.

2.2.22 Cell based assay for pDNA

2.2.22.1 Determination of relative LfR expression levels using fluorescence activated cell sorting (FACS)

For relative quantification of LfRs by FACS, HepG2, GL261 and A549 ($1X10^5$) cells were trypsinized and probed with primary anti-LfR antibody followed by secondary antibody conjugated with Alexa Fluor-488. The cells were washed thrice and analyzed using a FACSCaliberTM cell analyzer (BD Biosciences) as discussed previously.

2.2.22.2 LfR specific cellular uptake

In order to investigate the lactoferrin receptor targeting abilities of LfNPs, HepG2, GL261 and A549 (1×10^6) cells were incubated with LfNPs-Rh123 (100 μg ml^{-1}). In a separate experiment competitive ligand binding assay, cells were simultaneously incubated with free Lf in serum-free medium for 2 h in a 12-well plate. After incubation, cells were harvested and analyzed using flow cytometry.

2.2.22.3 *In vitro* transfection

To analyze the gene expression abilities of LfNPs, the above mentioned cell lines were seeded on 12 well plate (5×10^4 cells/well) 24 h prior transfection. Upon 80-90% confluency the transfection was initiated by incubating cells with pDNA-LfNPs (1μg equivalent DNA) in 200μl of serum-free medium for 6 h at 37°C in 5% CO2 incubator. Later cells were washed and replaced with 1 ml of complete medium and incubated further for 48 h. Finally the percentage GFP positive transfected cells were counted using flow cytometry.

2.2.23 Animal experiments

All animal experiments were conducted in accordance with protocols approved by the Institute's Animal Ethics Committee (IAEC) project numbers 41/2016. Adult C57BL/6 mice (22-24 g) were maintained at 22 ºC on a 12 h light and dark cycle in polyethylene cages with stainless steel lids with *ad libitum* access to food and water. All experiments were performed under anaesthesia using intraperitonial (i.p) injection of a mixture of Ketamine (120 mg kg^{-1}) and xylazine (6 mg kg^{-1}) in saline.

2.2.23.1 BBB crossing capability of LfNPs in healthy mice by immunoblotting and immunohistochemistry

Healthy C57BL/6 mice were intravenously injected with PBS and 100 μl of free Lf and LfNPs (equivalent dose 2 mg ml^{-1}). After 24 h mice were euthanized by cervical

dislocation. After perfusion of heart with 4% paraformaldehyde, brain tissues were extracted, snap frozen in liquid nitrogen and stored at -80°C. For immunoblotting brain tissues lysate was probed with primary anti-Lf antibody and secondary IgG conjugated with HRP substrate and processed as described earlier.

For immuno-histochemistry, frozen brain tissues were embedded in OCT tissue freezing medium (Leica, India) and cryosectioned to obtain 5 μm thick sections on positively charged slides. The tissue sections were fixed in iso-propanol for 5 min and incubated with anti-Lf antibody at RT for 1 h. Excess antibody was washed using PBST and the sections were further incubated with Alexa Fluor-488 labelled goat anti-rabbit secondary antibody. The sections were counterstained with propidium iodide (PI) and visualized under a confocal fluorescence microscope.

For transcytosis studies, C57BL/6 mice were intravenously injected with 100 μl of FL-LfNPs (2 mg ml^{-1}). Brain sections, obtained by the procedure described earlier, were blocked in 5% BSA for 1 h followed by incubation with CD31 antibody diluted in PBS containing 0.05% Tween 20 (1:300) for 12 h at 4°C. The sections were washed and incubated with cy3 conjugated secondary antibody and processed as described above. Autofluorescence was removed by treating brain sections with freshly prepared 1% (w/v) $NaBH_4$ in PBS for 20 min before immunostaining. Subsequently the sections were incubated in 1 mM cupric sulphate and 50 mM ammonium acetate solution (pH 5.0) for 1 h [85].

2.2.23.2 Pharmacokinetic studies

Healthy C57BL/6 mice were intravenously administered with free TMZ and TMZ-LfNPs (with an equivalent TMZ dose of 10 mg kg^{-1} body weight), via tail vein injection. 200 μl of blood was collected by retro-orbital plexus at indicated time points, 0.083, 0.25, 0.5,1, 2, 4, 8 and 24 h following injection. Plasma was separated from the blood samples, followed by 30 min incubation with equal volume of 20% $AgNO_3$ at RT. Subsequently, the homogenates were centrifuged at 11000 xg for 15 min at 4ºC and the supernatant was collected and filtered using a 0.2 μm syringe filter and assayed for TMZ concentration using HPLC as mentioned previously. At 24h mice were euthanized and brain was collected and assessed for TMZ uptake using HPLC. Pharmacokinetic parameters from quantified TMZ were calculated using Kinetica V.5.0 software with non-compartmental model of estimation.

2.2.23.3 Orthotopic glioma mice model generation

Tumor was developed by intracranial implantation of mouse glioma cells. Briefly, C57BL/6 mice (21-22 gm) were intracranially implanted with GL261 cells for generation of

orthotropic glioma mouse model. Mice were anesthetised by I.P. injection of Xylene/Ketamine and injected with 10,000 cells in 3 µl PBS, stereo-tactically into the right striatum (1.8 mm lateral to the bregma at 3 mm depth) using a Hamilton syringe (Harvard Apparatus, UK) along with a 26-gauge needle at 0.2 µl min^{-1} attached to a stereotaxic frame (Stoelting, USA). Wounds were closed with sutures and mice were carefully monitored until recovery from anaesthesia.

2.2.23.4 *In vivo* tumor targeting studies

The ability of systemically administered LfNPs to deliver TMZ at the tumor site was evaluated. Glioma bearing C57BL/6 mice were treated with free TMZ (5 mg kg^{-1} body weight) and equivalent dosage of TMZ in TMZ-LfNPs. Different parts of the brain tissue were isolated and TMZ was quantified using HPLC as described earlier.

2.2.23.5 *In vivo* tumor regression and survival studies of TMZ-LfNPs in glioma bearing mice

The established intracranial glioma bearing C57BL/6 mice, were randomly divided into three groups (n=3) and injected with either PBS or an equivalent dosage of 5 mg kg^{-1} body weight of TMZ and TMZ-LfNPs on 3^{rd}, 5^{th}, 7^{th} and 9^{th} day as described in the schedule given (*vide infra*). When all the PBS treated mice succumbed to death, tumor bearing brain samples were collected and fixed with 10% formalin in PBS for 48 h and then embedded in paraffin wax followed by, sectioning (5 µm sections) and staining with Haematoxylin and Eosin using standard protocols. The tumor area in the histology sections was measured using Image J software. To calculate the tumor volume (V), the maximum diameter (a) and minimum diameter (b) of tumor mass in the whole brain tissue was measured using vernier caliper and the tumor volume was calculated using the below formula:

$$\textbf{Tumor volume (V)} = 0.5\ ab^2$$

For survival curve analysis, another set of intracranial glioma bearing mice (n=6) were treated as in accordance with the treatment schedule mentioned and monitored for their survival till they became moribund. Survival data was analyzed with log-rank test in Kaplan Meier non-parametric analysis mode.

The *in vivo* response to TMZ-LfNPs was assessed by quantifying the level of apoptosis in tumor tissue using FITC Annexin V/dead cell apoptosis kit (Molecular probes). Briefly, the glioma bearing mice, after treatment with either TMZ or TMZ-LfNPs as described earlier were euthanized and the tumor bearing brain was harvested. Single-cell suspensions were obtained by collagenase digestion [86]. Subsequently cells were passed

through a 70 µm cell strainer (BD Falcon), stained according to the supplier's protocol and analyzed by flow cytometry as mentioned above. Apoptosis was further analyzed by determining the levels of cleaved (activated) Caspase-3 using western blot. Briefly brain tumor lysate was processed and 20 µg of protein was resolved on a 12% SDS-polyacrylamide gel, transferred to nylon membrane, and probed with antibody against Caspase-3 followed by secondary antibody conjugated with horse raddish peroxidase and the blot were developed as described above.

2.2.23.6 Toxicity studies in glioma bearing mice

Toxicity related parameters were tested at the end of the treatment in glioma bearing mice by collecting blood samples for haematological and serum chemistry analysis. The complete blood count from untreated control and treated mice was obtained using haematology analyzer Elite 5, as per manufacturer's protocol. The following enzymes were tested for hepatotoxicity; alanine aminotransferase (ALT), aspartate aminotransferase (AST) and alkaline phosphatase (ALP). For nephrotoxicity creatinine (CRE) and blood urea nitrogen (BUN) were studied. Lactose dehydrogenase (LDH) was monitored for cardiotoxicity. Activity of all above mentioned enzymes were measured by using biochemical kits as per the manufacturer's protocol (Tulip Pvt. Ltd.).

2.2.23.7 *In vivo* gene silencing in GBM mice

In order to investigate the desired gene silencing abilities of LfNPs, AKB-LfNPs (2 mg kg^{-1}) were systemically injected via tail vein injection. GBM mice were also injected with equivalent dosage of scrambled siRNA loaded LfNPs (scr. siRNA-LfNPs) for negative control. Post 48 h injection, all three groups (1) cancer untreated (2) AKB-LfNPs treated and (3) scr.siRNA-LfNPs were euthanized and brain samples were collected for gene silencing evaluation. Briefly brain tumor lysate was processed as mentioned earlier and 20 µg of protein was resolved on a 12% SDS-polyacrylamide gel, transferred to nylon membrane, and probed with antibody against AKB protein followed by secondary antibody conjugated with horse raddish peroxidase and the blots were developed as described above.

2.2.23.8 Tumor regression and survival studies

The established intracranial glioma bearing C57BL/6 mice, were randomly divided into four groups (n=3). The groups were injected with: (1) PBS, (2) four alternate dosage of TMZ (5 mg kg^{-1} BW) alone, (3) TMZ in combination with prior consecutive dosage of AKB-siRNA (2mg kg^{-1} BW) and (4) AKB-siRNA alone as described in the schedule (**Figure 5.11)**. When all the PBS treated mice succumbed to death, tumor bearing brain samples were

collected and processed for Haematoxylin and Eosin staining as described earlier. The tumor area in the histology sections was measured using Image J software.

For survival curve analysis, another set of intracranial glioma bearing mice (n=6) were treated as in accordance with the treatment schedule mentioned and monitored for their survival till they became moribund. Survival data was analyzed as described previously.

2.2.23.9 Subcutaneous GBM model generation

To investigate the therapeutic potential of pDNA delivered by LfNPs into the tumor tissues, and to potentiate the current TMZ chemotherapy, we selected pDNA against p53 tumor suppressor gene. Subcutaneous glioma tumor model were developed in C57BL/6 mice by injecting the GL261 cells intra-peritoneal (i.p) in the flank region.

2.2.23.10 *I*n vivo gene expression in GBM mice

After the tumor size attained an average dimension between 50~100 mm^3, the mice were randomly grouped and were treated with a single dose of p53-LfNPs. Post 48 h and 72 h injection, mice were euthanized and brain samples were collected for gene expression evaluation. Briefly, tumor lysate was processed as mentioned earlier and 20 μg of protein was resolved on a 12% SDS-polyacrylamide gel, transferred to nylon membrane, and probed with antibody against p53 protein followed by secondary antibody conjugated with horse raddish peroxidase and the blots were developed as described above.

2.2.23.11 Tumor regression studies

In order to access the tumor regression abilities of p53 gene delivered by LfNPs, mice were randomly divided in groups and injected with (i) four alternate dosage (5mg kg^{-1}) of TMZ, (ii) four alternated dosage (2mg kg^{-1}) of p53-LfNPs and (iii) TMZ with prior consecutive dosage of p53-LfNPs in combination. Mice that received PBS were used as a negative control for assessing the tumor suppression**.**

Chapter 3

Development of 5-FU loaded Lf nanoparticles & their efficacy in mouse melanoma cells

3.1 Introduction

Malignant melanoma is a belligerent form of skin cancer with high mortality rates. There has been a rapid increase in the occurrence of malignant melanoma in industrialized countries in the last 30 years [87]. As per the American Cancer Society's estimates around 87,110 new melanoma cases will be diagnosed in 2017 with a predictable mortality of 9730 people. It is one of the most common cancers in young adults (especially young women). Despite the fact that there is a greater understanding of the risk factors, along with the genetic and epigenetic causes of melanoma, the mortality rate from melanoma is quite predominant compared to any other types of cancers [88]. Risk factors of melanoma include gene polymorphism, skin type, many or unusual moles on body, family history, a previous melanoma occurrence, sensitivity towards sun, weakened immune system and excessive ultraviolet (UV) exposure. Common treatments for malignant melanoma involve surgical procedures, chemotherapy and radiotherapy. Despite these stated treatments, at least one third of patients with early-stage melanoma develop metastases, and the prognosis of metastatic melanoma remains dismal. Studies show that the melanoma patients have an alarmingly low median survival time of approximately 6–8 months. Moreover, it has been grimly observed that less than 5% of patients survive for a maximum of five years.

Various chemotherapeutic drugs have been ineffective against melanoma cells as these cells become resistance to apoptotic pathways which leads to poor clinical outcome [89]. 5-FU is one of the oldest standard drug used broadly for solid tumors. It is a fluorinated analog of pyrimidine base uracil, which gets converted intracellularly to its active form - fluorodeoxyuridine monophophate. This active form inhibits thymidylate synthase (TS) enzyme, required for the synthesis of thymidine, a nucleoside vital for DNA replication. This results in apoptosis of rapidly dividing cancerous cells due to thymine deficiency [90]. Although 5-FU is widely used for melanoma, it causes severe systemic toxicity of gastrointestinal, haematological, neural, cardiac, and dermatological origin [22]. 5-FU is sparingly soluble in water and its bioavailability is greatly limited in the blood, liver and other organs due to rapid metabolism by dihydropyramidine dehydrogenase enzyme. 5-FU has a very short plasma half-life of approximately 8 to 20 min [91]. Complications associated with 5-FU toxicity further limit the effectiveness of the treatment outcome and add detrimental impact on the patient's quality of life. Therefore, an efficient delivery system is vital to improve the bioavailability and safe delivery of 5-FU.

Nanoparticle based treatments have offered promising clinical outcomes due to their tuneable pharmacokinetic properties like prolonged half-life, larger surface to volume ratio, enhanced drug solubility and the likelihood for controlled release [92]. In particular, nanoparticles can be exploited for the targeted delivery of anticancer drugs at the tumor site. Target-specific nanoparticles render a new dimension to the standard conventional chemotherapy. A myriad of biomaterials including lipids, polymers and proteins have been used as matrix for nanoparticle formulations. Amongst these, proteins have garnered a significant interest as biomaterials due to three major advantages. Firstly, proteins are biocompatible and biodegradable in nature [93]. Secondly, drug-binding, imaging or targeting becomes much simpler in case of proteins as it offers numerous functional moieties for modification. Thirdly, due to the existence of charged groups in proteins they can be a better matrix in which drugs can be physically entrapped. There are many proteins *viz.* albumin [94], gelatin [95], transferrin [82] and elastin [96] which have been used as nanocarriers for several drugs. Nanoparticles mediated tumor targeting can be achieved by both active and passive targeting. The passive targeting is achieved by enhanced permeability and retention effect whereas active targeting can be achieved by ligand functionalization.

Lf plays an important role in iron transport along with other physiological functions. Due to its unique antimicrobial, antifungal, anticancer and anti-inflammatory properties, Lf seems to have great potential in clinical sector. There are several reports on using Lf as a targeting ligand by decorating them on nanoparticle surface [62, 97] however our group has utilized Lf as a matrix for nanoparticle preparation. This chapter provides insights into the development of 5-FU loaded Lf nanoparticles and their *in vitro* evaluation in mouse melanoma cells B16F10.

3.2 Result and Discussion

3.2.1 Physico-chemical characterization

Most protein based nanoparticle preparations involve coacervation or precipitation of the protein followed by cross-linking to hold the particles together [95]. The 5-FU-LfNPs were prepared by our previously reported sol-oil protocol [82]. This method does not require any precipitation or cross linking of the protein. The advantage of using Lf protein based nano-formulations, is that the formulation has least number of components and derivatization steps. It involves a biphasic mixture of buffer containing Lf and 5-FU in olive oil in a ratio of 1:20 (v/v). An emulsion is generated by sonication followed by snap freezing.

The oil in the preparation is later removed thorough washing with an organic solvent. The method is rapid and can be completed in less than 6 hours. We have attempted synthesis of particles in the range of 5 to 40 mg of Lf and have obtained reproducible yields and product quality.

The structure and morphology of the nanoparticles as characterized by TEM and SEM suggests that particles are spherical in shape with size in the range of 90-110 nm (**Figure 3.1 A and 3.1B**). The hydrodynamic diameter of the particles, as determined by DLS, was found to be 150 ± 20 nm (**Figure 3.1C**). DLS analysis account solvent shell around the particle, thus measures hydrodynamic radii of particles. Proteins due to their surface hydrophobic and hydrophilic projections facilitate an interactive solvent environment thus the apparent hydrodynamic radii is higher in DLS measurements, which was absent when analyzed in a dry state using TEM or SEM which is also in agreement with other report [44, 83].

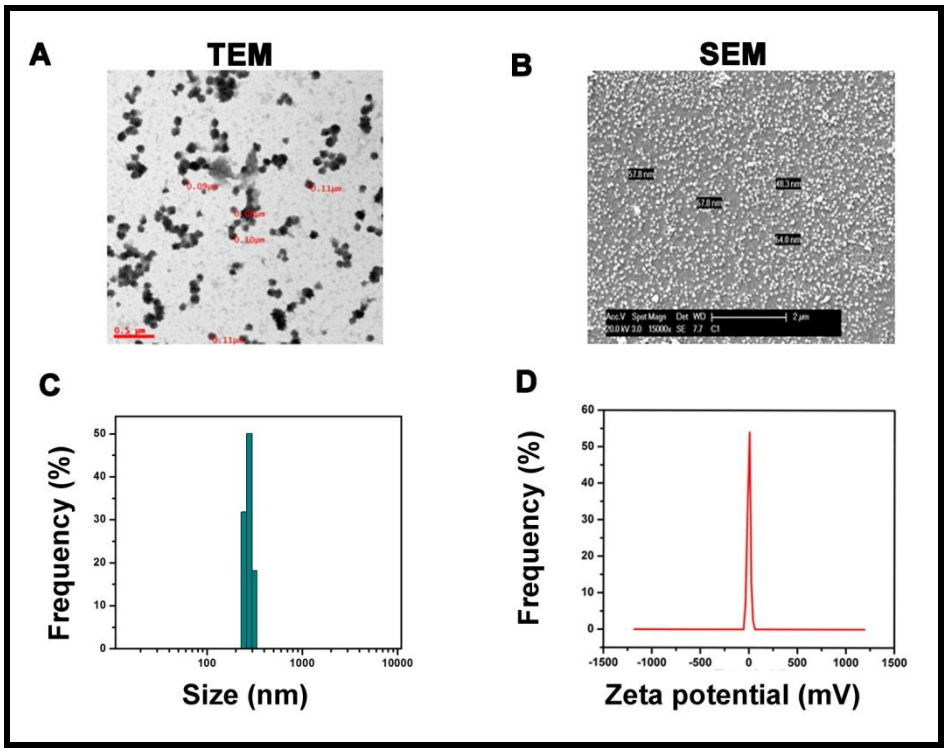

Figure 3.1: Characterization of 5-FU-LfNPs. (**A)** TEM and **(B)** SEM analysis of particles. **(C)** Hydrodynamic diameter and **(D)** Zeta-potential of LfNPs at pH 7.4.

The polydispersity index (PDI) value and zeta potential (**Figure 3.1D**) of the particles were found to be 0.332 ± 0.1 and -2.5 ± 1 mV respectively, an indicative of a narrow size distribution with near neutral surface charge on the nanoparticles suggesting a stable dispersion of nanoparticles in aqueous media. Particles size and surface charge play a

major role in cell uptake. The small size and a near neutral surface charge (ζ potential) of the LfNPs may help in evading their phagocytic uptake by macrophages, thereby prolonging there *in vivo* circulation providing an improved pharmacokinetics of 5-FU [98, 99].

The encapsulation efficiency (EE) of 5-FU in LfNPs was found to be 64 ± 3.60 % with a drug loading content (DLC) of 31.21 ± 2.5 %. The high encapsulation efficiency and DLC, suggest significantly high 5-FU encapsulation in the nanoparticles, which is much higher than the reports available [100]. Such high encapsulation efficiency of 5-FU in LfNPs could be attributed to the strong hydrophobic interactions between Lf and 5-FU. Taken together, the high drug encapsulation efficiency of LfNPs along with an optimum size and surface charge provides an increased advantage under *in vivo* conditions. The LfNPs may thus carry large amounts of drug to the site of action and increases the plasma half-life of 5-FU.

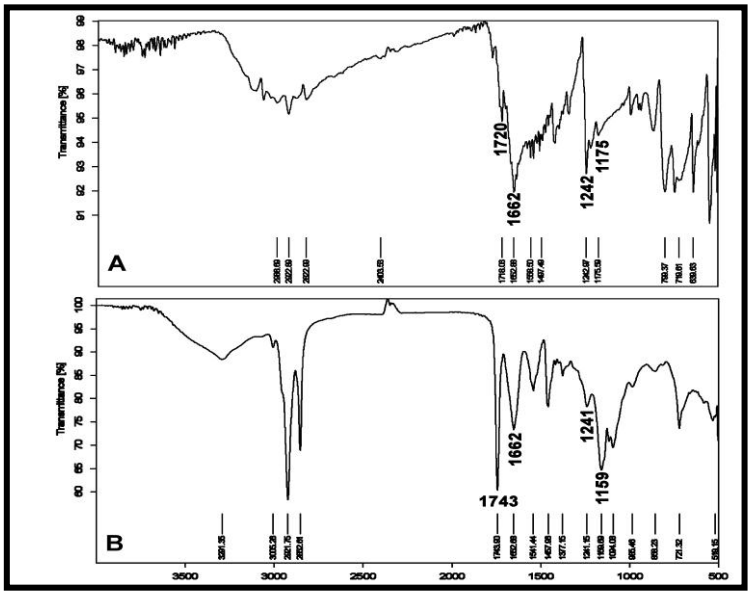

Figure 3.2: FT-IR spectra of **(A)** free 5-FU **(B)** 5-FU-LfNPs. It reveals that 5-FU is physically entrapped/adsorbed in LfNPs.

To confirm the entrapment of 5-FU in the LfNPs, FT-IR was performed. FT-IR spectra of Lf protein reveals characteristic peaks corresponding to the amide bonds *viz.* amide I (1636 cm), amide II (1539 cm), and C-O-C stretch (1069 cm). Almost similar pattern of stretching frequencies for amide I (1662), amide II (1541) and C-O-C stretch (1072) were observed in LfNPs **(Figure 3.2A & 3.2B)**. The characteristic peak positions of free 5-FU in FT-IR for C=O stretch, C-N stretch, C-H in plane and C-O were 1720, 1662, 1242 and 1175 respectively **(Figure 3.3A).** Likewise the characteristic peaks of 5-FU in 5-FU-LfNPs were in 1718, 1662, 1241, and 1159.69 respectively **(Figure 3.3B)**. Spectra of all four components

suggest that there was no loss or major shift in stretching frequency between free 5-FU and 5-FU entrapped in LfNPs. In addition, 5-FU-LfNPs exhibited characteristic peaks of both lactoferrin and 5-FU, suggesting successful encapsulation of 5-FU without any reactivity.

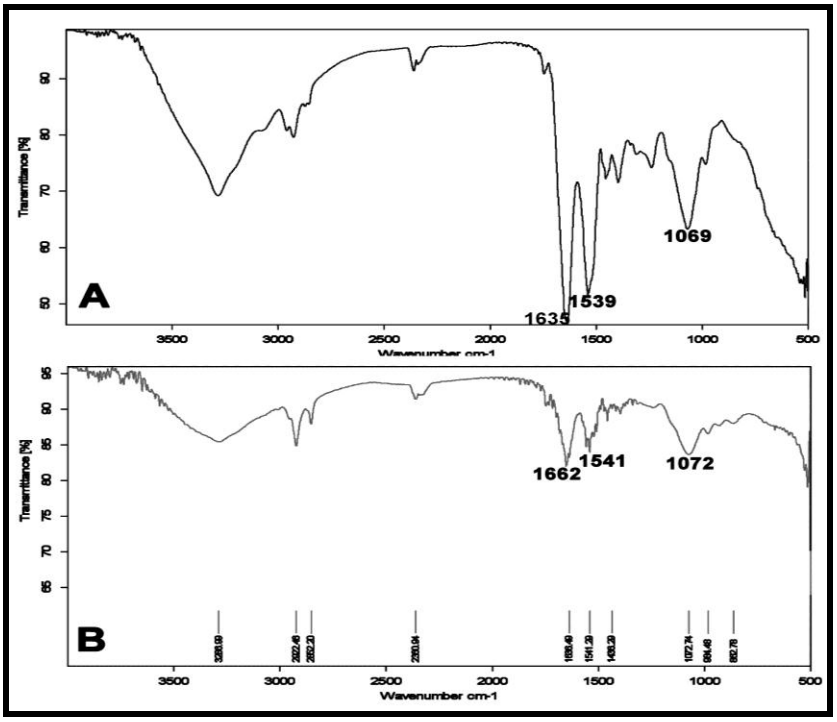

Figure 3.3: FT-IR spectra of **(A)** Lf **(B)** LfNPs. Lf maintain its structural integrity in the nanoparticlulate form as there was no major changes in the stretching frequency

3.2.2 Stability and biocompatibility of Lf nanoparticles

Long shelf-life and vehicle related safety of a carrier is pre-requisite to increase the translational potential of any formulation. Therefore, the storage stability of LfNPs was monitored by measuring their size over a period of 5 weeks. As shown in **(Figure 3.4A)**, the nanoparticles showed no significant size change when stored under refrigerated conditions in PBS (pH 7.4), suggesting the high stability of LfNPs. Further particle size also remained constant when tested in serum conditions **(Figure 3.4B)** suggesting particle stability. The increased particle stability in serum is expected to facilitate in their increased *in vivo* half-life.

Toxicity of the drug carrier is another major criterion in the success of any drug delivery system. Although Lf is a biocompatible protein, it was nevertheless important to assess the toxic effect of Lf nanoparticles on cells. B16F10 cells were treated with varying concentrations of LfNPs and subsequently analysed for cell death by PI uptake through flow cytometry. Flow cytometry (**Figure 3.4C)** data demonstrate that more than 80 % cell

survival even at the highest concentration of particles tested (1 mg ml^{-1}), suggesting minimal carrier related toxicity. The highest concentration used in this study was much higher (10 times) as compared to the particle concentration used for drug delivery studies, affirming the safety of LfNPs as nanocarriers for drug delivery.

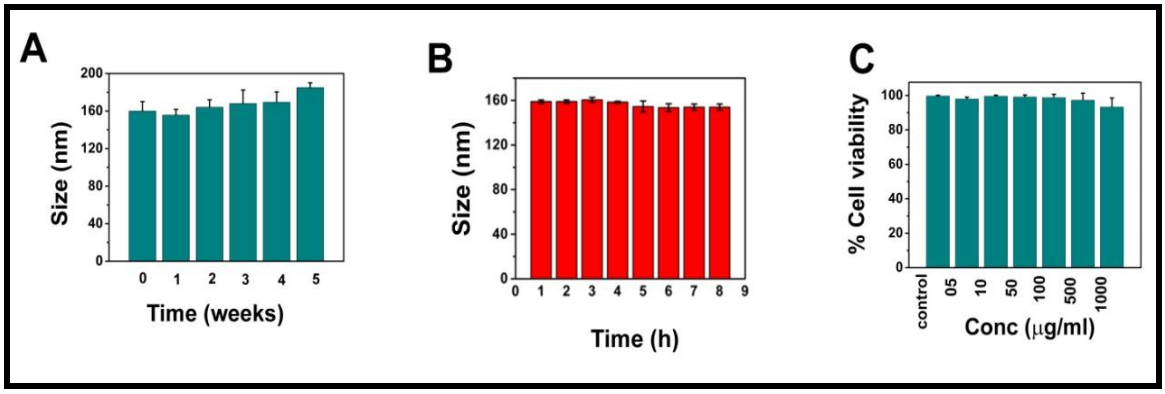

Figure 3.4: Stability and biocompatibity of LfNPs. (A) Size of 5-FU-LfNPs recorded for a period of 5 weeks at 4 ºC in PBS pH 7.4. (B) Size of 5-FU-LfNPs recorded for a several hours at RT in DMEM with 10 % serum. (C) Assessment of biocompatibility of LfNPs. B16F10 cells were treated with LfNPs at the indicated dosage followed by assessing the PI uptake using Flow cytometry 48 h post treatment. Cells treated with PBS were considered as controls having 100% viability. Graph represents data from three independent experiments (n = 3) and presented as mean ± SD.

3.2.3 Receptor mediated endocytosis

The Lf receptors (LfRs) mediated cellular uptake of Lf has been already reported [101]. We therefore carried out a competitive ligand binding assay to confirm the lactoferrin receptor mediated uptake of LfNPs in B16F10 cells. Flow cytometry results (**Figure 3.5A**) suggest a gradual decrease in the uptake of LfNPs (labelled with Rh123) by B16F10 cells with increasing amounts of free Lf. The results were further validated by a spectrophotometric estimation of the intracellular 5-FU concentration delivered through LfNPs in the presence and absence of Lf (**Figure 3.5B**). A significantly reduced uptake of 5-FU when delivered through LfNPs in the presence of free Lf was observed, suggesting a competitive inhibition of LfNP uptake by Lf. Our results corroborate with previous reports of LfR mediated uptake of LfNPs, suggesting that the targeting ability of Lf is preserved even in the nanoparticlulate formulation. However some fraction of LfNP uptake has been observed even after blocking the receptor, this could be due to some alternative pathways of entry.

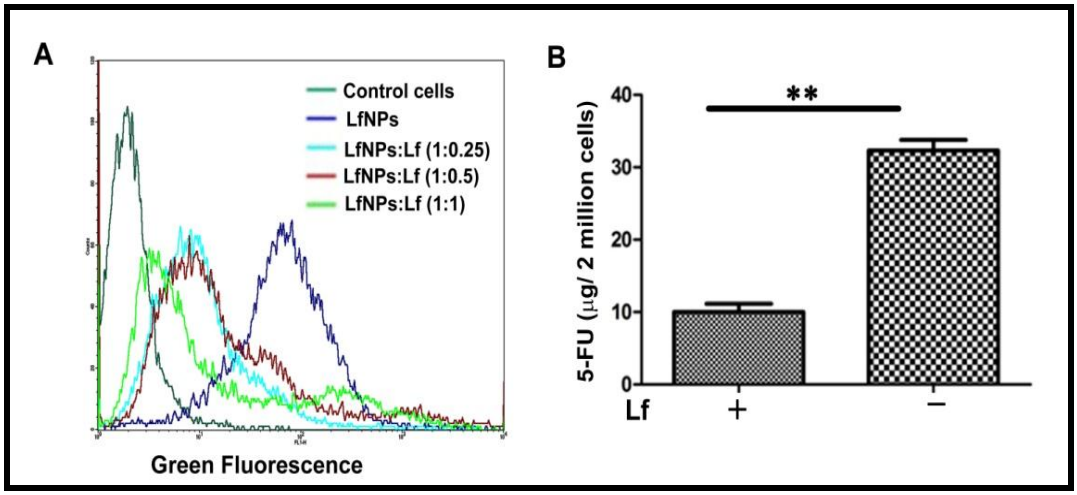

Figure 3.5: (A) Competitive ligand binding assay. B16F10 cells were treated with LfNPs-Rh123 and simultaneously with increasing dosage of free Lf. Cellular uptake of LfNP-Rh123 in presence of free Lf was studied by flow cytometry. **(B)** Quantification of intracellular 5-FU concentration in B16F10 cells treated with 5-FU-LfNPs in the presence and absence of Lf. 5-FU concentration was estimated in cell lysates using spectrophotometry. Graph represents data from three independent experiments (n = 3) and presented as mean ± SD.

3.2.4 5-FU release studies

To understand the release mechanism of 5-FU from 5-FU-LfNPs, a pH-dependent release study was carried out. Interestingly, it was found that approximately 60-80% of the entrapped 5-FU was released at a pH of 5.0 to 6.0 which is similar to endo-lysosomal pH **(Figure 3.6)**. The ability of LfNPs to release 5-FU at a mildly acidic pH as compared to neutral pH may facilitate a triggered release of 5-FU in response to low pH encountered in the tumor environment and inside the endosomes. The low pH release of 5-FU from 5-FU-LfNPs may be attributed to structural changes in the Lf protein molecules constituting the nanoparticles. Earlier studies has been reported, lactoferrin undergoes a structural transition with an increase in α-helical content (by 30 %) and decrease in β-sheet and random coil content (by 12 %) as the pH is lowered from 7.4 to 5 [102]. The pH triggered release of 5-FU may provide an advantage in enhancing the cytotoxic effects of 5-FU by increasing its therapeutic relevant dose specifically at the tumor site.

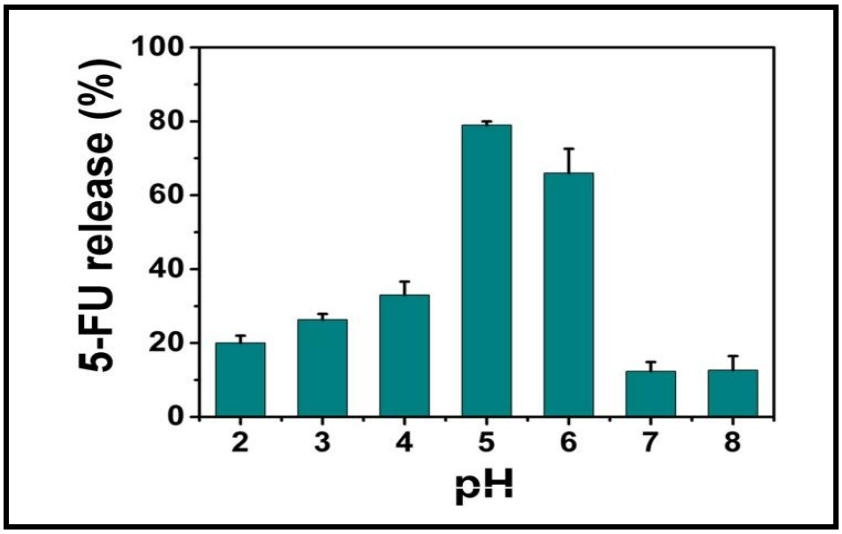

Figure 3.6: Release of 5-FU from LfNPs studied at different pH values. Maximum 5-FU release was observed at pH 5 and 6. Data represent from three independent experiments (n = 3) and presented as mean ± SD.

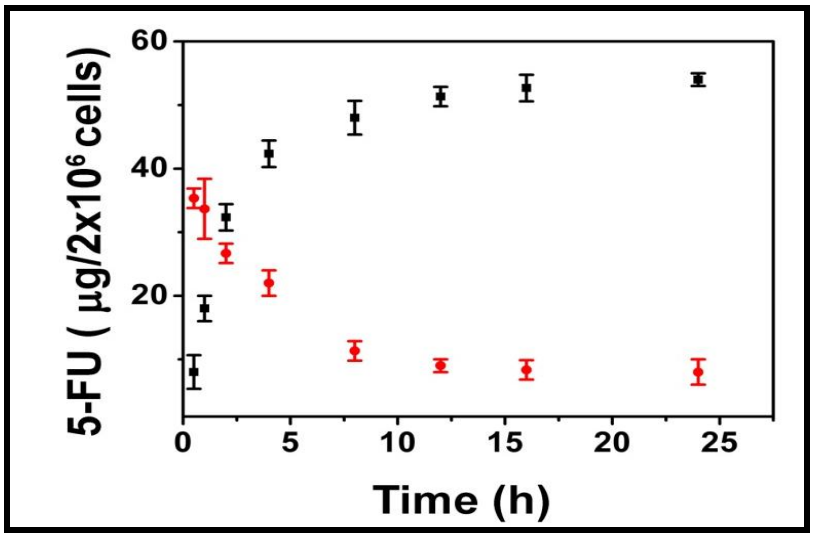

Figure 3.7: Comparative 5-FU uptake and clearance by B16F10 cells when delivered through LfNPs (square) and free 5-FU (circle), quantified using spectrophotometric studies. Graph represents data from three independent experiments (n = 3) and presented as mean ± SD.

3.2.5 Cellular uptake assay by HPLC

The cellular uptake and the comparative intracellular concentration of the 5-FU-LfNPs was carried out using spectrophotometric estimation of 5-FU. Our results (**Figure 3.7**), indicate that the intracellular concentration of free 5-FU was high at 30 min followed with a constant decrease thereafter up to 24 h. However, the intracellular concentration of 5-

FU, delivered through LfNPs, significantly increased from 30 min to 4 h in a linear fashion and remained constant thereafter up to 24 h.

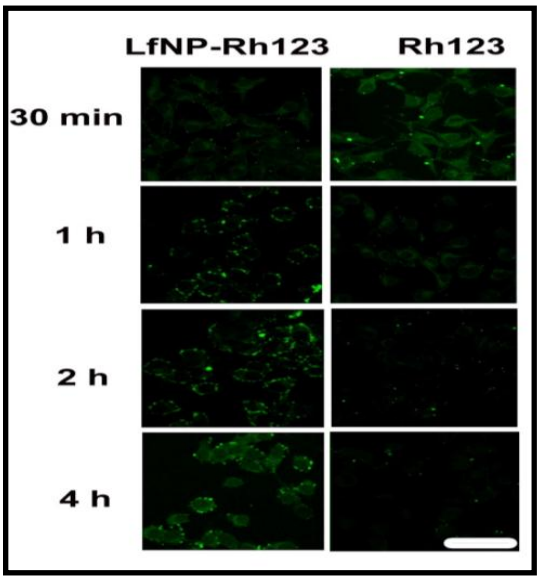

Figure 3.8: Time based cellular uptake of LfNP-Rh123 compared with free Rh-123 in B16F10 cells. Time course experiment shows that nanoparticles are retained for longer time in cells as compared to free Rh-123 that enters cells rapidly but gets cleared within 30 min, scale bar=25μm.

3.2.6 Cellular uptake by confocal microscopy

The prolonged retention of LfNPs was further confirmed by comparative uptake of free Rh123 and LfNP-Rh123 through confocal studies (**Figure 3.8**). It has been observed that although free Rh123 enters cells quickly (within 30 min), they get cleared rapidly (within 1 h). Whereas the uptake of LfNP-Rh123 was found to be low at 30 min but increases gradually with time and was retained up to 4 h. The rapid clearance of free Rh123 could be due to the fact that enters the cells through diffusion mechanism in contrast to the receptor mediated uptake mechanism of LfNPs-Rh123 which is slow at the beginning but retained for longer time.

3.2.7 Enhanced antiproliferative activity of 5-FU-LfNPs

5-FU, the standard drug widely used for melanoma treatment is not effective because of the inability to achieve therapeutic dosage at the target site due to its non-specificity. In addition, associated systemic toxicity greatly limits its therapeutic index which in due course leads to poor prognosis. A delivery system that can enhance the potency of drug by reducing its IC_{50} value would be desirable. The cytotoxic effect of 5-FU-LfNPs was measured using

MTT assay. The results suggest that 5-FU-LfNPs exhibited more cytotoxic effect over all the experimental concentrations (**Figure 3.9**). Also, there was a significant decrease (3-fold) in IC_{50} value of 5-FU-LfNPs (21.5 ± 2.56 μg ml^{-1}) as compared to free 5-FU (59 ± 3.0 μg ml^{-1}). The enhanced cytotoxicity of 5-FU delivered through LfNPs may be attributed to the higher intracellular concentration and prolonged retention of the drug achieved through delivery with LfNPs.

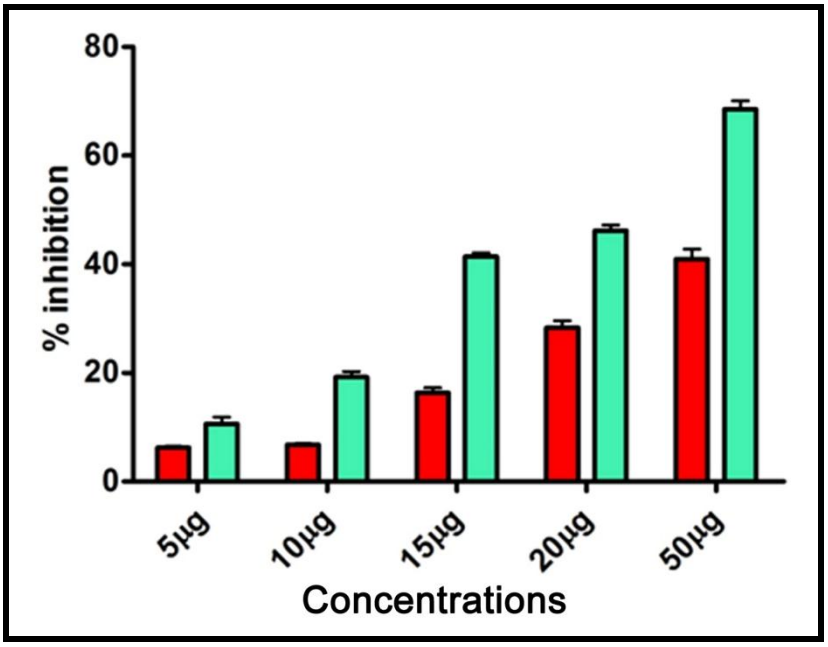

Figure 3.9: Enhanced cytotoxicity of 5-FU-LfNPs. B16F10 cells treated with various equivalent dosage of 5-FU (red) and 5-FU-LfNPs (cyan). Graph show an enhanced cytotoxicity of 5-FU-LfNPs compared to free 5-FU. Graph represents data from three independent experiments (n = 3) and presented as mean ± SD.

3.3 Conclusion

The present work deals with development of a nanoparticle based drug carrier system using lactoferrin protein as a matrix molecule. The LfNPs developed in the study demonstrate a highly efficient delivery of 5-FU to melanoma cells. The 5-FU-LfNPs is featured with high drug loading capacity, modest particle size (150 ± 20 nm) and narrow size distribution. A high 5-FU release at mild acidic pH values, as observed in our studies might be favourable for targeting tumor cells and reducing toxicity to normal cells. Moreover, 5-FU-LfNPs exhibited receptor mediated cellular uptake, prolonged retention and enhanced cytotoxicity in melanoma cells. Thus our results suggest LfNPs might be used as potential delivery vehicles to elevate the anticancer effects of chemotherapeutic drugs such as 5-FU.

Chapter 4

Analysis of TMZ-loaded Lf nanoparticles & their therapeutic efficacy in orthotopic GBM model

4.1 Introduction

Clinical outcome of glioma, the most common malignant brain tumor, is poor [103]. According to a recent study, 64 individuals among every million are reported for glioma every year with an expected mean survival time of 12 months [104]. The inadequate treatment outcomes are mainly due to poor prognosis and lack of an effective treatment after diagnosis. The exact cause(s) of glioma are unknown and several genes have been implicated in its origin [104]. Conventional treatment involves surgical resection followed by radiotherapy and chemotherapy [105]. Originating from astrocytes, a type of glial cells in brain, the tumor infiltrates into other brain tissues as well. The proliferative nature of the tumor and the inaccessibility of brain to a number of small and large molecules are the major reasons for treatment failures and hence recurrence after surgical resection [106].

Temozolomide, a DNA alkylating agent, is the preferred drug for glioma treatment and has been shown to provide clinically meaningful survival benefits in patients. Clinical trials have established a 2 to 5 year increase in median survival of glioma patients treated with a concomitant TMZ and radiotherapy [107]. However, a prolonged therapy leads to TMZ resistance and subsequently poor responsiveness, thus leading to tumor recurrence in 60-75% of patients [107]. In addition, due to low solubility of TMZ in physiological media and a short plasma half life (1.8 h), TMZ therapy requires continuous administration [24]. Though TMZ is well tolerated at the administered dosage, the dose escalation is limited due to its haematological toxicity [25], acute cardiomyopathy [26], oral ulceration, hepatotoxicity [27] and pneumocystis pneumonia [28] which results in discontinuation of the treatment regimen. The severe side effects associated with TMZ therapy thus highlight the need for a delivery vehicle to increase the therapeutic index of TMZ.

Several carriers of TMZ including liposomes, solid lipid nanoparticles, polymeric nanoparticles, etc have been tested for their efficacy, with limited success [26, 27, 108]. The superiority of a delivery vehicle largely depends on its ability to cross BBB and subsequent accumulation at the tumor site. A design approach should thus incorporate two ligands, one for facilitating transcytosis across the BBB and the other targeting over-expressed receptors on tumor cells for preferential accumulation.

Targeting BBB and brain tumor cells using a single ligand is further expected to enhance the therapeutic value in terms of specificity and also in simplifying the design of the nanoparticles. The over-expression of Lf receptors on the surface of glioma is a hall-mark

feature [81]. Moreover, Lf is also known for its BBB crossing ability and therefore has been extensively exploited as a targeting ligand for the delivery of several drugs [109, 62].

This chapter focuses on the development and characterization of TMZ loaded Lf nanoparticles (TMZ-LfNPs) and the subsequent evaluation of its therapeutic efficacy using a combination of *in vitro* and *in vivo* studies. The BBB crossing ability of Lf has been exploited in healthy mice and tumor regression abilities of TMZ-LfNPs were assessed in orthotopic GBM mice model.

4.2 Results and Discussion

4.2.1 Characterization of TMZ-LfNPs

The morphology and size of the TMZ-LfNPs were characterized by Transmission Electron Microscopy (TEM). TEM analysis suggested a spherical shape of the particles with size in the range of 70-90 nm **(Figure 4.1A)**. The hydrodynamic diameter of the particles at pH 7.4, as determined by DLS **(Figure 4.1B)**, was found to be 160 ± 13.3 nm, which is excepted as DLS provides size of hydrated particles, compared to the dry state size obtain by TEM. The polydispersity index (PDI) and zeta potential (**Figure 4.1C**) of the particles were 0.24 ± 0.1 and 2.5 ± 2 mV respectively, suggesting a narrow size distribution and near neutral surface charge of the particles.

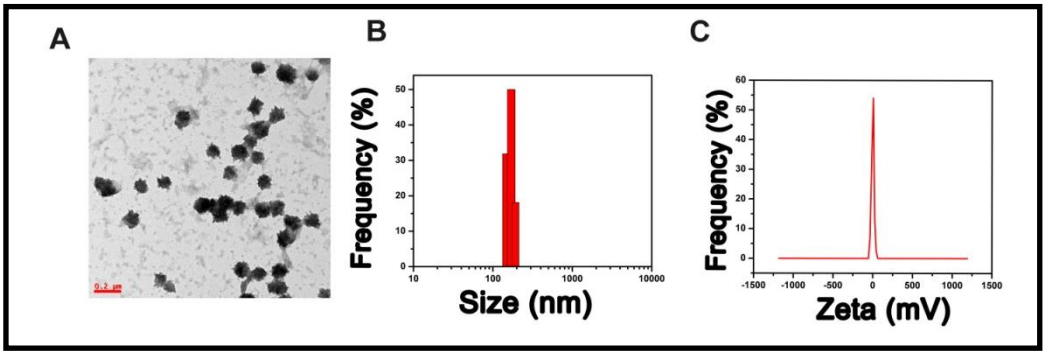

Figure 4.1: Characterization of TMZ-LfNPs. (A) TEM analysis of particles (B) Hydrodynamic diameter and (C) Zeta potential

The encapsulation efficiency (EE) of TMZ in LfNPs was found to be 42 ± 4.9% (n=3) with a drug loading content (DLC) of 17.5 ± 2.5% (n=3). The high EE and DLC achieved in the present study, as compared to the previous reports, [108] [110] [111] is probably due to the partitioning of TMZ in the hydrophobic patches of the Lf particles.

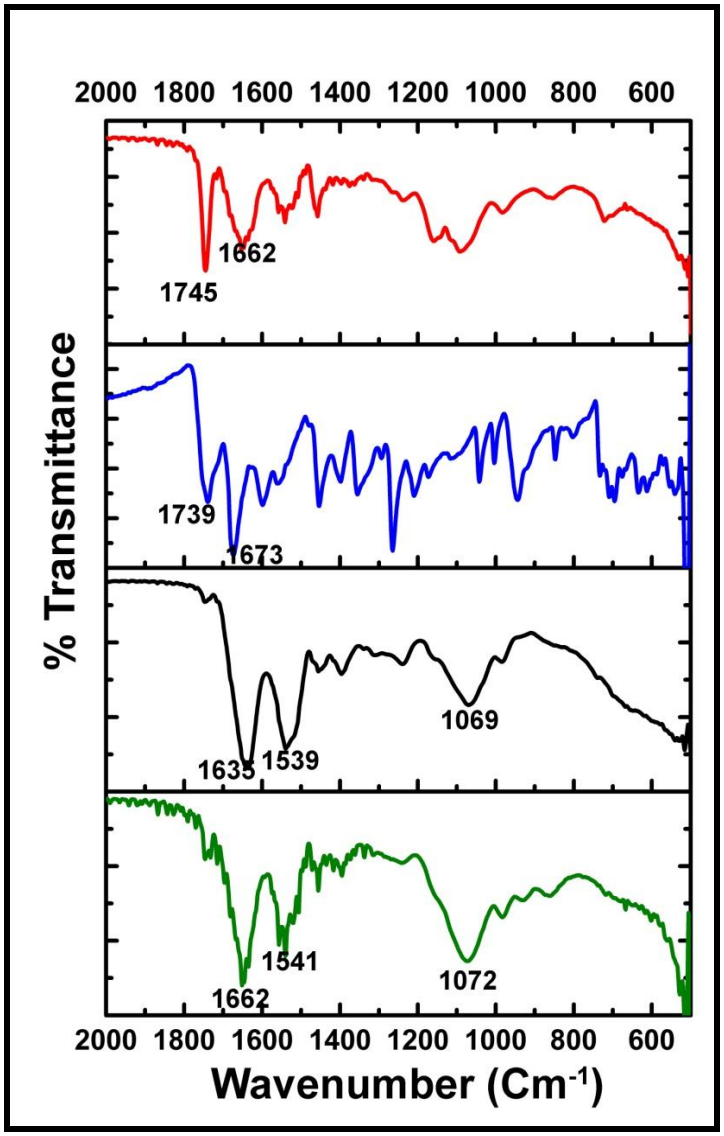

Figure 4.2: FT-IR spectra of TMZ (blue), TMZ-LfNPs (red), Lf (black) and LfNPs (green). It reveals that TMZ is physically entrapped/adsorbed within the TMZ-LfNPs and also stretching frequencies of Lf is intact even in nanoparticulate formulation**.**

The entrapment of TMZ in the LfNPs was confirmed by FT-IR of TMZ-LfNPs. As shown in **Figure 4.2,** characteristic bands of TMZ corresponding to the C=C or C=N stretching vibration frequencies were observed at 1673 cm^{-1} and 1739 cm^{-1}.The presence of similar bands (1662 cm^{-1} and 1745 cm^{-1}) in the FT-IR spectra of TMZ-LfNPs suggested an encapsulation of TMZ. The FT-IR spectra of Lf shows peaks characteristic of amide I (C=O stretch), amide II (C-N coupled with N-H bonding mode), and C-O-C stretching frequency at 1636 cm^{-1}, 1539 cm^{-1} and 1669 cm^{-1} respectively. Almost similar pattern of stretching frequencies (1662, 1541, and 1072 cm^{-1}) were observed for LfNPs, listed in **Table 4.1**. The

similarity in the band frequencies of Lf and LfNPs suggests that no major changes have occurred in Lf after formation of nanoparticle, which would aid in the lactoferrin receptor (LfR) targeting abilities of Lf.

Table 4.1: Major FT-IR peaks observed for Lf, LfNPs, TMZ and TMZ-LfNPs

Functional Groups	Lf	LfNPs	TMZ	TMZ-LfNPs
Amide I (C=O)	1636	1662	-----	-----
Amide II (C-N and N-H bending)	1539	1541	-----	-----
C-O-C	1069	1072	-----	-----
C=C	-----	-----	1673	1662
C=N	-----	-----	1739	1745

In addition to the high encapsulation efficiency, the inhibition of toxic effects of various drugs, in particular poorly water-soluble drugs, is also critically important and significant to achieve optimum therapeutic outcome. Mildly acidic nature of specific intracellular compartments (such as endosomes) and tumor environment has been exploited to trigger the release of drugs from the nanoparticles. To test the ability of LfNPs, to release TMZ in various pH conditions, TMZ-LfNPs were incubated in buffer solutions of various pH values. As shown in **Figure 4.3A**, maximum TMZ release (60-70%) from LfNPs was found in buffers of pH 5.5 and 6.5, which are reported tumor environments. However the release of TMZ from LfNPs at neutral pH 7.4 was minimal (10-20 %). We further monitored the TMZ release kinetics over a period of 72 h. As shown in **Figure 4.3B**, TMZ release from LfNPs at pH 5.5 (black line) followed a biphasic profile with an initial burst (about 60-70%) in the first 10 h, followed by a slow and sustained release till 72 h (15 to 20 %). However, the release of TMZ at pH 7.4 was found to be slow and was sustained over a period of 72 h (red line). The release of drugs at mildly acidic pH by Lf nanoparticles has been earlier reported by our group [45, 46].

4.2.2 Receptor-mediated endocytosis of LfNPs

Lf receptors (LfRs) are known to be over-expressed in a variety of cancer cells. We assessed the expression of LfRs in HepG2 cell lines reported as positive [112] along with GL261 used in this study and A549 used as a negative control.

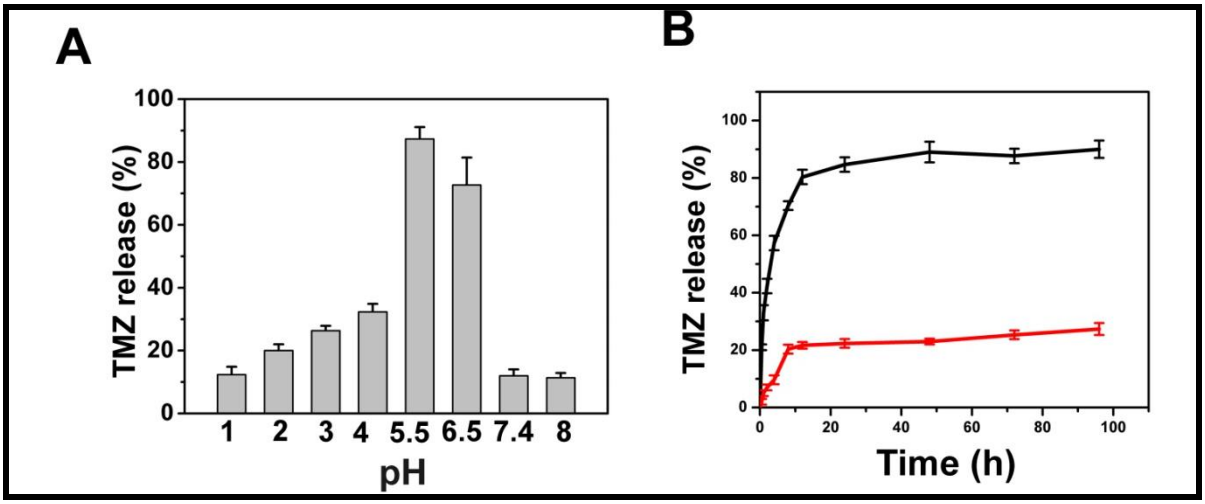

Figure 4.3: (A) Release of TMZ from LfNPs studied at different pH values. Maximum TMZ release was observed at pH 5.5 and 6.5 (B) Cumulative TMZ release from LfNPs at pH 5.5 (black) and pH 7.4 (red). All experiments were repeated independently at least thrice (n = 3), and all values expressed as mean ± SD.

Western blot analysis suggests **(Figure 4.4A**) the expression of LfRs is highest in HepG2 followed by GL261 cells. The expression of LfRs was low and not detected in A549 cells, a cell line previously reported negative for LfR expression [113]. Having ascertained the LfR expression in GL261 cells, the role of LfRs in nanoparticle uptake was validated by a receptor blocking assay using confocal fluorescence microscopy.

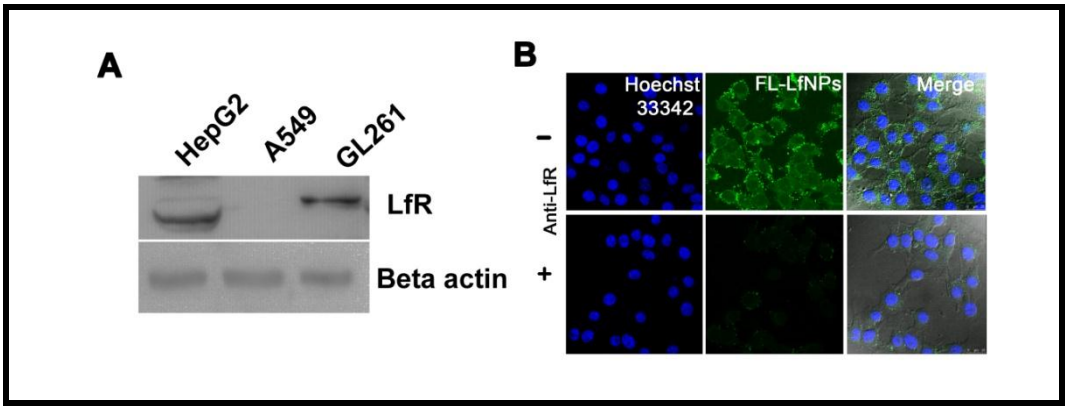

Figure 4.4: Receptor mediated endocytosis of LfNPs. (A) Lf receptor screening in GL261, HepG2 and A549 cells using western blot. (B) Receptor blocking assay. GL261 cells were pre-incubated for 1 h without (B, top panel) and with (B, bottom panel) anti-LfR antibodies and then treated with FL-LfNPs. Scale bar = 25 μm.

As shown in **Figure 4.4B**, particle uptake was found to be higher (top panel) in untreated cells as compared to cells treated with receptor antibody (anti-LfR). The reduced uptake suggests that LfRs play an essential part in the entry of LfNPs in the cells.

Receptor mediated intracellular uptake of LfNPs was further validated by estimating the intracellular TMZ concentration (using HPLC) in GL261 cells after receptor blocking by anti-LfR antibody. As shown in **Figure 4.5A,** receptor blocking also leads to a significantly lesser intracellular TMZ uptake, when presented as TMZ-LfNPs. However, the uptake of free TMZ was found to be independent of the presence of LfR antibody. Since, the cellular uptake of LfNPs is largely dependent on the presence of LfRs, the intracellular TMZ levels achieved through LfNPs was found to be significantly higher (3-folds) as compared to free TMZ. The uptake kinetics further indicate that intracellular TMZ concentration, when the cells were exposed to free TMZ, was found to be high at initial time points (up to1 h), followed with a steep decrease till 24 h **(Figure 4.5B)**. In contrast, the intracellular levels of TMZ obtained, when delivered through LfNPs was found to increase gradually up to 4 h and remained constant (up to 24 h). This difference in the uptake kinetics could be attributed to their different uptake mechanism. While TMZ uptake is largely diffusion based and hence rapid, the uptake of TMZ-LfNPs, as mentioned earlier, is receptor mediated and hence comparatively slow. Moreover, the high TMZ intracellular concentrations maintained for longer duration in the TMZ-LfNPs treated cells could be due to the large carrying capacity of LfNPs and steady release of TMZ from the particles.

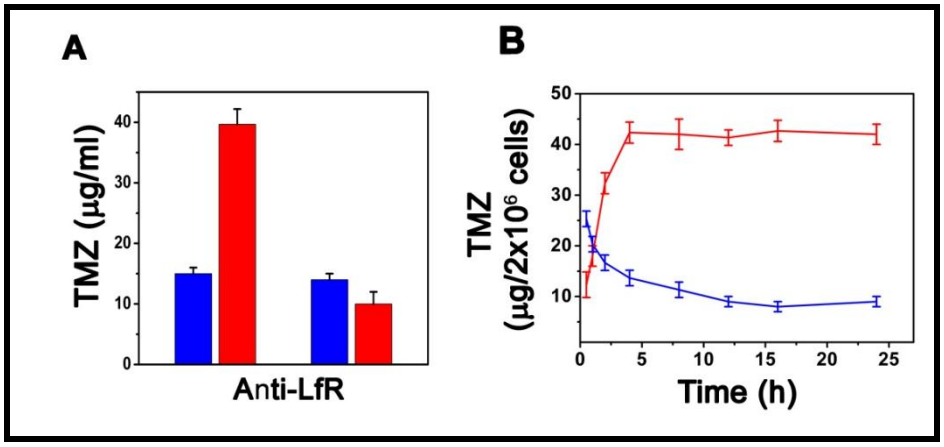

Figure 4.5. (A) Intracellular TMZ concentration, estimated in cell lysates by HPLC, in presence and absence of anti-LfR in GL261 cells. (B) Comparative TMZ uptake and clearance by GL261 cells treated with TMZ-LfNPs (red) and free TMZ (blue), quantified using HPLC. Graph represents data from three independent experiments (n = 3) and presented as mean ± SD.

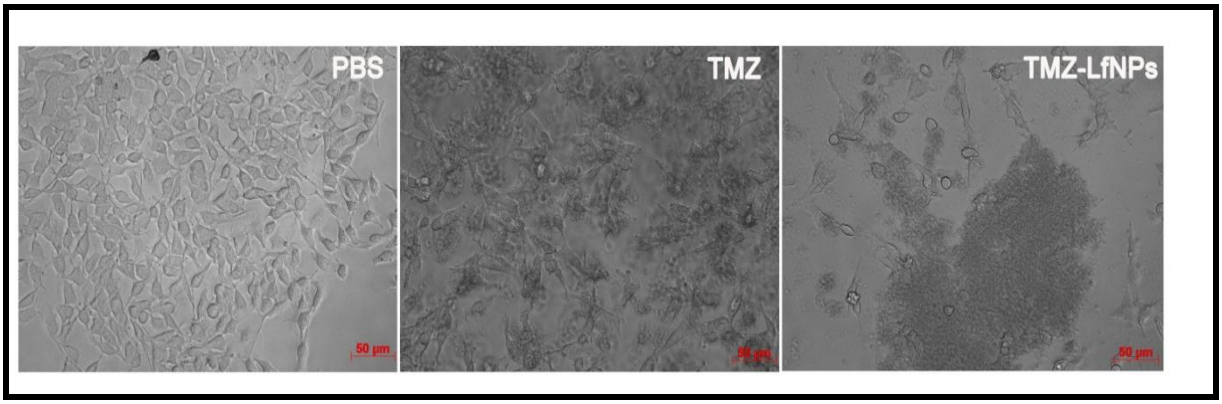

Figure 4.6: Enhanced Cytotoxicity of TMZ-LfNPs. Representative microscopic images of control cells (left), 100 µg/ml-^{1} of TMZ treated (middle) and TMZ-LfNPs (equivalent to free TMZ) treated cells (right).

4.2.3 *In vitro* cytotoxicity of TMZ-LfNPs

To assess the enhanced cytotoxic effect of TMZ-LfNPs, a microscopic examination of GL261 cells treated with free TMZ and equivalent amount of it in TMZ-LfNPs was conducted. Cells treated with TMZ-LfNPs showed significant detachment from the surface, blebbing and round edges as suggested by microscopic images (**Figure 4.6**). Observed cell fragmentation and decrease in number also indicated significantly higher cell death in TMZ-LfNPs treated cells as compared to cells treated with free TMZ.

The enhanced cytotoxic effect of TMZ-LfNPs was further confirmed by cell viability assay. Glioma cells in general exhibits high IC_{50} values (in the millimolar range) for TMZ [114]. The IC_{50} values of TMZ and TMZ-LfNPs in GL261 cells were determined by treating GL261 cells with varying concentrations of the same. As shown in **Figure 4.7**, the IC_{50} of free TMZ and TMZ-LfNPs was found to be 94.3 $\pm$ 2.3 and 9.3 $\pm$ 1.32 µg ml^{-1} respectively. A 10-fold lower IC_{50} value for TMZ-LfNPs as compared to free TMZ was observed. This could be attributed to the enhanced retention and a sustained release of TMZ when delivered through LfNPs.

We further studied the effect of TMZ-LfNPs on proliferation and migration of GL261 cells. In a wound healing-migration assay, a gap in the monolayer of GL261 cells was made and the rate of migration of cells towards the gap was monitored microscopically (**Figure 4.8A**). Upon addition of TMZ-LfNPs and free TMZ, the gap covered by the migrated cells at 8 h and 24 h time points was recorded. As shown in **Figure 4.8B**, the number of cells migrating towards the gap in untreated cells at the 8 h time point was higher as compared to that of TMZ treated samples. However, the migration in TMZ-LfNPs

treated cells was significantly lower than free TMZ treated samples. The treatment effect was more evident at 24 h time point. In control cells the gap was covered by cells completely; while in TMZ treated cells about 70% of gap was covered.

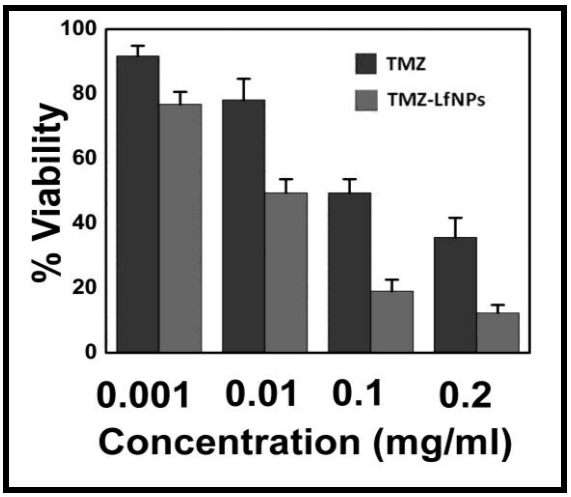

Figure 4.7: GL261 cells treated with different concentrations of TMZ and equivalent dosage of the drug in TMZ-LfNPs. Figure show a reduced IC_{50} for TMZ-LfNPs as compared to free TMZ for GL261 cell line.

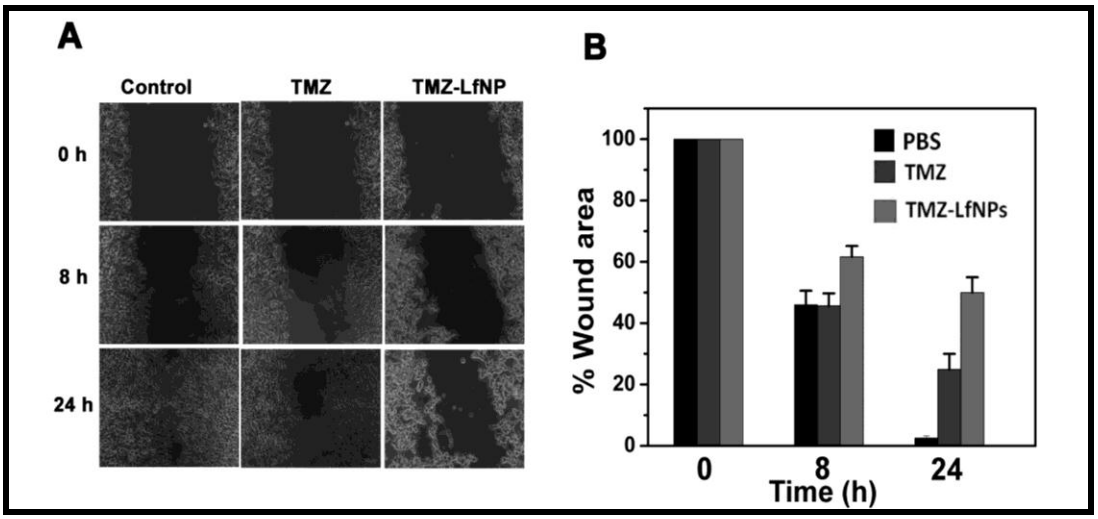

Figure 4.8: (A) Representative images of wound in control (left), TMZ (middle) and TMZ-LfNPs (right) treated Gl261 cells at different time points (0, 8, and 24 h). Images depict the inability of cells treated with TMZ-LfNPs to migrate and invade the wound area as compared to free TMZ and control. (B) Quantitative plots of the wound area at different time points when treated with free TMZ and TMZ-LfNPs. Graph represents data from three independent experiments (n = 3) and presented as mean + SD.

However, the gap was covered by only 50% in TMZ-LfNPs treated cells. Our results suggest that apart from inducing cell death, both TMZ and TMZ-LfNPs markedly reduce proliferation and migration of GL261 cells, with the effect being most pronounced in cells treated with TMZ-LfNPs.

4.2.4 Blood-brain barrier crossing capability of LfNPs in normal mice

Receptor-mediated transcytosis of Lf across BBB has been established [115]. To assess the transcytosis abilities of particulate Lf (LfNPs), healthy C57BL/6 mice were injected with equivalent amount of free Lf and LfNPs via tail vein injection. 24 h after injection, animals were euthanized and the amount of Lf protein was estimated in the brain tissue lysate as described in the methods section. Immunoblotting analysis showed higher band intensity in LfNPs treated animals compared to free Lf treated animals **(Figure 4.9A).**

The higher brain accumulation of LfNPs could be attributed to the decreased plasma clearance of LfNPs as compared to free Lf. To obtain a cytological evidence for the presence of LfNPs in the brain, animals injected with LfNPs and PBS (negative control) were processed for immuno-histochemistry. Mice were euthanized 24 h post-delivery of the particles and all the major organs, including brain were dissected, sectioned, probed with Lf antibodies and visualized under confocal microscope as described in the methods. Fluorescence signals (Alexa^{488}) corresponding to LfNPs was observed in the brain cortex compared to PBS controls (**Figure 4.9B)**.

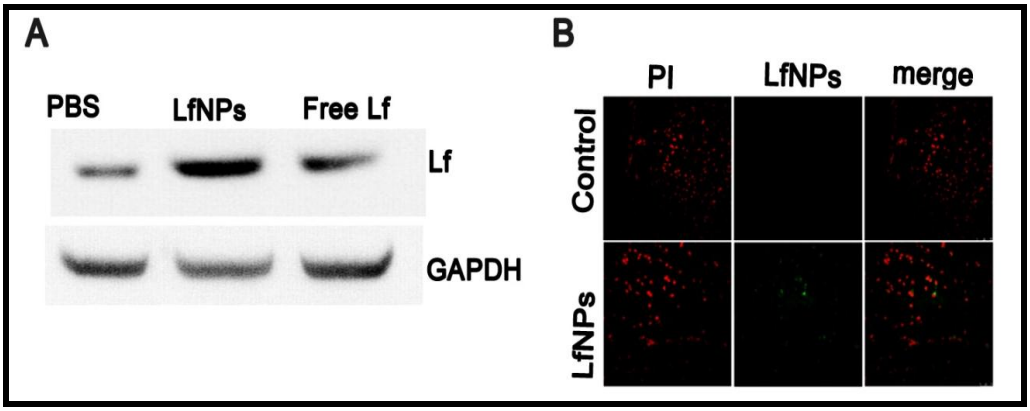

Figure 4.9: Localization of LfNPs in brain. (A) Comparative uptake of free Lf and LfNPs in brain. Representative immunoblots of brain lysates of PBS, Lf and LfNPs treated mice probed with anti-Lf antibody (n=3 mice for each group). GAPDH is used as protein loading control. (B) Immuno-histochemistry images of brain tissues of control and LfNPs treated animals probed with anti-Lf antibody using secondary antibody tagged with Alexa Fluor ^{488} (green) and counter stained with PI (red).

To further validate the ability of LfNPs to cross BBB, animals injected with FL-LfNPs were sacrificed 24 h after injection and the sections were probed with CD31 antibody (secondary antibody labelled with cy3), a marker for endothelial brain capillaries. Tile scan on the brain section was performed to substantiate the localization of CD31 and FL-LfNPs. Scans show distinctly visible fluorescence corresponding to FL-LfNPs in the cerebral cortex above the hippocampus region (**Figure 4.10A,** inset in the merged image was zoomed for clarity), clearly indicating transcytosis of LfNPs across the BBB. Non-specific fluorescence in the brain sections was eliminated by $NaBH_4$ and $CuSO_4$ treatment of tissue sections as described in the methods. A lack of fluorescence in the lung, kidney and spleen (**Figure 4.10B**) indicate that the LfNPs do not accumulate in these tissues.

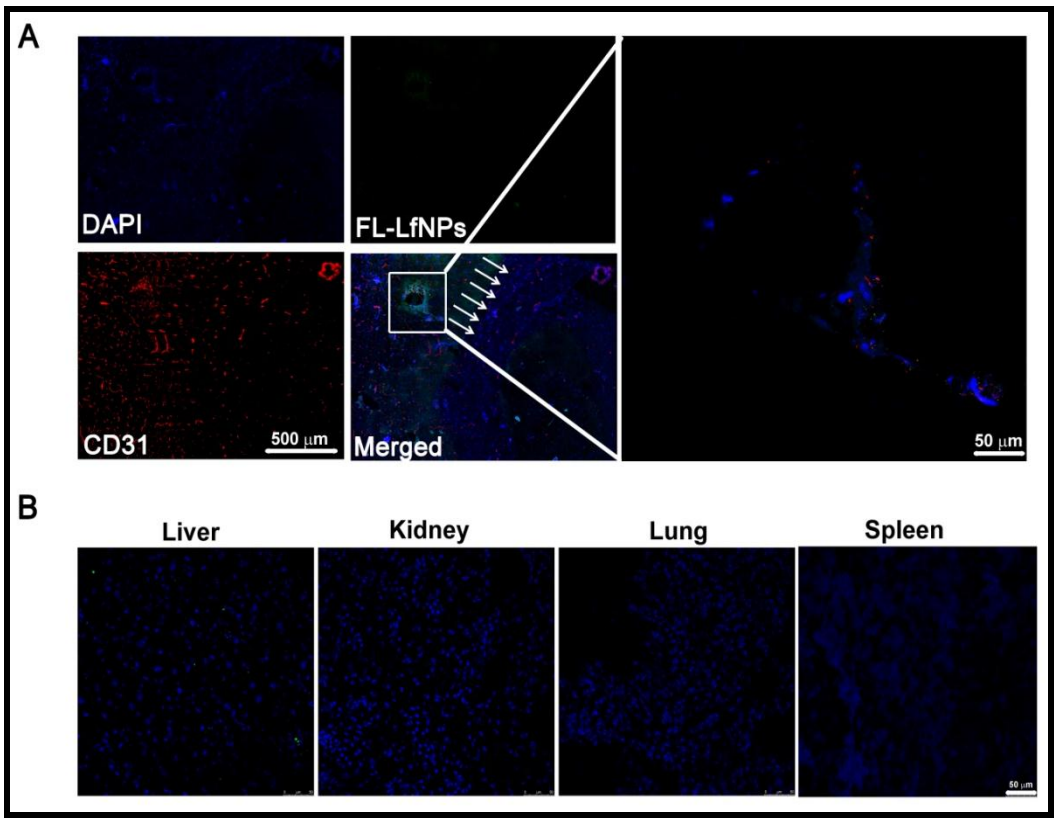

Figure 4.10: (A) Partial projection of a representative tile scan of the mouse brain depicts strong fluorescence corresponding to FL-LfNPs in the brain cortex (inset) above the hippocampus (white arrows). The brain slice (8μm thickness) was imaged using confocal microscopy with 40X objective. The image in the inset depict the zoomed scan of the boxed where fluorescence of FL-LfNPs (green) and brain micro vessels stained with anti-CD31 using secondary antibody tagged with Cy3 (red) was visualized. Scale bar = 500 μm and 50 μm (inset). (B) Organ bio-distribution of FL-LfNPs. Representative confocal images depicts fluorescence in the liver unlike lung, kidney and spleen.

Fluorescence observed in liver tissue sections indicates the accumulation of particles due to expression of Lf receptor and also being the first pass organ for the particles.

4.2.5 Pharmacokinetic studies of TMZ-LfNPs

Pharmacokinetic studies of free TMZ and TMZ-LfNPs were carried out by administering these as a single equivalent dose of TMZ (10 mg kg^{-1} body weight) into healthy C57BL/6 mice intravenously (IV bolus). 200 µl of blood was collected by retro-orbital plexus at indicated time points (0.083, 0.25, 0.5,1, 2, 4, 8 and 24 h) post injection and brain was collected after 24 h. As shown in **Figure 4.11A**, the blood clearance of free TMZ and TMZ-LfNPs followed biexponential kinetics. Free TMZ was cleared rapidly from the blood with a plasma concentration of only 0.21% ID ml^{-1} at 15 min.

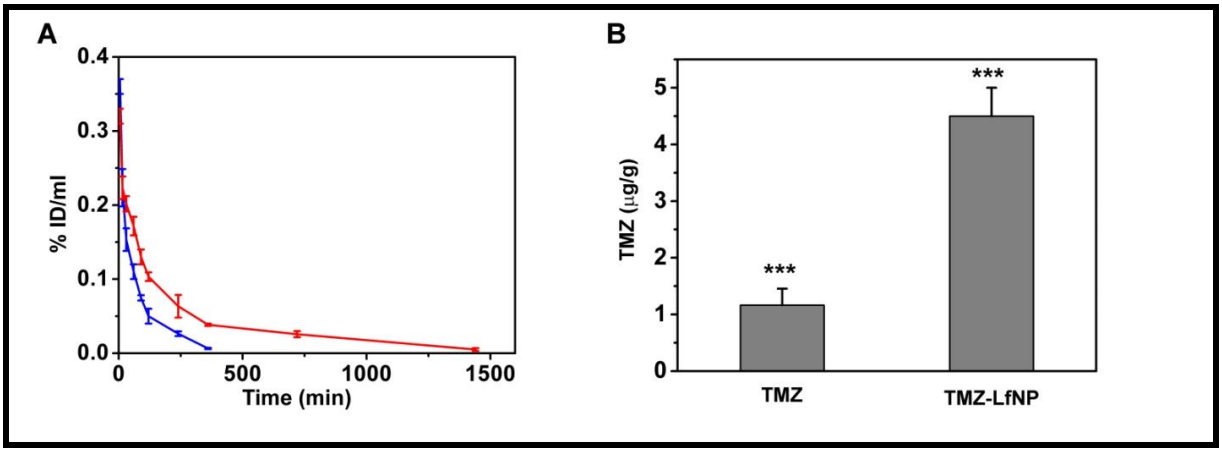

Figure 4.11: (A) Pharmacokinetic studies. % ID/mL of plasma TMZ is plotted versus time after i.v. injection of free TMZ (blue) and TMZ-LfNPs (red) with an equivalent dose of 10 mg kg^{-1} of TMZ in C57BL/6 mice. (B) Brain uptake of TMZ in healthy mice 24 h post intravenous injection of TMZ and TMZ-LfNPs with an equivalent dose (10 mg kg^{-1}) show a higher accumulation of TMZ when delivered through LfNPs as compared to free TMZ. Data represent mean ± SD (n = 3 mice), ***P < 0.001.

On the contrary, the plasma TMZ concentration in TMZ-LfNPs treated animals remained high for a longer period of time. Even at 24 h after administration, the plasma concentration for TMZ-LfNPs was 0.02% ID ml^{-1}. However, the free TMZ was completely eliminated from the plasma and could not be detected. The plasma concentrations of TMZ when delivered in free form and through LfNPs, as obtained from HPLC analysis, were analysed using Kinetica 5 software and the pharmacokinetic parameters are listed in **Table 4.2**. Our results show that the plasma clearance (CI) rate of TMZ significantly decreased from 0.04 ± 0.001 to 0.01 ± 0.03 (ug)/(µg ml^{-1})/min when injected as free TMZ as

compared to TMZ-LfNPs respectively. Also there is significant increase in plasma half-life ($T_{1/2}$) by 5-fold, area under the curve (AUC) by 2-fold, and Mean Residence Time (MRT) by 4-fold as compared to free TMZ. Further TMZ uptake in brain after 24 h **(Figure 4.11B)** suggests that targeting efficiency of TMZ-LfNPs was significantly higher (3-fold) than free TMZ. Our data suggests that TMZ exhibits an improved pharmacokinetic profile and increased brain targeting ability when delivered through nanoparticles. This is in corroboration with our earlier studies which also showed improved PK profile of other drugs delivered through Lf nanoparticles [47].

Table 4.2: The comparative plasma pharmacokinetic parameters after intravenous injection of free TMZ and TMZ-LfNPs with an equivalent TMZ dose of 10 mg kg^{-1} in mice (n=3).

Parameters	TMZ	TMZ-LfNPs
$T_{1/2}$ (min)	68 ± 2.13	360 ± 70.86
MRT (min)	88 ± 7.4	367 ± 18.33
AUC (min)*(µg ml^{-1})	4639.66 ± 109.24	10998 ± 754

AUC-The area under curve, $T_{1/2}$ - elimination half-life of drug, MRT- mean residence time of drug in the plasma.

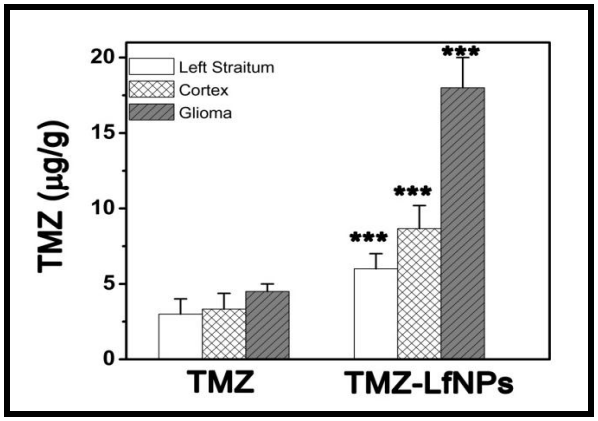

Figure 4.12: Brain uptake of TMZ in glioma bearing mice after intravenous injection of TMZ and TMZ-LfNPs with an equivalent dose (5 mg kg^{-1}) show a higher accumulation of TMZ when delivered through LfNPs especially in the glioma region (right striatum) as compared to free TMZ. Data represent mean ± SD (n = 3 mice), ***P < 0.001.

4.2.6 TMZ-LfNPs bio-distribution in GBM mice model

Having confirmed the passage of LfNPs across BBB and the ability to deliver higher dosage of TMZ into the brain as compared to free TMZ in normal mice, we studied the tumor targeting ability of TMZ-LfNPs in glioma bearing mice. Intracranial glioma model was generated using GL261 cell. The GL261 cells, although from murine origin, closely mimic human gliomas in a number of significant ways, especially in its invasive and angiogenic properties, thereby representing the relevant biology of human gliomas.

The brain distribution of TMZ, estimated by HPLC (**Figure 4.12)** suggests a 3-fold higher accumulation in TMZ-LfNPs treated animals compared to free TMZ-treated animals. TMZ uptake was highest especially in the glioma region (right striatum) among other brain areas (cortex and left striatum) in TMZ-LfNPs treated animals.

4.2.7 Tumor regression studies in glioma mice model

To study the improved anti-tumor effect of TMZ-LfNPs over free TMZ, glioma mice models were generated by intracranial injection of GL261 cells as described in methods. Preliminary findings showed an aggressive tumor growth and all the untreated mice died after two weeks. Based on this observation mice were randomly divided into three treatment groups (n=4 mice) and injected with PBS, free TMZ and TMZ-LfNPs with an equivalent TMZ dose of 5 mg kg^{-1} body weight (X 4 dosage) starting from day 3 after tumor implantation up to 9^{th} day, alternately as shown in **Figure 4.13.** On 14^{th} day when all the PBS treated mice died, other groups were also sacrificed and brain tissues were extracted and processed for histology and other molecular analysis.

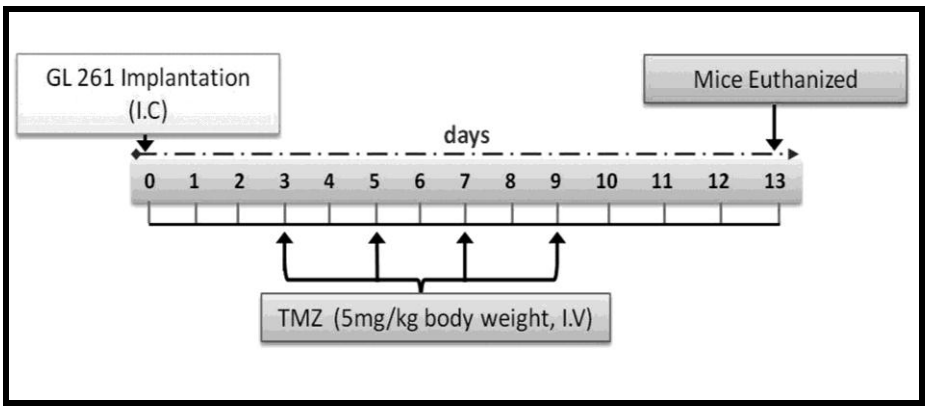

Figure 4.13: Treatment schedule. Mice were given 4 dosage of TMZ intravenously on alternate days.

Glioma development was confirmed by the cancerous growth profile in the brain histology sections. As evident from **Figure 4.14A, i-iv**, PBS treated mice show huge tumor burden, infiltrating tumor cells surrounded by large necrotic areas and numerous atypical cells. Glioma bearing mice treated with free TMZ showed preventive infiltration of tumor and caused moderate shrinkage of the tumor relative to PBS treated mice **(Figure 4.14B, i-iv).** However, the tumor burden was found to be negligible when treated with TMZ-LfNPs as illustrated in the whole brain microphotograph **(Figure 4.14C, i-iv)**. This was further supported by replacement of glioma cells by normal brain parenchyma cells.

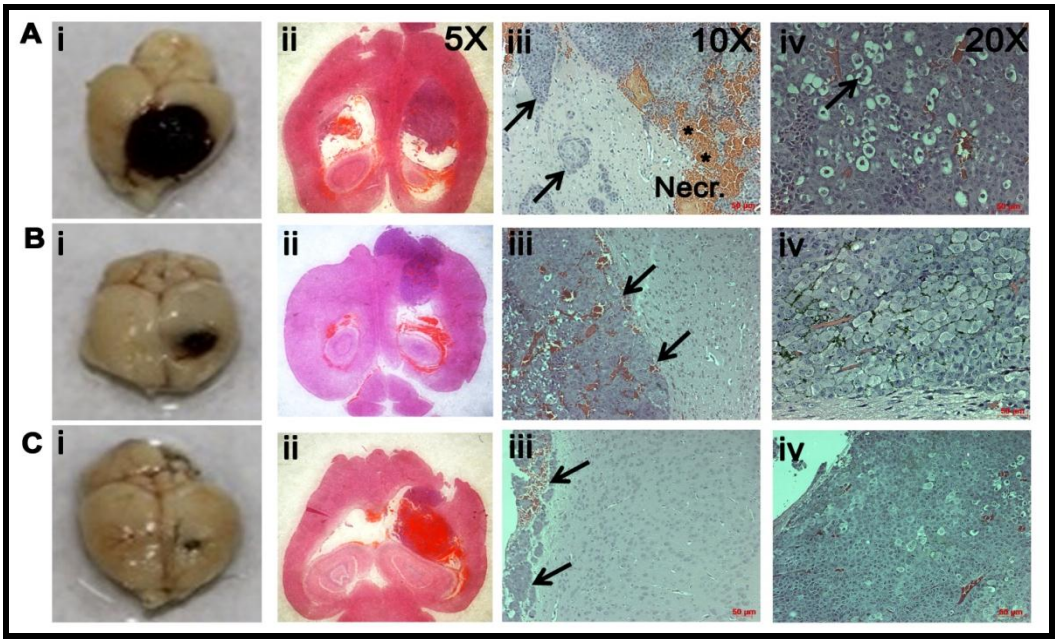

Figure 4.14: (A, i-iv) Photomicrographs of brain dissected from PBS treated glioma bearing mice, show huge necrotic area which was reduced when treated with TMZ and TMZ-LfNPs with the effect most pronounced in TMZ-LfNP. (B, i-iv) TMZ treated mice show, relatively reduced tumor burden compared to control. (C, i-iv) TMZ-LfNPs treated tumor shows negligible tumor burden as compared to TMZ treated mice and well-delineated tumor/brain interface (arrows) representing reduced tumor area restricted to the boundaries without any invasion into the surrounding tissue and tumor cells were replaced by monomorphic brain parenchyma cells.

The tumor volume and tumor area was estimated as described in methods and were plotted for different treatment groups. Our results **(Figure 4.15A and 4.15B)** show a

significant decrease in tumor volume and area in TMZ-LfNPs treated mice as compared to mice treated with free TMZ.

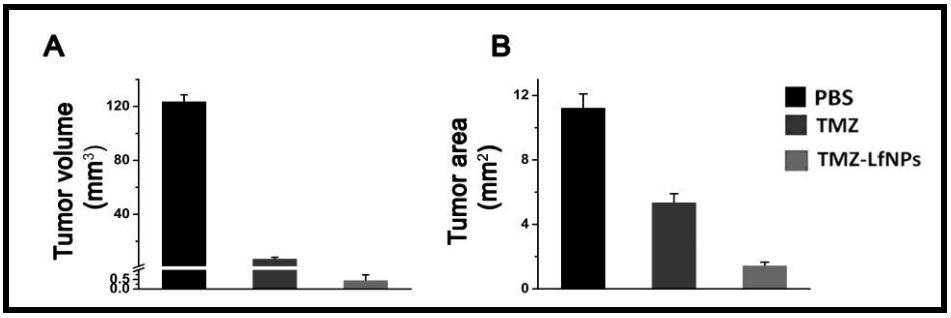

Figure 4.15: (A) Tumor volume from the whole brain was quantified as described in methods in the three different groups. (B) Tumor area quantified by image J analysis in histological sections in three treatment groups**.**

The primary mechanism of TMZ induced cell death is through apoptosis. TMZ methylates the O-6 residue in guanine bases of DNA, which may lead to cell cycle arrest at G2/M phase resulting in apoptosis [116]. The PI/annexin V-FITC based apoptotic quantification of tumor brain was carried out using flow cytometry. As shown in **Figure 4.16A**, the percentage of apoptotic cells was found to be significantly higher in TMZ-LfNPs treated mice as compared to those treated with free TMZ.

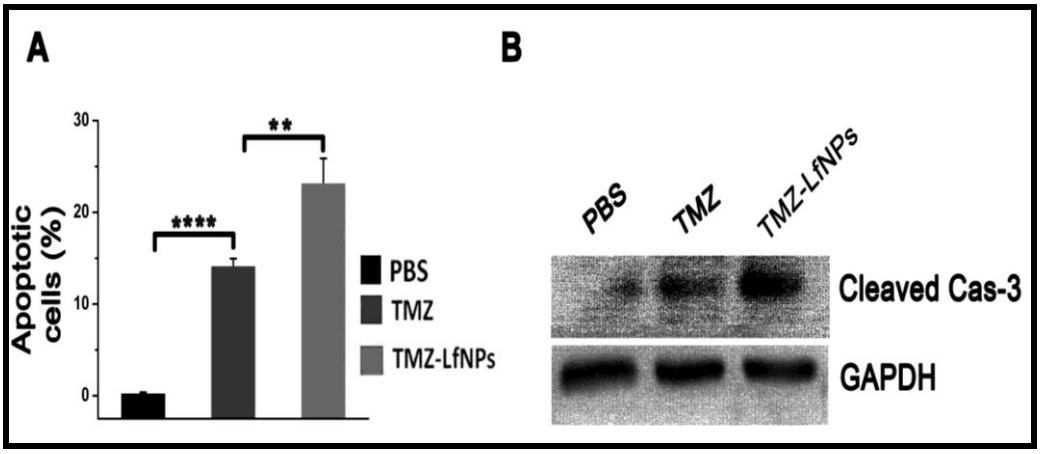

Figure 4.16: (A) Quantification of the percentages of Annexin V positive cells in the tumor tissue using flow cytometry, in different groups. The percentages of Annexin V positive cells (apoptotic response) represented in mean ± SD, n = 3. **P ≤ 0.01, ***P ≤ 0.001, ****P ≤ 0.0001. (B) Western blots of cleaved Cas-3 in representative brain tumor lysates. GAPDH is used as protein loading control. (n=3)

Further, the enhanced apoptotic activity of TMZ was analysed through Caspase-3 activation using western blot. Activation of Cas-3 was shown by higher intensity bands of cleaved cas-3 in the TMZ-LfNP treated mice as compared to free TMZ treated mice **(Figure 4.16B)**. These observations put together suggest that TMZ-LfNPs markedly enhance the anti-tumor ability of TMZ by its targeted localization in glioma.

In order to assess the effect of improved anti-tumor effect of TMZ on survival of glioma bearing mice, the difference in survival time between free TMZ and TMZ-LfNPs was recorded and analysed. Life-span extension curve obtained from glioma bearing mice treated with multiple dosage of TMZ and TMZ-LfNPs (equivalent dose of 5 mg kg^{-1}) on day 3, 5, 7, and 9 after GL261 implantation is shown in **Figure 4.17**. The median survival time of PBS treated (black curve) mice was 10 days as compared to 18 days when treated with TMZ (blue curve). However, the increase in median survival was found to be highest in the mice treated with TMZ-LfNPs (25 days, red curve). The increase in survival time (IST) of the group treated with TMZ-LfNPs was 2.5 times more as compared to PBS treated and 1.4 times more than free TMZ treated group. Our results indicate that the improved anti-tumor activity of TMZ-LfNPs leads to a significant enhancement in survival time of glioma bearing mice.

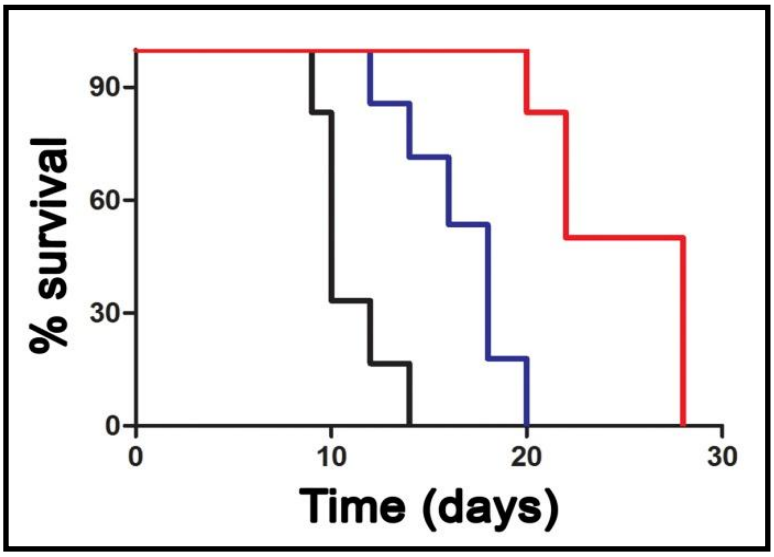

Figure 4.17: Kaplan Meier survival curve; comparison of the survival-promoting effects of PBS (black curve), TMZ (blue curve) and TMZ-LfNPs (red curve) treatment in glioma bearing mice (n=6).

Dose related haematological and organ toxicity is a major concern in TMZ chemotherapy. Previous studies have suggested a TMZ dose ranging from 5 - 75 mg/m^2/day

for tumor regression in glioma model [117]. A desirable host response of chemotherapy depends on the balance between anti-tumor efficacy and safety. While a sub therapeutic dose (15 mg/m^2/day) gives rises to inadequate clinical outcomes, a high dose regimen (75 mg/m^2/day) leads to systemic toxicity and discontinuation of treatment [27]. In the present study, we found that the glioma bearing mice, after treatment with free TMZ, show a significant reduction in the number of leukocytes, lymphocytes and platelets as compared to the mice treated with TMZ-LfNPs. These parameters in case of TMZ-LfNPs treated mice were found to be similar to untreated controls. The liver and kidney toxicity caused by TMZ *vs.* TMZ-LfNPs was also tested by monitoring the levels of SGOT, SGPT, creatinine and blood urea nitrogen. Our results as summarized in **Table 4.3**, suggest that the toxicity of TMZ is high in heart, liver and kidney which however is reduced substantially when administered through LfNPs.

Table 4.3: Effect of TMZ and TMZ-LfNPs treatment on haematological and biochemical parameters in mice

Parameters	Untreated	TMZ	TMZ-LfNPs
Blood Count			
Leukocytes (x10^9/L)	8.27 ± 0.86	6.23 ± 0.36 (L)	8.98 ± 0.62
Lymphocyte (%)	47.5 ± 1.25	40 ± 0.45 (L)	68 ± 3.60
Thrombocytes (x10^9/L)	982.00 ± 41.00	600 ± 25.00 (L)	1044.67 ± 32.13
Blood Chemistry			
ALP (U/L)	100 ± 6.42	70.40 ± 9.34 (L)	93.80 ± 13.46
ALT (U/L)	39 ± 4.36	63.20 ± 3.62 (H)	33.40 ± 1.86
AST (U/L)	197 ± 46.50	300 ± 46.07 (H)	98.20 ± 25.85
BUN (mg dL^{-1})	17 ± 2.00	21.20 ± 0.73 (H)	17.60 ± 1.03
Creatinine (mg dL^{-1})	0.15 ± 0.05	0.13 ± 0.10	0.12 ± 0.02
LDH (U/L)	75 ± 0.45	180 ± 0.23 (H)	82 ± 2.33

ALT: alanine transaminase, AST: aspartate aminotransferase, ALP: alkaline phosphatase, LDH: lactose dehydrogenase, BUN: blood urea nitrogen. (L): lower, (H): higher represent more than 25% change from the untreated base line. Values are reported as mean ± SD for 3 mice in each group.

4.3 Conclusion

Prepared from natural and abundant protein with no modifications, Lf nanoparticles were shown to be a safe carrier of drugs. The reproducible and scalable preparation method and excellent entrapment efficiency of TMZ by Lf particles is attractive. LfR specific uptake and subsequent toxicity on GL261 cells and significant reduction in tumor burden in orthotopic glioma model substantiates the utility of this formulations in glioma treatment. LfNPs, being of particular interest, due to their ability to cross the BBB and target glioma efficiently. LfNPs are safe and with targeting abilities, has potential to be an efficient carrier of TMZ for glioma treatment. The pictorial representation of ability of TMZ-LfNPs to cross BBB and target glioma is demonstrated in **Figure 4.18**. The limited access of TMZ through BBB restricts the clinical outcome of the therapy, however when TMZ is delivered via Lf nanoparticles, can efficiently cross BBB by LfR mediated transcytosis. Furthermore, the tumor targeting abilities of TMZ-LfNPs show improved median survival in orthotopic GBM mice model as depicted below.

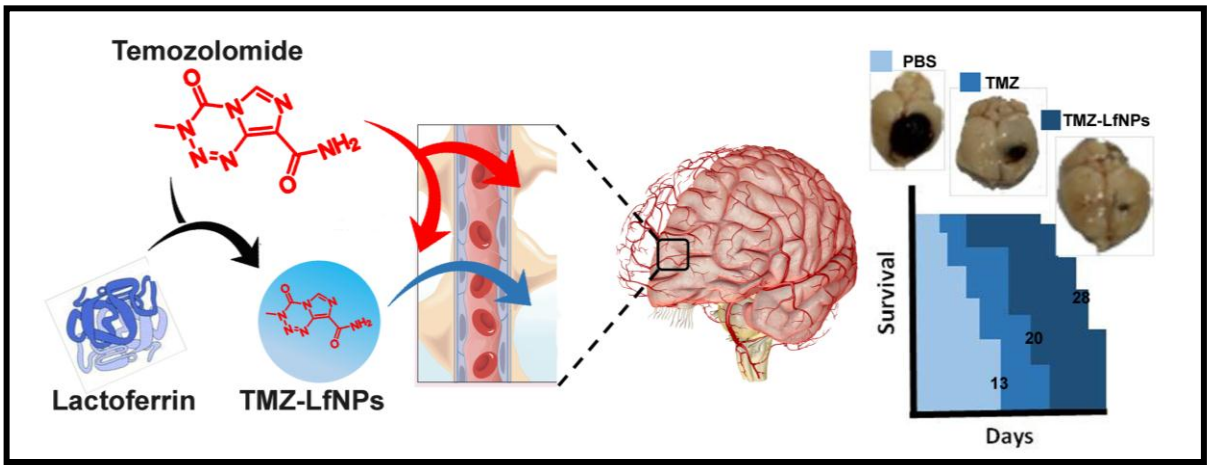

Figure 4.18: Schematic representation of working model .TMZ, the only chemotherapeutic drug for glioma has limited access to BBB, however TMZ-LfNPs can readily permeate BBB, deliver significantly higher amount of TMZ and thereby markedly reduces tumor burden and helps in survival progression of glioma bearing mice.

Chapter 5

Enhancing drug sensitivity in TMZ resistant orthotopic GBM using AKB-siRNA loaded Lf nanoparticles

5.1 Introduction

The current treatment strategies of GBM include only palliative treatment or surgical resection which is challenging because of the proximity of tumor to the vital structures of brain. In addition GBM exhibits a high resistance to current chemotherapy. TMZ, the only approved drug displays a limited efficacy upon repeated dosing owing to an increased resistance to TMZ in GBM tumors [118] due to induction of enhanced levels of repair enzymes involved in TMZ mediated DNA methylation. While higher doses of TMZ may result in positive outcomes by way of causing extensive tumor kill, the resulting toxic effects of TMZ do not permit dose escalation. Therefore to achieve maximum therapeutic efficacy of TMZ at approved dosage, effective down-regulation of over expressed oncogenes perhaps will be a logical approach to overcome recurrence of glioma after resection. Silencing of genes by siRNA was successfully used as a therapeutic strategy against several cancers.

The first siRNA developed for wet age-related macular disease entered into Phase I clinical trials in 2004, six years after their breakthrough indicating the importance of siRNA technology [119]. There are several advantages of siRNA therapeutics over others such as (1) the high specificity and ability to efficiently silence a large number of diverse genes involved in a number of distinct cellular pathways, (2) gene silencing at extremely low concentration of siRNA due to the efficient protein regulatory expressions in mammalian cells, (3) possibility of designing siRNA targeted to any disease-causing pathogenic gene. The siRNA based therapy is important particularly for the disease condition which are not treatable by other conventional therapies such as small molecular inhibitors and therapeutic antibodies. Majority of human diseases essentially involve aberrant gene functioning. The ability of siRNA to regulate gene expression for several genetic diseases and cancers, making it a potential therapeutic means [120, 121]. However, the major challenge of siRNA therapeutics is the need for devising a safe, stable and effective carrier system capable of delivering therapeutic dosage of siRNA into the cytoplasm of target cells. siRNA, an oligomer of 20-22 nucleotide, is anionic and has poor stability in biological milieu. A large number of carriers including liposomes [122, 123] and cationic nanoparticles [120] have been tested with variable success. Multi modal approaches to treat cancer are shown to be more effective. Simultaneously addressing more than one pathway involved in cancer pathogenesis may yield better outcomes.

. In this work we have focused on inhibiting Aurora kinases (AKs), crucial for cell cycle control, simultaneously with treatments with TMZ. AKs are over expressed in several

cancers, thus implicating their role in tumorigenesis. AKs are a family of serine/threonine kinases involved in centrosome separation, mitotic spindle assembly, chromosome condensation, segregation and cytokinesis. All the three mitotic protein kinases (Auroras A, B and C) have been found to be over expressed in various types of cancers [124]. Aurora Kinase B (AKB) is referred as a chromosomal passenger protein, involved in chromosomal segregation and spindle check points [125]. Furthermore AKB, negatively regulates the tumor suppressor gene p53 by accelerating its phosphorylation and ultimately its degradation resulting in tumor development [126, 127]. Over expression of AKB mRNA and protein is common in malignant glioma and other human cancers [128] making it an attractive target for cancer therapeutics. The signalling pathway of AKB is often compromised in GBM. Moreover knockdown of AKB has been shown to increase the sensitivity of highly resistant GBM against chemotherapeutic drug, TMZ [129]. These studies suggest AKB silencing as a logical approach to potentiate the efficacy of TMZ-based therapy. However, prior to the potential of AKB inhibition as a means to enhance TMZ-based chemotherapy can be realized, it is necessary to have a safe and effective means to transport siRNA across the blood-brain barrier (BBB) and deliver it selectively to brain tumors. The promise of siRNA technology in brain tumor is critically dependent on development of effective delivery vehicles for carrying siRNA across the BBB. The delivery vehicle should be optimized to stabilize the siRNA under the biological environment and should facilitate the localization of siRNA at all the stages from target-cell recognition and uptake to association into RISC complex and mRNA cleavage. Moreover, it should be able to cross BBB and reach the tumor target. Brain targeting abilities of Lf for delivering drug have been already discussed in previous chapters. In a recent study a siRNA-delivering CPP, bLFcin6, isolated from Lf has been tested for its ability to cross BBB [130]. Carriers that protect siRNA and transport it across the BBB are critical for the therapy.

In the previous chapter, we have established the brain targeting of lactoferrin nanoparticles (designated as LfNPs) loaded with TMZ. In this work we have employed lactoferrin based nanoparticle formulation that combines the ability to entrap siRNA in nanoparticles and also facilitates transport across BBB. By combining the siRNA loaded Lf nanoparticles with TMZ treatment, we are able to demonstrate a significant reduction in the tumor burden and extension of survival in orthotopic mouse models.

5.2 Results and Discussions

5.2.1 Gel binding assay and nanoparticle characterization

The nucleic acid binding abilities of Lf have been well characterized. To determine the binding affinity of Lf with siRNA, we initially performed a gel binding assay by preparing complex of siRNA and Lf at various molar ratios. A faint siRNA band at 1:1 molar ratio and absence of bands at higher ratios indicated strong binding of Lf to siRNA (**Figure 5.1**). Using this molar ratio, siRNA loaded Lf nanoparticles were prepared as described in method sections.

TEM analysis suggested a spherical shape of the particles with size in the range of 50-70 nm **(Figure 5.2A)**. The hydrodynamic diameter of the particles at pH 7.4, as determined by DLS **(Figure 5.2B)**, was found to be 150-165 nm, which is excepted as DLS provides size of hydrated particles, compared to the dry state size obtain by TEM. The polydispersity index (PDI) and zeta potential of the particles were 0.22 ± 0.1 and -2.5 ± 1 mV respectively, suggesting a narrow size distribution and near neutral surface charge of the particles.

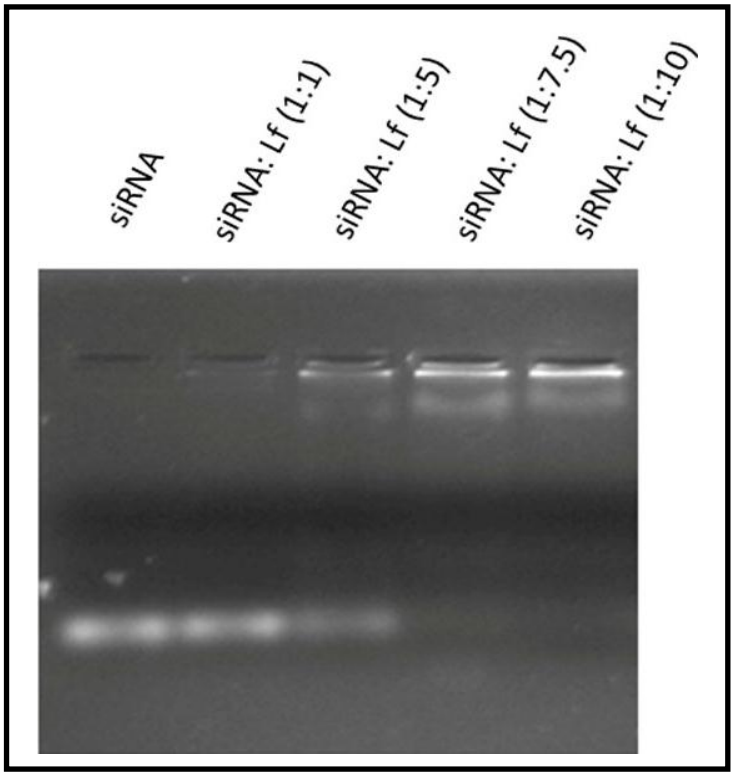

Figure 5.1: Gel binding assay. Representative image of agarose gel assay depicting binding of Lf to siRNA. Retardation in mobility of siRNA in the wells at higher mole ratios indicates strong affinity of Lf to siRNA.

5.2.2 Nuclease protection assay and serum stability

An important aspect of gene delivery is the protection of siRNA from endo-nucleases present in the biological environment. Hence to investigate the nuclease protection of encapsulated siRNA in the LfNPs, the siRNA-LfNPs were subjected to RNaseA treatment. Post treatment the siRNA was extracted using phenol chloroform and the integrity of the entrapped siRNA was determined by subjecting to agarose gel electrophoresis. As shown in **Figure 5.3A**, siRNA entrapped in LfNPs remains unaffected from the harsh effects of RNaseA treatment. Under similar conditions, free siRNA was completely degraded and was thus not visualised in the agarose gel. Our results confirm that siRNA encapsulated in LfNPs was resistant to degradation by RNaseA. Moreover siRNA-LfNPs incubation with serum which contains nucleases and proteases does not affect their size over a period of time (**Figure 5.3B)** confirming their serum stability.

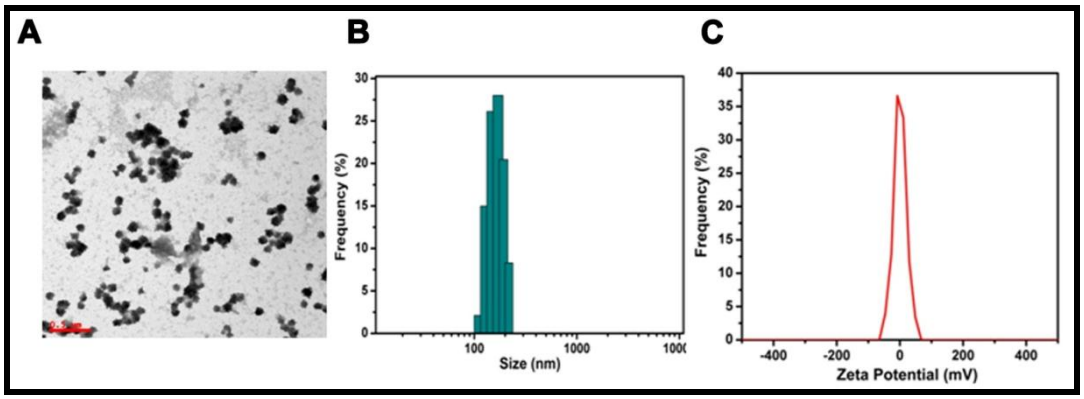

Figure 5.2: Characterization of siRNA-LfNPs. (A) TEM analysis (B) hydrodynamic redii (C) zeta potential.

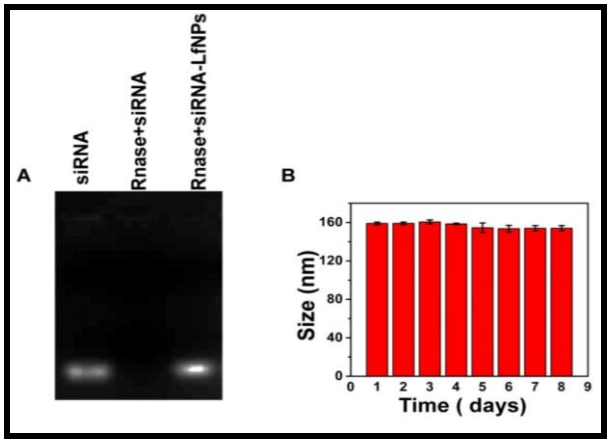

Figure 5.3: RNase protection and serum stability of siRNA-LfNPs. (A) Agarose gel electrophoresis of RNaseA digested siRNA-LfNPs following phenol chloroform extraction. Treated siRNA alone was used as a positive control for enzyme activity. (B) Hydrodynamic redii measured using DLS up to 9 h in presence of 20 % serum at 37 ºC.

5.2.3 Comparative cellular uptake by Flow cytometry

LfNP-mediated cellular uptake of siRNA was assessed in GL261 cells using flow cytometry. Cell were treated with Fluorescently labelled siRNA loaded Lf nanoparticles. After 2 h of treatment cells were thoroughly washed with PBS to remove any surface bound fluorescence nanoparticles and then analyzed by flow cytometry. Lipofectamine complexed with siRNA was used as a positive control.

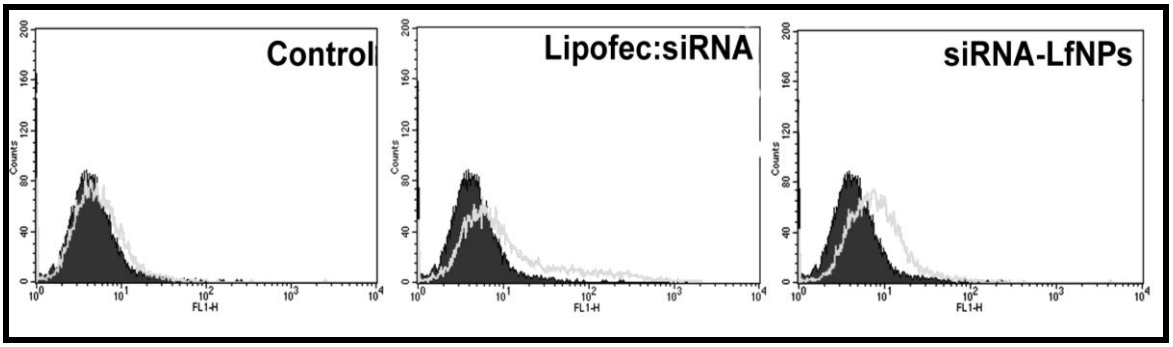

Figure 5.4: Uptake of siRNA by GL261 cells. Representative FACS pattern of cells treated with either 20 pmoles of siRNA-FAM alone or equivalent amounts of siRNA-LfNPs. Cells treated with Lipofectamine acts as positive control.

There was a significant uptake of siRNA when delivered through LfNPs (53.29 %) as compared to lipofectamine (30.17 %) suggesting efficient and receptor specific delivery of siRNA via LfNPs. However the uptake of siRNA alone was minimal (5.27 %) as siRNA was unable to enter the cells on its own due to its large size and negative charge (**Figure 5.4**).

5.2.4 Cellular uptake and endo-lysosomal escape

Nanoparticle mediated delivery of gene influences their intracellular pathway, which eventually influence their final fate and thereby therapeutic efficacy. Thus, an understanding of the intracellular trafficking of the delivery vehicle is necessary. To monitor the release of siRNA from LfNPs, both siRNA and LfNPs were labelled separately with FAM (green) and Alexa-633 (red) fluorescence. Merged fluorescence of LfNPs and siRNA at the 3 h time point (**Figure 5.5 A**) suggest that siRNA and LfNPs are co-localized or siRNA is still entrapped in LfNPs. However prominent individual fluorescence corresponding to siRNA and LfNPs at later 6 h time point suggest release of siRNA from nanoparticles.

After intracellular uptake, the major challenge for siRNA is to escape from endo-lysosome to cytosol for binding with RISC complex. Hence to establish the endosomal escape ability of LfNPs we performed endo-lysosomal colocalization studies of LfNPs at the

indicated time points. Confocal images **(Figure 5.5B)** suggest merged fluorescence of Fam-siRNA and Lysotracker at the initial 3 h time point however the signals were separated into their individual fluorescence at 6 h time point suggesting that a great portion of siRNA efficiently escaped from endo-lysosome. However, certain questions pertaining to the mechanism of endosomal escape of siRNA remain unaddressed.

Earlier studies on histidine-rich peptides have demonstrated that endosomolytic activity of these peptides is responsible for releasing the nanoparticles from the endosomes into the cytoplasm [131]. We believe that being highly cationic in nature (rich in histidine and arginine residues), Lf protein may have assisted in endosomal release of the siRNA.

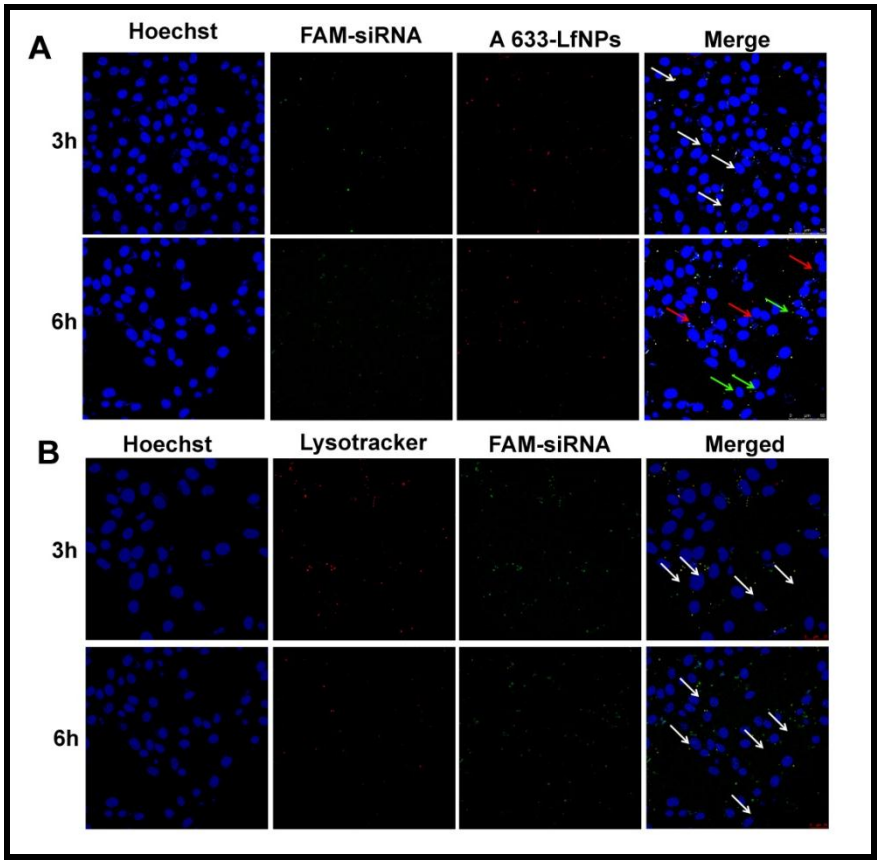

Figure 5.5: (A) Cellular uptake of LfNPs at the indicated time points. White arrows correspond to merged fluorescence of Fam-siRNA and Alexa-633-LfNPs at 3h, however the absence of colocalization at 6 h suggests siRNA release from LfNPs. (B) Trafficking of siRNA-LfNPs within the endo-lysosome at the indicated time points. White arrows correspond to merged fluorescence of Fam-siRNA and Lysotracker red at early time point 3h, however the absence of the same at 6 h suggests endo-lysosomal escape of siRNA.

5.2.5 AKB-LfNPs mediated down-modulation of AKB expression in GBM cells

To assess the efficiency of siRNA delivered by LfNPs, gene silencing studies was performed by treating cells with 50 nM AKB gene-specific siRNAs entrapped in LfNPs. Extent of gene silencing was monitored by estimating the mRNA levels using quantitative real-time PCR and protein levels using immunoblotting of the AKB genes in GL261 cells. Cells treated with AKB siRNA-Lipofectamine complexes were used as a positive control. After 48 h of treatment, we observed significant reduction in the expression level of AKB gene at mRNA and protein level (**Figure 5.6**).

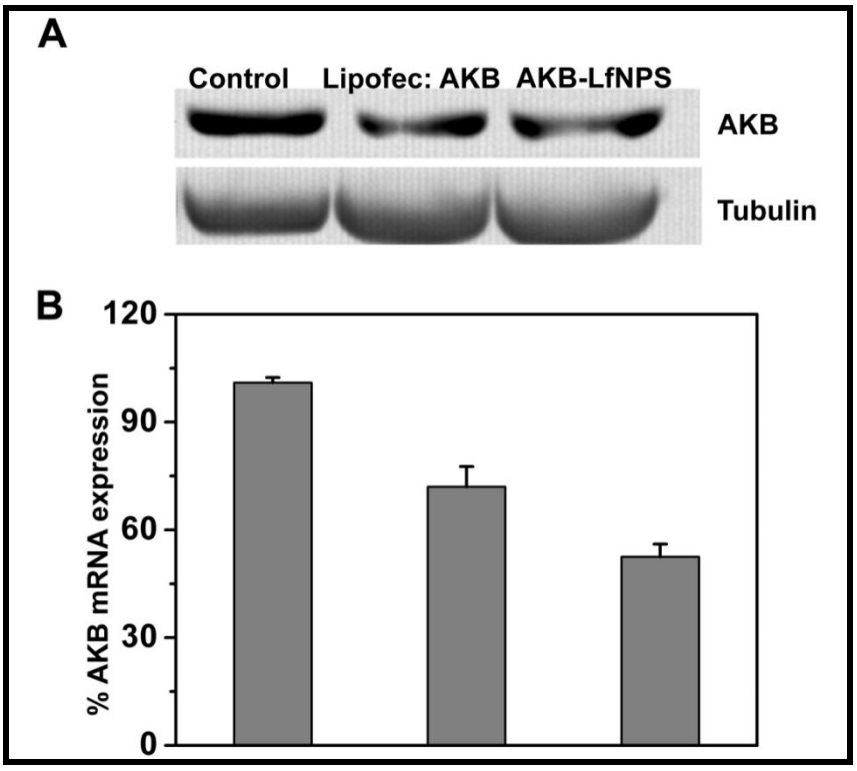

Figure 5.6: AKB gene silencing after the treatment with the AKB-LfNPs (A) Immunobloting of AKB and tubulin (normalized control) expression in GL261 cells transfected with siRNA-LfNPs (50 nM equivalent dose of AKB-siRNA) (B) RT-PCR analysis of AKB protein levels at 48 h post treatment of TMZ-resistant GL261 cells. Lipofectamine was used as positive control. Tubulin protein was utilized as an internal protein loading control.

5.2.6 Potentiating cytotoxicity of TMZ and increased apoptosis using AKB-LfNPs in TMZ-resistant GL261 cells.

To assess the ability of AKB-LfNPs to sensitize glioma cells to TMZ, GL261 cells were transfected with AKB-LfNPs for 48 h and then treated with increasing concentrations

of TMZ (0 to 500 μM) for an additional 24 h. Cells either treated with TMZ alone or transfected with the AKB-LfNPs were used as controls. Three days later, the number of untreated cells had increased to confluence without any cell detachment. In contrast, microscopic examination (**Figure 5.7)** of cells treated with AKB-LfNPs resulted in significantly increased response to TMZ. On the contrary no significant cell death was observed in cells treated with TMZ alone at lower dosage suggesting TMZ based cell death in a dose-dependent manner. It was also evident that transfection with AKB-LfNPs alone had better cytotoxic effect on GL261 cells, greater than that of TMZ alone even at the highest dosage. Moreover, the degree of cell death observed in the groups treated with the combination of AKB-LfNPs and TMZ was significantly higher than with either TMZ or AKB-LfNPs alone. These results indicate sensitization of GL261 cells to TMZ leading to a major increase in TMZ-induced cell death as a result of combination treatment with AKB-LfNPs.

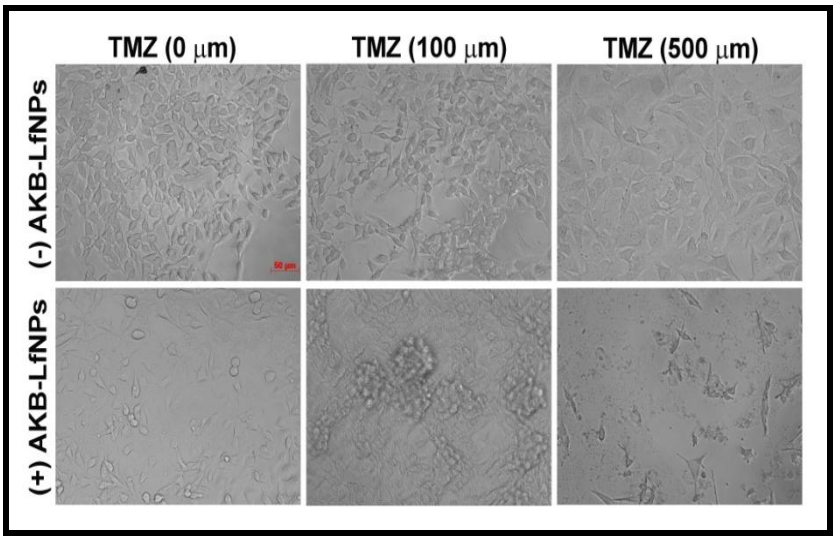

Figure 5.7: AKB-LfNPs mediated enhancement of TMZ cytotoxicity in TMZ-resistant mouse glioma cells. GL261 cells were treated with the indicated concentrations of TMZ, either alone or after prior treatment with the AKB-LfNPs. Photomicrographs of representative area of the cell monolayer 3 days after treatment. Scale bar indicates 50 μm.

The primary mechanism of TMZ induced cell death is via apoptosis. TMZ methylates O-6 guanine residues in DNA, leading to increase in sub G1 population (sign of dead cells) and cell cycle arrest at G2/M phase, subsequently resulting in apoptosis [116]. The combinatorial treatment of AKB-LfNPs and TMZ also affected the cell cycle profile analysed by flow cytometry (**Figure 5.8**). The increase in sub-G1 population (1.13 % to 5.26

%) with increasing TMZ dosage (100 μM to 500 μM) suggests a dose dependent TMZ apoptotic response. Combinatorial treatment of cells with TMZ and AKB-LfNPs also suggests that cytotoxic effect of AKB-LfNPs is dependent on the concentration of TMZ used. Higher dosage of TMZ (500 μM) shows an increased sub-G1 population as compared to a lesser dose (100 μM). The combination of AKB-LfNPs and TMZ treatment significantly increased the sub-G1 population, as studied by flow cytometry, compared to TMZ treatment alone; suggesting AKB-LfNPs increases the cytotoxic effects of TMZ in resistant GL261 cells.

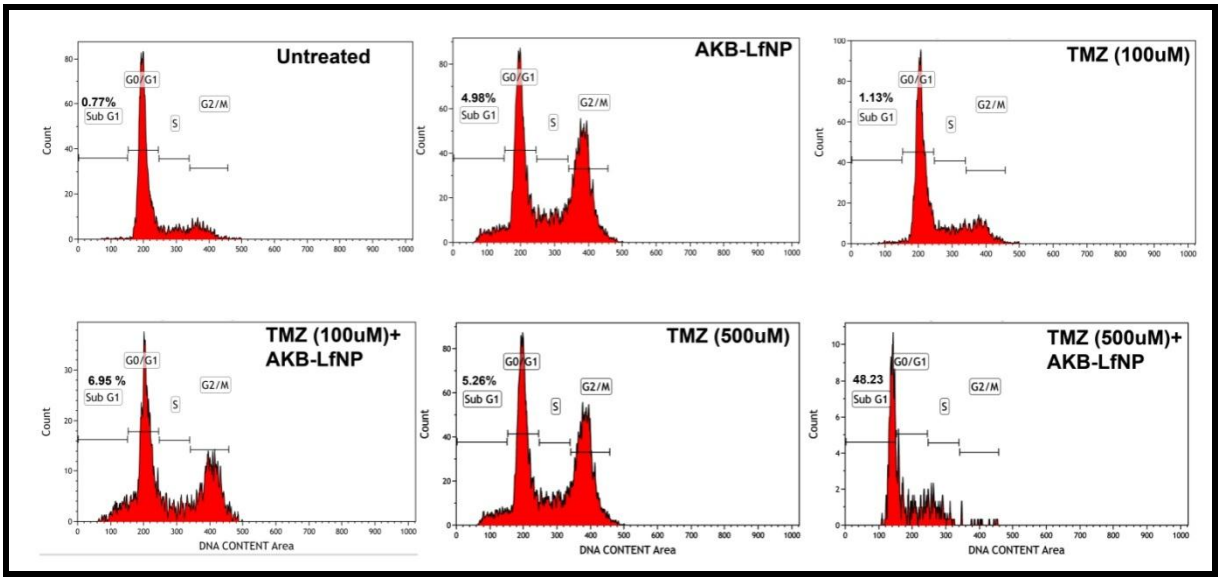

Figure 5.8: Cell cycle profiles of GL261 cells post-treatment with either TMZ alone or in combination with AKB-LfNPs. The numbers indicate the percentages of sub-G1 cells.

5.2.7 Animal studies

5.2.7.1 Distribution of fluorescent siRNA loaded LfNPs in mouse brain

Based on the efficient siRNA entrapment and cellular uptake when delivered via LfNPs, the specificity of siRNA-LfNPs was further tested for its *in vivo* potential to cross the BBB using Lf receptors specific transcytosis and get localized in the brain. To visualise the bio-distribution fluorescent labelled siRNA loaded LfNPs were administered systemically in healthy mice models. 6 h post systemic administration of siRNA-LfNPs, mice were euthanized and all the major organs, including brain were dissected, sectioned and visualized. In the representative brain sections (**Figure 5.9 A**) of mice injected with cy5-siRNA-LfNPs, the localization of fluorescent siRNA is distinctly visible in the brain parenchyma along with endothelial micro vessels stained with CD31 (Alexa 488), which clearly indicates transcytosis of the siRNA-LfNPs across the BBB. PBS injected mice were used as negative controls to

eliminate the background fluorescence. Further the bio-distribution studies suggest a small fraction of accumulation of siRNA in liver which is in concomitant with our previous results in chapter 3 and earlier studies from our group. However the absence of any fluorescence in the other organs like kidney, lung and spleen indicate receptor specific uptake of siRNA in brain.

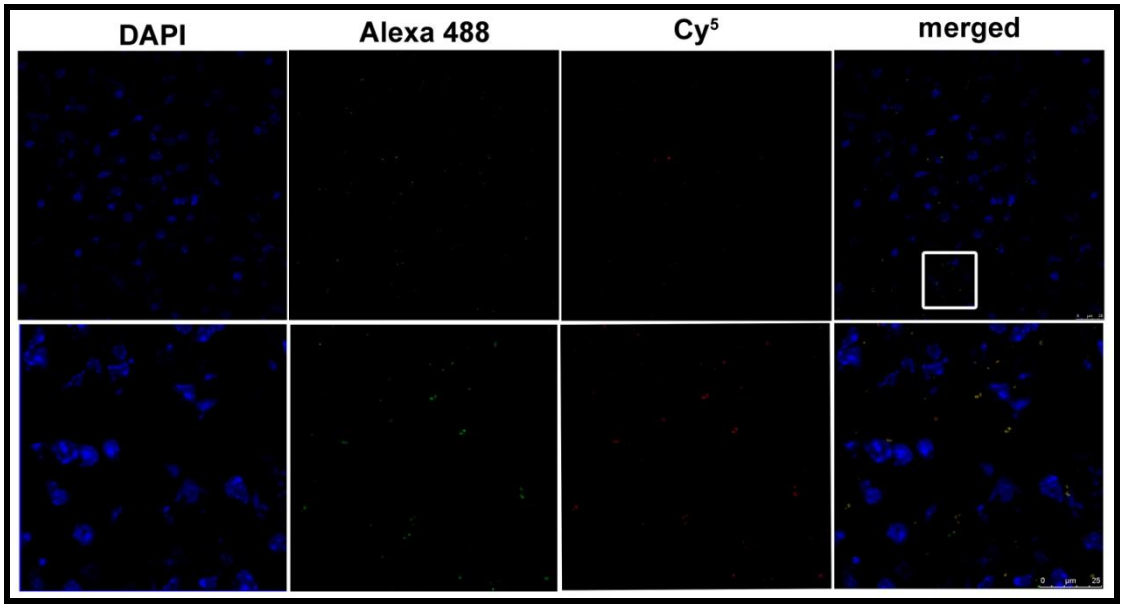

Figure 5.9: (A) *In vivo* bio-distribution of fluorescently labelled siRNA-LfNPs. Representative scan of mouse brain (Top panel) show a strong fluorescence (cy5) in the brain parenchyma (top panel). The brain slice (8μm thickness) was imaged using confocal microscopy with 63x oil objective. The panels below depict the scan of the boxed expanse where fluorescence of brain micro-vessels stained with anti-CD31 antibody was visualized using secondary antibody tagged with Alexa Fluor 488 (green).

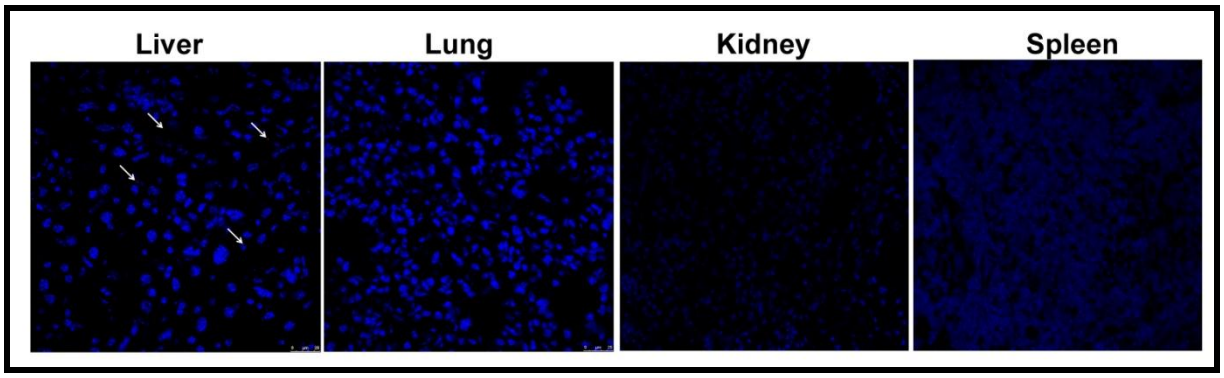

Figure 5.9: (B) Organ bio-distribution of siRNA-LfNPs. Representative confocal images depict fluorescence in the liver unlike lung, kidney and spleen. Scale bar = 25μm.

5.2.7.2 *In vivo* gene silencing

The ability of systemically injected AKB-LfNPs to silence the AKB protein *in vivo* was assessed in GBM mice. Western blot (**Figure 5.10)** indicates a significant decrease in AKB protein when the AKB siRNA is delivered via LfNPs. Scrambled siRNA (scr.siRNA) was used as negative control.

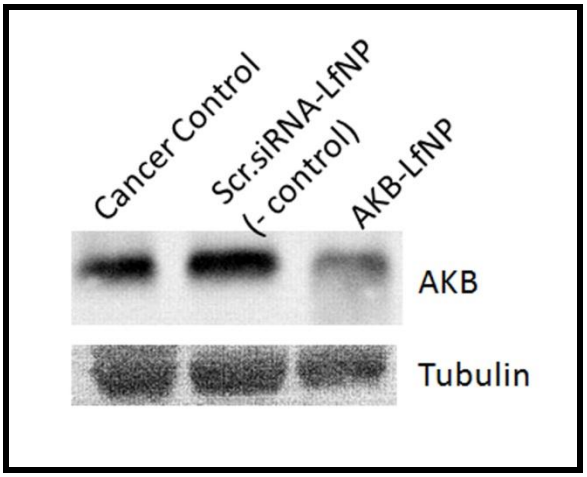

Figure 5.10: *In vivo* gene silencing. GBM mice were systemically injected with AKB-LfNPs. Scr.siRNA-LfNPs used as negative control.

5.2.7.3 Tumor regression studies in glioma mice

To study the anti-tumor effect of AKB-LfNPs and their potentiating effect on TMZ chemotherapy, GBM mice models were generated by intracranial injection of GL261 cells as described in methods. Preliminary experiments showed an aggressive tumor growth and all the mice died after two weeks.

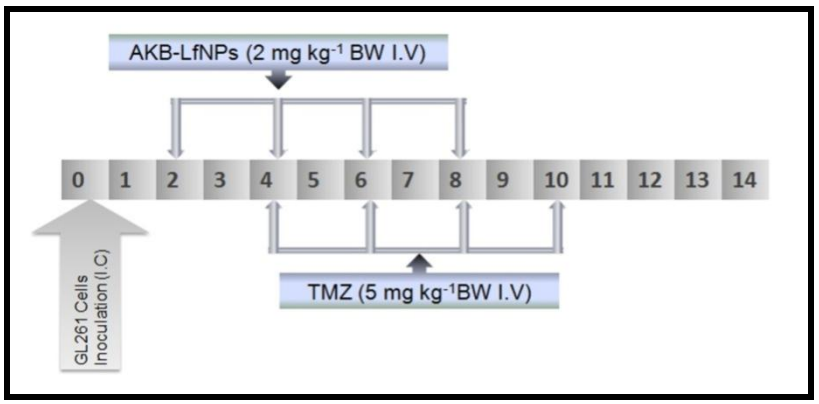

Figure 5.11: Treatment schedule. Mice were given four alternative dosage of TMZ (5 mg kg^{-1}) along with four prior consecutive dosage of AKB-LfNPs (equivalent to 2mg kg^{-1} of AKB-siRNA).

Based on these observations, mice were randomly divided into three treatment groups (n=3 mice) and injected with four dosage of TMZ either alone or in combination with prior consecutive dosage of AKB-LfNPs starting from day 4 after tumor implantation up to 10th day, as shown in **Figure 5.11.** On 14th day when all the PBS treated mice succumbed to death, other groups were also sacrificed and brain tissues were extracted and processed for histology and tumor regression analysis.

Glioma development was confirmed by a cancerous growth as seen in the brain histology sections. Histology results (**Figure 5.12)**, suggest that PBS treated mice showed huge tumor burden, large necrotic areas. Glioma bearing mice treated with free TMZ caused moderate shrinkage of the tumor relative to PBS treated mice**.** However, as illustrated in the whole brain photomicrographs as well as the histology sections, the tumor burden was found to be significantly reduced in mice treated with AKB-LfNPs and a combination of AKB-LfNPs and TMZ.

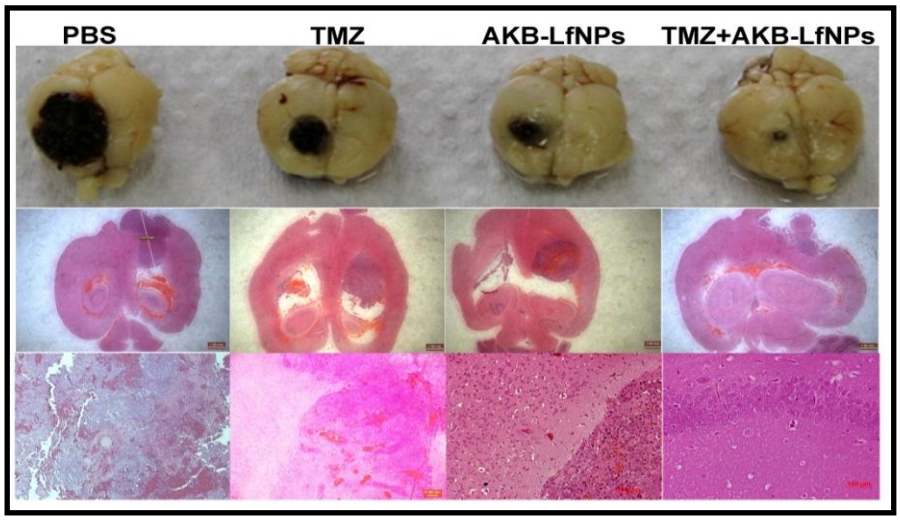

Figure 5.12: Photomicrographs of brain dissected from PBS treated glioma bearing mice, show huge necrotic area (top most panel). Histology section observed under 5X magnification (Middle panel) and under 10X magnification (bottom panel) depicts tumor area and necrosis with larger areas of haemorrhage respectively in all treated groups. It is clearly evident that the combination of AKB-LfNPs and TMZ treated groups had maximum tumor regression than independently treated group.

In order to assess the improved anti-tumor effect of AKB-LfNPs as well as combination therapy on survival of GBM mice, in a separate experiment the survival time in

all treatment groups was monitored and analysed. Life-span extension curve (**Figure 5.13)** obtained from glioma bearing mice treated with multiple dosage of either TMZ alone or AKB-LfNPs alone show a median survival time of 20 days and 27 days respectively. However, when treated with a combination of both, the survival time was increased up to 33 days. PBS treated mice show the least median survival of 14 days. Our results indicate that the chemosensitization of resistant GBM with AKB-LfNPs leads to a significant enhancement in survival time of TMZ treated glioma bearing mice. Thus, lactoferrin nanoparticles provide an efficient vehicle for delivery of AKB-siRNA and significantly enhancing tumor regression. Additionally combination therapy of AKB-siRNA and TMZ potentiates the TMZ efficacy by sensitizing GBM against TMZ, resulting in significant improvement of survival.

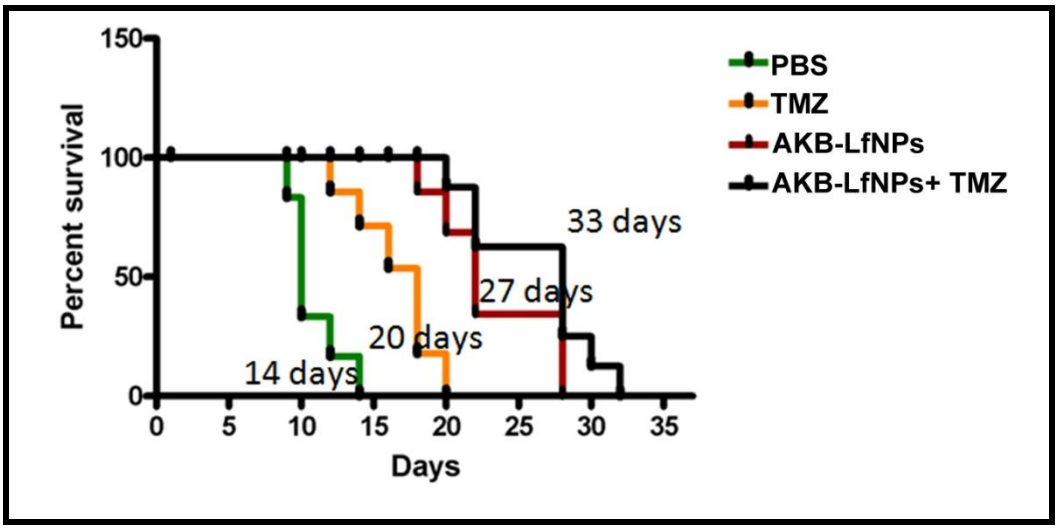

Figure 5.13: Kaplan Meier survival curve. Comparison of the survival-promoting effects of individual treatment groups and in combination in glioma bearing mice (n=6).

5.3 Conclusion

The data presented here suggests a potential application of LfNPs as a carrier for the therapeutic delivery of siRNA into mouse brain. We have demonstrated that the LfNPs mediated delivery of therapeutic siRNA against Arora kinase B, significantly reduces tumor burden and also potentiates the current TMZ chemotherapy by chemosensitizing resistant GBM ensuing promising clinical outcome.

Chapter 6

Potentiating TMZ activity by p53-loaded Lf nanoparticles in subcutaneous GBM model

6.1 Introduction

Tumor suppressor gene p53 is frequently (~50%) mutated in primary and secondary GBM tumors. The signalling pathway of p53 gene is often compromised in GBM, resulting in more aggressive disease with greater resistance to chemotherapy and radiation therapy. Temozolomide, an alkylating agent, is the first line of treatment for glioma and provide survival benefits. However, a prolonged therapy leads to TMZ resistance and subsequently poor responsiveness, thus leading to tumor recurrence in 60-75% of patients [107]. The increased resistance against TMZ is largely due to increase in the O^6-methyl guanine methyl transferase (MGMT) levels [132, 133]. MGMT is a DNA repair enzyme that removes the methyl group added by TMZ to an internal cysteine within its active site and repairs the damaged DNA [134] [133]. MGMT expression level is directly correlated with the TMZ resistance in glioma and is considered as a diagnostic marker for successful TMZ based clinical outcome. There are several approaches that have been utilized to down-modulate the MGMT to improve the efficacy of TMZ based therapy in resistant GBM tumor, including MGMT inhibitors and more recently developed siRNA based silencing of MGMT. Though O^6 - Benzyl guanine (O^6-BG), an MGMT inhibitor, relatively increases the sensitivity of resistant cells against TMZ, it causes severe systemic toxicity in glioma patients [135]. Also, there has been many efforts on the p53-mediated down-modulation of MGMT, as wild type 53 (wtp53) is a negative regulator of MGMT [136]. Moreover, over expression of wtp53 has been shown to increase the sensitivity of cancer cells to TMZ in both *in vitro* and *in vivo* models [137]. These findings suggest that restoration of wtp53 is a rational approach to silence MGMT and improve the efficacy of the current TMZ-based therapy by reversing the chemo-resistance. However, before p53-based augmentation of TMZ therapy can be realized, there is a need for safe and efficient delivery vehicle.

Mainly gene therapy is limited by the lack of efficient gene delivery vehicles and there is a growing demand for designing methods for gene delivery without the involvement of viral vectors due to their immunogenicity, carcinogenicity and unknown long-term side effects. The advantages of using non-viral vectors include no risk of infection, absence of immunogenicity, facilitation of multi-dose scheduling and cost effectiveness. Several non-viral gene delivery vehicles, especially nanoparticle systems, have been developed so far using polymers such as PLGA [12], chitosan [138] lipids [139] and polypropylenimine (PPI) [13]. However, the success rate associated with these non-viral gene delivery systems is moderate due to non-specificity and the toxicity linked with the carrier materials. Also the existing

delivery vehicle may not confer *in vivo* advantage due to their likely interaction with serum proteins, lack of target selectivity and tendency to aggregate. Ideally, a delivery vehicle should be target specific; should aid in cellular entry of the plasmid; protect the plasmid from any form of degradation; should escape endo/lysosome compartment; and should have nuclear localization sequences (NLSs) [140]. Owing to unique features of LF *viz.* an ability to bind DNA, efficient transport of gene to nucleus due to its NLS domain and specificity to over-expressed Lf receptors on cancer cell, it has been utilized as a potential targeting ligand for plasmid DNA delivery to human bronchial epithelial cells and hepatocytes [113] [141]. The focus of this chapter is to develop plasmid DNA loaded Lf nanoparticles and their Lf receptor specific efficient delivery in LfR positive cells. Further we have demonstrated the systemically injected p53-loaded lactoferrin nanoparticles (p53-LfNPs) significantly reduces the tumor burden alone or in combination with TMZ in subcutaneous GBM model. More over the combination therapy of pDNA-LfNPs and TMZ, chemo-sensitize resistant GBM and provides survival benefits to the GBM mice model.

6.2 Results and Discussion

Synthetic gene delivery through artificial polymers, although successful, is still over-shadowed when compared to viral vectors. Designing a system for gene delivery applications requires smart modifications of the existing polymers in an attempt to increase efficiencies at one or more steps involved in the process (binding to the cell surface, endocytosis, endo-lysosomal escape, gene unpacking and translocation to the nucleus). Lf, owing to its biocompatible and biodegradable nature can serve as a suitable candidate for gene delivery vehicle. Moreover, the DNA binding capability of lactoferrin makes it a perfect candidate for gene delivery applications.

6.2.1 Preparation and characterization of plasmid loaded LfNPs

pDNA loaded LfNPs and blank LfNPs were synthesised as mentioned in chapter 2. TEM visualization of the particles revealed a uniform distribution with a spherical shape. The mean diameter of the unloaded LfNPs and pDNA-LfNPs was found to be in range of 50 ± 20 nm and 70 ± 20 nm respectively (**Figure 6.1A and 6.1B**). Size and poly-dispersity index of the LfNPs further determined by DLS suggests a little larger size around 180 ± 20 nm for pDNA-LfNPs as compared to the unloaded LfNPs which was around 100 ± 5 nm (**Figure 6.1C**). They show a narrow size distribution with a PDI of 0.1 which could be attributed to the formation of stable complexes between Lf and DNA. The near neutral (-0.2

± 1) surface charge of pDNA-LfNPs (**Figure 6.1D**) may attribute reduced interaction with serum proteins and thereby increased biological stability [142].

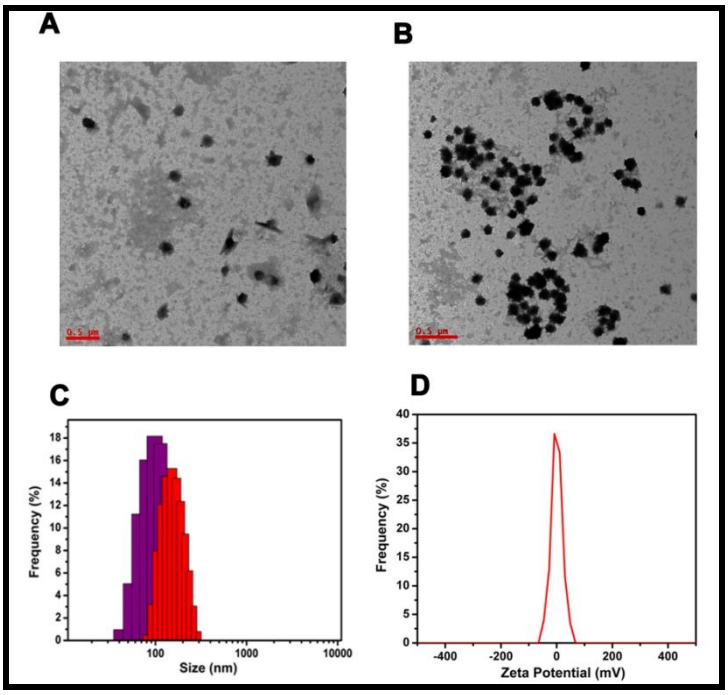

Figure 6.1: Characterization of pDNA-LfNPs. (A) TEM analysis of blank LfNPs and (B) pDNA-LfNPs (C) Relative hydrodynamic diameter of blank LfNPs (purple) and pDNA-LfNPs (red) and (D) Zeta potential of pDNA-LfNPs.

The loading efficiencies of the particles determined by SYBER GREEN assay was found to be 58% ± 2.6. The high loading efficiency by LfNPs could be due to a charge based interaction between Lf and pDNA. The theoretical pI of Lf is approximately 8.5, as it possesses many basic amino acids (Arg + Lys + His = 100). At neutral pH, Lf therefore carries a net positive charge. Moreover, Lf is known to possess DNA binding domain which may further help in DNA binding. Our studies are in corroboration with earlier reports where in Lf has been utilized in gene delivery applications for its properties of DNA binding through charge based interactions.

6.2.2 Gel binding assay and nuclease protection

In order to confirm the encapsulation of DNA, the pDNA-LfNPs were subjected to agarose gel electrophoresis. As shown in **Figure 6.2A**, DNA encapsulated in the LfNPs was observed in the wells of the agarose gel and failed to migrate when subjected to electrophoresis as compared to the control plasmid which migrated under the influence of

the electric field applied. Retardation in the migration of DNA, suggests its encapsulation in the nanoparticles.

An important aspect of delivery vehicle is the protection of DNA from endonucleases in the biological environment. Hence, to further investigate the nuclease protection of encapsulated DNA in the LfNPs, the pDNA-LfNPs were subjected to Dnase I treatment. Post DNase I treatment the pDNA was extracted using phenol-chloroform extraction method and the integrity of the entrapped DNA was determined by subjecting to agarose gel electrophoresis. As shown in **Figure 6.2B**, DNA entrapped in LfNPs remains unaffected from the harsh effects of DNase I treatment. Under similar conditions, free DNA was completely degraded, as a result of which it is not visualised in the agarose gel. Results indicate the inaccessibility of nuclease to pDNA when encapsulated in LfNPs.

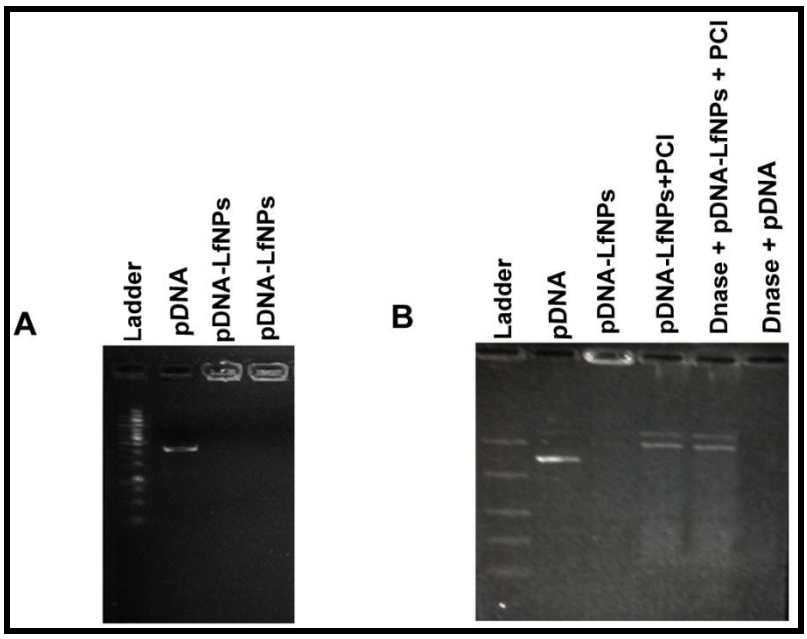

Figure 6.2: Gel retardation and nuclease protection assay of pDNA-LfNPs. (A) Agarose gel electrophoresis of pDNA-LfNPs confirms DNA encapsulation as pDNA-LfNPs fails to migrate from the wells (B) Electrophoretic analyses of pDNA-LfNPs following DNase I digestion. All samples were run on a 1% agarose gel and stained with ethidium bromide.

6.2.3 Stability studies of pDNA-LfNPs

Stability of a formulation is an important aspect in the pharmaceutical industry. In the present study we analysed the stability of the LfNPs synthesised by monitoring their size over a period of 10 weeks. As shown in **Figure 6.3A**, the nanoparticles showed no significant change in size or surface charge during the entire duration of the study. The

stability of the particles was also studied in culture media DMEM with 20% serum at 37 ºC for several hours. As shown in **Figure 6.3B**, the presence of serum (as studied up to 8 h) had no effect on particle size, suggesting particle integrity under physiological conditions.

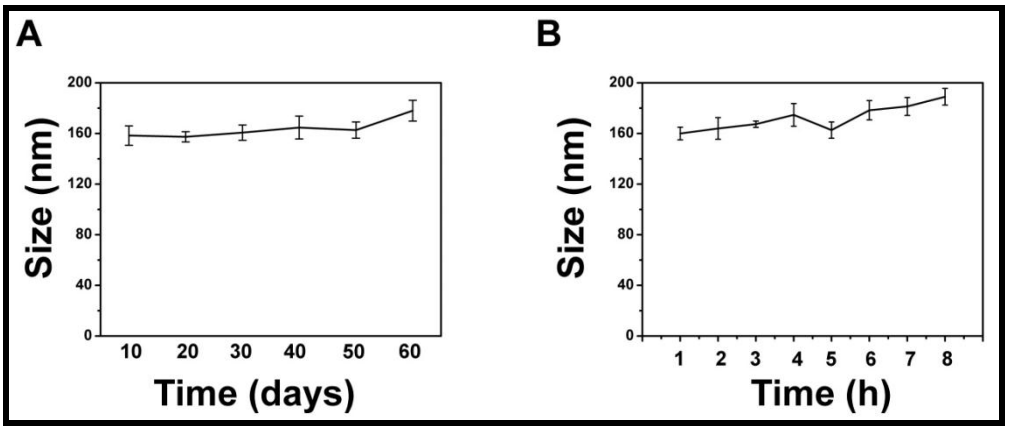

Figure 6.3: Stability of LfNPs (A) in PBS pH 7.4 at 4 ºC and (B) in culture medium with 20% serum. The minimal change in the size suggest the stability of particles in physiological conditions.

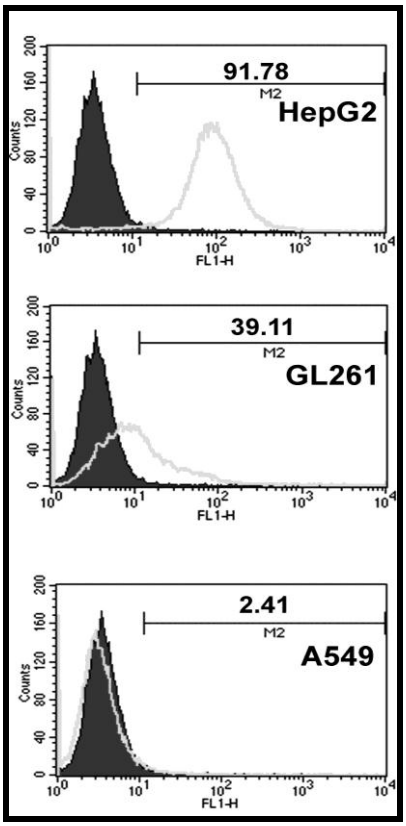

Figure 6.4: Lf receptor expression levels in HepG2, GL261 and A549 cells using flow cytometry.

6.2.4 Lf Receptor expression

The LfR expression levels in the indicated cell lines were analysed by flow cytometry. Our results (**Figure 6.4)** show a significant variation of LfR expression among 3 cell lines presented in decreasing order: HepG2 (91.78) >> GL261 (39.11%) >> A549 (2.41). The flow cytometry results are in agreement with our immunoblotting analysis in chapter 4, **Figure 4.4A**. Our results are consistent with the earlier findings, where lack of LfR expression in A549 cells has been reported [113].

6.2.5 Receptor mediated uptake and gene transfection abilities of LfNPs

We examined the receptor mediated uptake of LfNPs using flow cytometry. Quantitative analysis of cells, treated with fluorescently labelled nanoparticles showed (**Figure 6.5A, 6.5B and 6.5C**) LfNPs uptake was highest (92%) in HepG2 followed by (88%) in GL261.

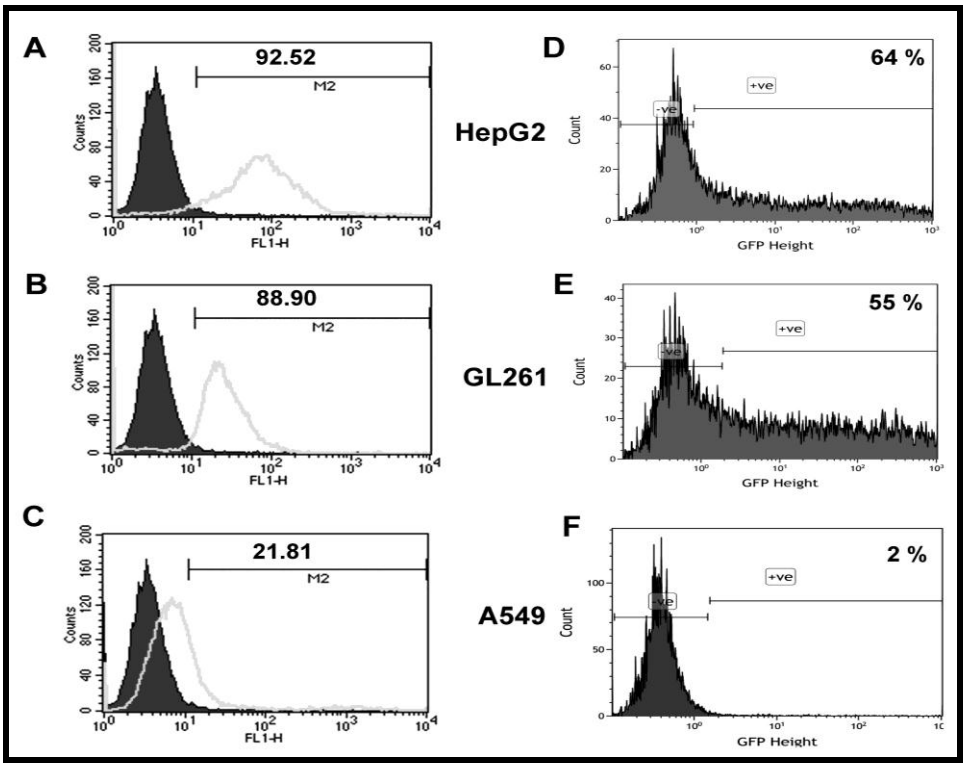

Figure 6.5: Intracellular Uptake and pDNA transfection. LfNPs uptake in HepG2, GL261 and A549 cells and their relative transfection efficiency in LfR positive cell lines.

However the uptake of LfNPs was found to be minimal in A549 (21%) as indicated by cell associated fluorescence. The lesser uptake of LfNPs in A549 was expected due to a lack of expression of LfRs in A549 cells as described earlier. These results demonstrated that

LfNPs cellular uptake is highly receptor specific. However, being small in size, a minute fraction of nanoparticle uptake through some other alternative pathways cannot be ruled out.

Gene delivery is assessed by the ability of the delivery system in localizing the gene to target organelle namely nucleus and to express protein for the particular gene of interest. GFP gene carrying plasmid construct (pDNA) was loaded into Lactoferrin nanoparticles and incubated with LfR positive and LfR negative cells lines. Flow cytometry analysis **(Figure 6.5D, 6.5E and 6.5F)** demonstrate a high expression of GFP protein in HepG2 cells followed by GL261 with minimal GFP expression in A549 cells, which might be attributed to the level of LfR expression in the indicated cells lines, suggest that LfNPs enters cells through LfR receptor.

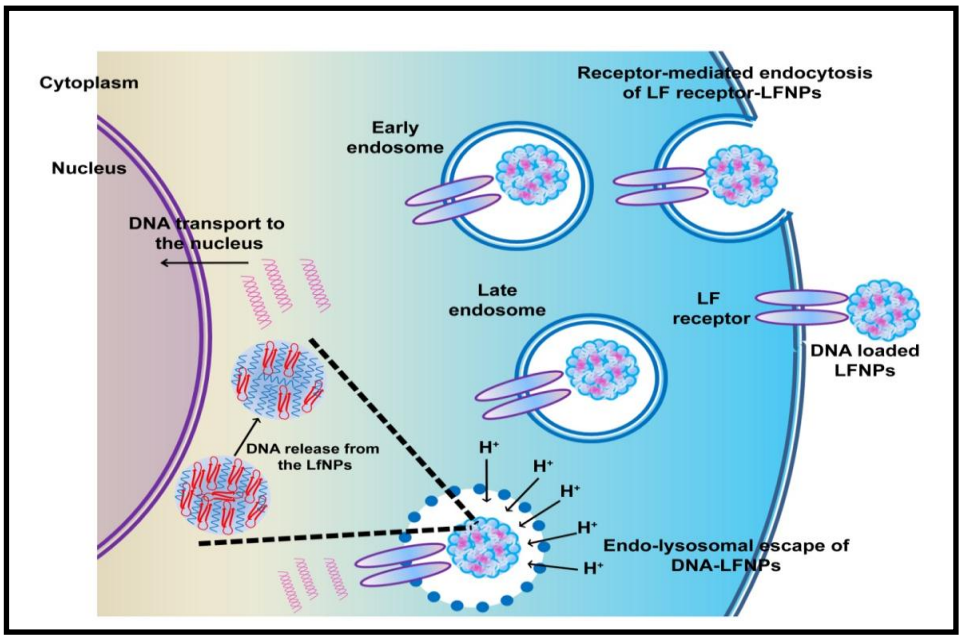

Figure 6.6: Proposed mechanism of Lf receptor mediated uptake of DNA loaded LfNPs. DNA loaded LfNPs enters cells through receptor mediated endocytosis, internalized in the endosomes followed with subsequent escape from endo-lysosome and transport of DNA to nucleus.

We hypothesize that the ability of DNA loaded LfNPs to transfect cells may be a direct consequence of the intrinsic proton-sponging capability of lactoferrin (due to rich in histidine residues) which may aid in endo-lysosomal escape of the nano-particle delivered. Post release from the endosomes, the DNA could be carried to the nucleus either through Lf, due to its nuclear localization signal, or through other DNA transporting proteins. As

lactoferrin has been shown to have DNA binding capabilities and a nuclear localization signal, the transfer of DNA from LfNPs to other DNA transport proteins may be dependent on the affinity of the transporter proteins to extract DNA from the LfNPs and carry it into the nucleus. However, the transport of DNA into the nucleus through LfNPs cannot be completely ruled out as shown in the proposed LfR mediated endocytosis model (**Figure 6.6**).

6.2.6 Biocompatibility assay

Toxicity is another major issue in synthetic polymer based gene delivery. Although lactoferrin is a biocompatible protein, nevertheless it was important to confirm its toxic effect on the indicated cell lines. As shown in **Figure 6.7**, MTT assay performed in cells treated with varying concentrations of LfNPs suggested no significant effect on cell viability. The percentage of viable cells was found to be more than 90%, 46 h post-treatment in cells treated with LfNPs (5 mg ml^{-1}). The highest concentration used in the cytotoxicity study was much higher compared to the particle concentration used for gene transfection studies, suggesting that LfNPs may prove to be safe as a vector for gene delivery.

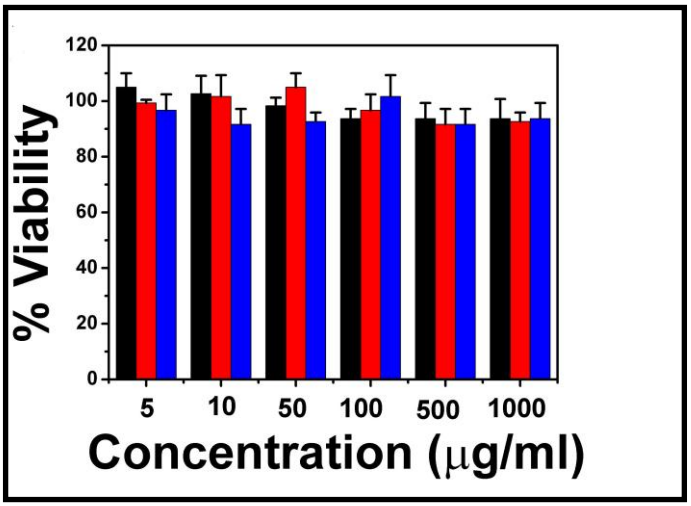

Figure 6.7: Evaluation of cell viability: HepG2 (black), GL261(red) and A549 (blue) cells were treated with LfNPs at the indicated amount followed by assessing cell viability using MTT, 48 h post treatment. Cells treated with PBS were considered as controls having 100% viability. All experiments were repeated independently at least thrice (n = 3) and all values expressed as mean ± SD.

6.2.7 Animal studies

6.2.7.1 Tumor regression studies in glioma mice

After confirming the *in vitro* receptor specific delivery of plasmid DNA via LfNPs, the ability of the p53-loaded LfNPs to restore the expression of tumor suppressor gene p53 and suppress tumor growth in subcutaneous GBM was investigated. Subcutaneous GBM mice models were generated by intra-peritoneal injection (IP) of GL261 cells as described in methods. After attaining the tumor size with an average dimension between 50~100 mm^3, the mice were randomly divided into four treatment groups (n=3 mice)- 1) PBS, 2) TMZ alone, 3) p53-LfNPs and 4) combination of p53-LfNPs and TMZ. Mice that received PBS were used as a negative control for assessing the tumor suppression. Mice were systemically injected with indicated treatment groups at every alternative days and the volume of the tumor was measured manually by using vernier caliper. During the experiment, we observed significant suppression of tumor growth in mice treated with p53-LfNPs alone and combination therapy of both TMZ and p53-LfNPs. However, the size of the tumors in control mice grew rapidly (**Figure 6.8**). The tumor regression in TMZ alone groups were higher than PBS control however lesser than other two groups suggest its improved efficacy in combination with p53 gene therapy.

Figure 6.8: Tumor regression studies**.** Representative photomicrographs of tumor organs dissected from control (PBS) and treatment groups after the end of experiment. The images were taken at the end of the experiment by sacrificing the animals. PBS treated mice show huge tumor volume (left most panel) compare to the mice treated with either p53-LfNPs alone or in combination with TMZ. Mice sensitized with p53-LfNPs prior to TMZ treatment show a significantly higher tumor regression than TMZ alone.

6.2.7.2 *In vivo* gene expression

To determine whether suppression of the tumor is due to the restoration of tumor suppressor gene p53, we quantified the p53 protein levels in the tumor tissues isolated from

control and treatment groups. Results showed a significant p53 expression when delivered via LfNPs at 48 h and 72 h (**Figure 6.9)** time point. Taken together, the results confirmed an efficient uptake of LfNPs by the tumor tissues and subsequent expression of their cargo p53 gene.

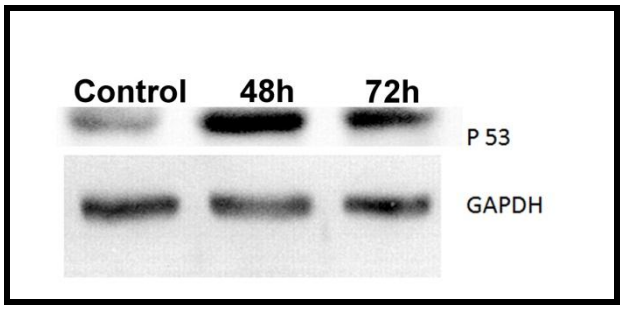

Figure 6.9: *in vivo* gene expression. Western blot of tumor tissue lysate of C57BL/6 mice, systemically injected with p53-LfNPs post 48 h and 72 h.

6.3 Conclusions

The results presented in this chapter suggest that LfNPs deliver plasmid DNA in a receptor specific manner and were able to express the encapsulated plasmid DNA *in vitro* in GL261 cells. Further, our finding established that the expression of p53 encoding gene when delivered through LfNPs in subcutaneous glioma model could significantly regress tumor alone and in combination with TMZ. Furthermore the combination therapies of p53-LfNPs significantly potentiate the TMZ treatment outcome by chemosensitizing the resistant GBM.

Chapter 7

Summary and Future Directions

7.1 Summary

Cancer is a lethal disease with poor treatment outcomes. The existing treatment options are surgery, radiotherapy, chemotherapy and gene therapy. Although, chemotherapy is a vital option to deal with various type of cancers, however its use is limited due to severe systemic toxicity, off-target effects and cancer cells developing resistant to a variety of chemotherapeutic drugs. In addition to that chemotherapeutic drugs have limitations such as low aqueous solubility, short plasma half-life and rapid clearance of drugs which greatly restricts their therapeutic index. A number of efforts have been put forth to overcome these limitations, amongst them nanomedicine based targeted therapy is rapidly evolving as the potential treatment alternatives. Nanocarriers help in sustained release of drugs, improves the bioavailability and pharmaco-kinetic profile of drugs. Drug loaded nanocarriers with tumor targeting abilities maintain optimum therapeutic level of the drug at the site of action, thereby improves the efficacy of the drug while reducing side effects; hence vital in cancers that require effective and specific targeting.

Glioma is an aggressive brain tumor with poor clinical outcome. The inadequate treatment outcomes are mainly due to the presence of an impermeable barrier. BBB, comprises of specialized endothelial cells having continuous tight junctions, absence of fenestrae, minimal pinocytosis and high level expression of efflux transporters, making it impermeable for most of the biologics. Poor ability of biologics to cross BBB renders inadequate clinical outcome.

Lf has been extensively used for targeting brain diseases as it can permeate across BBB through receptor mediated transcytosis mechanism. Several nanoparticles decorated by Lf have been used for drug delivery applications for targeting to specific sites or to permeate across BBB in brain diseases. Our group has developed a novel nano-particulate platform made up of lactoferrin protein and successfully demonstrated the improved efficacy of various drugs using this nano-formulation in *in vitro* and *in vivo* models. Lf nanoparticles maintains the targeting ability without the involvement of any further ligand unlike ligand decorated nanoparticles, which makes them distinctive from others. Our group has exploited lactoferrin nanoparticles due to their ability to target over expressed lactoferrin receptors on cancer cells for the drug delivery applications in various cancers. The present work introduces a novel drug/siRNA/gene delivery vehicle with excellent potential for treating melanoma and GBM. The major findings of work can be summarized as below-

- Lf nanoparticles were found to be less than 100 nm in size with spherical morphology and narrow size distribution. Moreover, the near neutral charge on

nano-formulations surface attributes to their long term colloidal stability. Drugs are encapsulated in the lactoferrin nanoparticles by non-covalent interactions and found to be stable in nanoformulations. Additionally LfNPs show a surprising ability to release the encapsulated drug at mild acidic condition that may trigger an enhanced localized drug release at the tumor site. 5-FU and TMZ show enhanced retention and improved cytotoxicity in melanoma and glioma cells respectively when delivered through LfNPs compared to their free forms. LfNPs were found to be very safe delivery systems and TMZ toxicity was substantially reduced when delivered via LfNPs compare to free form. We have shown that systemically administered LfNPs can cross the intact BBB in healthy mice and moreover delivery through LfNPs resulting in an enhanced and sustained intracellular concentration of TMZ in *in vitro* along with improving its *in vivo* pharmacokinetics and brain accumulation. TMZ-LfNPs treatment results in a significant tumor reduction, higher tumor cell apoptosis and improved median survival in glioma bearing mice.

- To overcome the GBM resistance against TMZ and to make them chemosensitize, combination of chemotherapy and gene therapy has been exploited. As the over expression AKB and mutation of p53 gene is linked with TMZ resistance, AKB-siRNA and plasmid p53 loaded Lf nanoparticles were developed. LfNPs found to protect siRNA and plasmid DNA against nucleases, increased serum stability, improves cellular uptake and gene silencing, facilitates the current TMZ based therapy by chemosensitizing resistant GBM. Also higher plasmid uptake and high gene expression in LfR positive cells potentiates the TMZ efficacy in resistant GBM tumor and provide survival benefits in glioma mice models.
- Prepared from natural and abundant protein, with no modifications, lactoferrin nanoparticles are very safe and efficient delivery platform for biologics.

7.2 Future directions

Current findings in the thesis require further evaluation for pre-clinical toxicology and bioequivalence studies to place LfNPs in consideration for clinical evaluation. Our research group is working in this direction.

Bibliography

Bibliography

[1] Pollock PM, Meltzer PS. Cancer: Lucky draw in the gene raffle. Nature. 2002;417:906-7.

[2] Hanahan D, Weinberg RA. Hallmarks of cancer: the next generation. cell. 2011;144:646-74.

[3] McKinnell RG. The biological basis of cancer: Cambridge University Press; 1998.

[4] Stein GS, Pardee AB. Cell cycle and growth control: biomolecular regulation and cancer: John Wiley & Sons; 2004;3-15.

[5] Sandru A, Voinea S, Panaitescu E, Blidaru A. Survival rates of patients with metastatic malignant melanoma. Journal of medicine and life. 2014;7:572.

[6] Purdy JA, Perez CA, Poortmans P. Technical Basis of Radiation Therapy: Practical Clinical Applications: Springer Berlin Heidelberg; 2012.

[7] Danyu M, Huile G, Wei G, Zhiqing P, Xinguo J, Jun C. Anti glioma effect of doxorubicin loaded liposomes modified with angiopep-2. African Journal of Pharmacy and Pharmacology. 2011;5:409-14.

[8] Riemenschneider MJ, Jeuken JW, Wesseling P, Reifenberger G. Molecular diagnostics of gliomas: state of the art. Acta neuropathologica. 2010;120:567-84.

[9] Marquet G, Dameron O, Saikali S, Mosser J, Burgun A. Grading glioma tumors using OWL-DL and NCI thesaurus. AMIA Annual Symposium Proceedings: American Medical Informatics Association; 2007;508-12.

[10] Zhang X, Zhang W, Cao W-D, Cheng G, Zhang Y-Q. Glioblastoma multiforme: Molecular characterization and current treatment strategy. Experimental and therapeutic medicine. 2012;3:9-14.

[11] Lawrence TS, Ten Haken RK, Giaccia A. Principles of radiation oncology. Cancer: principles and practice of oncology 8th ed Philadelphia: Lippincott Williams and Wilkins. 2008;2043-83.

[12] Prabha S, Zhou W-Z, Panyam J, Labhasetwar V. Size-dependency of nanoparticle-mediated gene transfection: studies with fractionated nanoparticles. International journal of pharmaceutics. 2002;244:105-15.

[13] Omidi Y, Hollins AJ, Drayton R, Akhtar S. Polypropylenimine dendrimer- gene expression changes: the effect of complexation with DNA, dendrimer generation and cell type. Journal of drug targeting. 2005;13:431-43.

[14] Prabha S, Labhasetwar V. Nanoparticle-mediated wild-type p53 gene delivery results in sustained antiproliferative activity in breast cancer cells. Molecular pharmaceutics. 2004;1:211-9.

[15] Dunne M, Corrigan O, Ramtoola Z. Influence of particle size and dissolution conditions on the degradation properties of polylactide-co-glycolide particles. Biomaterials. 2000;21:1659-68.

[16] Kwon GS. Polymeric micelles for delivery of poorly water-soluble compounds. Critical Reviews™ in Therapeutic Drug Carrier Systems. 2003;20.

[17] Stavrovskaya A. Cellular mechanisms of multidrug resistance of tumor cells. BIOCHEMISTRY C/C OF BIOKHIMIIA. 2000;65:95-106.

[18] Longley D, Johnston P. Molecular mechanisms of drug resistance. The Journal of pathology. 2005;205:275-92.

[19] Chabner BA, Roberts TG. Chemotherapy and the war on cancer. Nature Reviews Cancer. 2005;5:65-72.

[20] Sawyer AJ, Piepmeier JM, Saltzman WM. New methods for direct delivery of chemotherapy for treating brain tumors. Yale J Biol Med. 2006;79:141-52.

[21] Longley DB, Harkin DP, Johnston PG. 5-fluorouracil: mechanisms of action and clinical strategies. Nature Reviews Cancer. 2003;3:330-8.

[22] Di Paolo A, Danesi R, Falcone A, Cionini L, Vannozzi F, Masi G, et al. Relationship between 5-fluorouracil disposition, toxicity and dihydropyrimidine dehydrogenase activity in cancer patients. Annals of oncology : official journal of the European Society for Medical Oncology / ESMO. 2001;12:1301-6.

[23] Heggie GD, Sommadossi J-P, Cross DS, Huster WJ, Diasio RB. Clinical pharmacokinetics of 5-fluorouracil and its metabolites in plasma, urine, and bile. Cancer research. 1987;47:2203-6.

[24] Newlands ES, Blackledge GR, Slack JA, Rustin GJ, Smith DB, Stuart NS, et al. Phase I trial of temozolomide (CCRG 81045: M&B 39831: NSC 362856). British journal of cancer. 1992;65:287-91.

[25] Berrocal A, Perez Segura P, Gil M, Balana C, Garcia Lopez J, Yaya R, et al. Extended-schedule dose-dense temozolomide in refractory gliomas. Journal of neuro-oncology. 2010;96:417-22.

[26] Huang G, Zhang N, Bi X, Dou M. Solid lipid nanoparticles of temozolomide: potential reduction of cardial and nephric toxicity. International journal of pharmaceutics. 2008;355:314-20.

[27] Kim SS, Rait A, Kim E, DeMarco J, Pirollo KF, Chang EH. Encapsulation of temozolomide in a tumor-targeting nanocomplex enhances anti-cancer efficacy and reduces toxicity in a mouse model of glioblastoma. Cancer letters. 2015;369:250-8.

[28] Tentori L, Graziani G. Recent approaches to improve the antitumor efficacy of temozolomide. Current medicinal chemistry. 2009;16:245-57.

[29] Zhang J, FG Stevens M, D Bradshaw T. Temozolomide: mechanisms of action, repair and resistance. Current molecular pharmacology. 2012;5:102-14.

[30] Gabizon A, Shmeeda H, Barenholz Y. Pharmacokinetics of pegylated liposomal Doxorubicin: review of animal and human studies. Clinical pharmacokinetics. 2003;42:419-36.

[31] Mukherjee S, Ray S, Thakur RS. Solid lipid nanoparticles: a modern formulation approach in drug delivery system. Indian journal of pharmaceutical sciences. 2009;71:349-58.

[32] Weber C, Coester C, Kreuter J, Langer K. Desolvation process and surface characterisation of protein nanoparticles. International journal of pharmaceutics. 2000;194:91-102.

[33] Kratz F. Albumin as a drug carrier: design of prodrugs, drug conjugates and nanoparticles. Journal of controlled release. 2008;132:171-83.

[34] Lohcharoenkal W, Wang L, Chen YC, Rojanasakul Y. Protein nanoparticles as drug delivery carriers for cancer therapy. BioMed research international. 2014;2014:180549.

[35] Latha MS, Lal AV, Kumary TV, Sreekumar R, Jayakrishnan A. Progesterone release from glutaraldehyde cross-linked casein microspheres: in vitro studies and in vivo response in rabbits. Contraception. 2000;61:329-34.

[36] Metzmacher I, Radu F, Bause M, Knabner P, Friess W. A model describing the effect of enzymatic degradation on drug release from collagen minirods. European journal of pharmaceutics and biopharmaceutics 2007;67:349-60.

[37] Maeda M, Tani S, Sano A, Fujioka K. Microstructure and release characteristics of the minipellet, a collagen-based drug delivery system for controlled release of protein drugs. Journal of controlled release.1999;62:313-24.

[38] Kuijpers AJ, van Wachem PB, van Luyn MJ, Brouwer LA, Engbers GH, Krijgsveld J, et al. In vitro and in vivo evaluation of gelatin-chondroitin sulphate hydrogels for controlled release of antibacterial proteins. Biomaterials. 2000;21:1763-72.

[39] Muvaffak A, Gurhan I, Hasirci N. Cytotoxicity of 5-fluorouracil entrapped in gelatin microspheres. Journal of microencapsulation. 2004;21:293-306.

[40] Ahsan SM, Rao CM. Structural studies on aqueous gelatin solutions: Implications in designing a thermo-responsive nanoparticulate formulation. International journal of biological macromolecules. 2017;95:1126-34.

[41] Flenniken ML, Liepold LO, Crowley BE, Willits DA, Young MJ, Douglas T. Selective attachment and release of a chemotherapeutic agent from the interior of a protein cage architecture. Chemical communications. 2005:447-9.

[42] Furgeson DY, Dreher MR, Chilkoti A. Structural optimization of a "smart" doxorubicin-polypeptide conjugate for thermally targeted delivery to solid tumors. Journal of controlled release. 2006;110:362-9.

[43] Megeed Z, Haider M, Li D, O'Malley BW, Jr., Cappello J, Ghandehari H. In vitro and in vivo evaluation of recombinant silk-elastinlike hydrogels for cancer gene therapy. Journal of controlled release. 2004;94:433-45.

[44] Ahmed F, Ali MJ, Kondapi AK. Carboplatin loaded protein nanoparticles exhibit improve anti-proliferative activity in retinoblastoma cells. International journal of biological macromolecules. 2014;70:572-82.

[45] Golla K, Cherukuvada B, Ahmed F, Kondapi AK. Efficacy, safety and anticancer activity of protein nanoparticle-based delivery of doxorubicin through intravenous administration in rats. PloS one. 2012;7:e51960.

[46] Kumari S, Kondapi AK. Lactoferrin nanoparticle mediated targeted delivery of 5-fluorouracil for enhanced therapeutic efficacy. International journal of biological macromolecules. 2016;95:232-7.

[47] Kumar P, Lakshmi YS, C B, Golla K, Kondapi AK. Improved Safety, Bioavailability and Pharmacokinetics of Zidovudine through Lactoferrin Nanoparticles during Oral Administration in Rats. PloS one. 2015;10:e0140399.

[48] Sinha R, Kim GJ, Nie S, Shin DM. Nanotechnology in cancer therapeutics: bioconjugated nanoparticles for drug delivery. Molecular cancer therapeutics. 2006;5:1909-17.

[49] Haley B, Frenkel E. Nanoparticles for drug delivery in cancer treatment. Urologic Oncology: Seminars and original investigations: Elsevier; 2008. p. 57-64.

[50] Pelicano H, Martin DS, Xu RH, Huang P. Glycolysis inhibition for anticancer treatment. Oncogene. 2006;25:4633-46.

[51] Yatvin MB, Kreutz W, Horwitz BA, Shinitzky M. pH-sensitive liposomes: possible clinical implications. Science. 1980;210:1253-5.

[52] Gottesman MM, Fojo T, Bates SE. Multidrug resistance in cancer: role of ATP-dependent transporters. Nature reviews Cancer. 2002;2:48-58.

[53] Bareford LM, Swaan PW. Endocytic mechanisms for targeted drug delivery. Advanced drug delivery reviews. 2007;59:748-58.

[54] Tyagi N, Ghosh PC. Folate receptor mediated targeted delivery of ricin entrapped into sterically stabilized liposomes to human epidermoid carcinoma (KB) cells: effect of monensin intercalated into folate-tagged liposomes. European Journal of Pharmaceutical Sciences. 2011;43:343-53.

[55] Werner ME, Karve S, Sukumar R, Cummings ND, Copp JA, Chen RC, et al. Folate-targeted nanoparticle delivery of chemo- and radiotherapeutics for the treatment of ovarian cancer peritoneal metastasis. Biomaterials. 2011;32:8548-54.

[56] Wang S, Low PS. Folate-mediated targeting of antineoplastic drugs, imaging agents, and nucleic acids to cancer cells. Journal of Controlled Release. 1998;53:39-48.

[57] Li X, Ding L, Xu Y, Wang Y, Ping Q. Targeted delivery of doxorubicin using stealth liposomes modified with transferrin. International journal of pharmaceutics. 2009;373:116-23.

[58] Kobayashi T, Ishida T, Okada Y, Ise S, Harashima H, Kiwada H. Effect of transferrin receptor-targeted liposomal doxorubicin in P-glycoprotein-mediated drug resistant tumor cells. International journal of pharmaceutics. 2007;329:94-102.

[59] Sahoo SK, Ma W, Labhasetwar V. Efficacy of transferrin-conjugated paclitaxel-loaded nanoparticles in a murine model of prostate cancer. International journal of cancer. 2004;112:335-40.

[60] Pulkkinen M, Pikkarainen J, Wirth T, Tarvainen T, Haapa-aho V, Korhonen H, et al. Three-step tumor targeting of paclitaxel using biotinylated PLA-PEG nanoparticles and avidin-biotin technology: Formulation development and in vitro anticancer activity. European journal of pharmaceutics and biopharmaceutics. 2008;70:66-74.

[61] Zhang ZH, Wang XP, Ayman WY, Munyendo WL, Lv HX, Zhou JP. Studies on lactoferrin nanoparticles of gambogic acid for oral delivery. Drug delivery. 2013;20:86-93.

[62] Su Z, Xing L, Chen Y, Xu Y, Yang F, Zhang C, et al. Lactoferrin-modified poly(ethylene glycol)-grafted BSA nanoparticles as a dual-targeting carrier for treating brain gliomas. Molecular pharmaceutics. 2014;11:1823-34.

[63] Huang R, Ke W, Han L, Liu Y, Shao K, Jiang C, et al. Lactoferrin-modified nanoparticles could mediate efficient gene delivery to the brain in vivo. Brain research bulletin. 2010;81:600-4.

[64] Tseng C-L, Su W-Y, Yen K-C, Yang K-C, Lin F-H. The use of biotinylated-EGF-modified gelatin nanoparticle carrier to enhance cisplatin accumulation in cancerous lungs via inhalation. Biomaterials. 2009;30:3476-85.

[65] Hadjipanayis CG, Machaidze R, Kaluzova M, Wang L, Schuette AJ, Chen H, et al. EGFRvIII antibody-conjugated iron oxide nanoparticles for magnetic resonance imaging-guided convection-enhanced delivery and targeted therapy of glioblastoma. Cancer research. 2010;70:6303-12.

[66] Liu D, Liu F, Liu Z, Wang L, Zhang N. Tumor specific delivery and therapy by double-targeted nanostructured lipid carriers with anti-VEGFR-2 antibody. Molecular pharmaceutics. 2011;8:2291-301.

[67] Han HD, Mangala LS, Lee JW, Shahzad MM, Kim HS, Shen D, et al. Targeted gene silencing using RGD-labeled chitosan nanoparticles. Clinical cancer research. 2010;16:3910-22.

[68] Kim KH, Dmitriev I, O'Malley JP, Wang M, Saddekni S, You Z, et al. A phase I clinical trial of Ad5.SSTR/TK.RGD, a novel infectivity-enhanced bicistronic adenovirus, in patients with recurrent gynecologic cancer. Clinical cancer research. 2012;18:3440-51.

[69] Jin H, Lovell JF, Chen J, Lin Q, Ding L, Ng KK, et al. Mechanistic insights into LDL nanoparticle-mediated siRNA delivery. Bioconjugate chemistry. 2011;23:33-41.

[70] Corbin IR, Chen J, Li H, Cao W, Zheng G. Functionalizing low-density lipoprotein nanoparticles for in vivo near-infrared optical imaging of cancer. European Conference on Biomedical Optics: Optical Society of America; 2007;6626:1-7.

[71] Banerjee R, Tyagi P, Li S, Huang L. Anisamide-targeted stealth liposomes: A potent carrier for targeting doxorubicin to human prostate cancer cells. International journal of cancer. 2004;112:693-700.

[72] Zensi A, Begley D, Pontikis C, Legros C, Mihoreanu L, Wagner S, et al. Albumin nanoparticles targeted with Apo E enter the CNS by transcytosis and are delivered to neurones. Journal of Controlled Release. 2009;137:78-86.

[73] Kreuter J. Nanoparticulate systems for brain delivery of drugs. Advanced drug delivery reviews. 2001;47:65-81.

[74] Sharma G, Modgil A, Layek B, Arora K, Sun C, Law B, et al. Cell penetrating peptide tethered bi-ligand liposomes for delivery to brain in vivo: Biodistribution and transfection. Journal of Controlled Release. 2013;167:1-10.

[75] Qian ZM, Li H, Sun H, Ho K. Targeted drug delivery via the transferrin receptor-mediated endocytosis pathway. Pharmacological reviews. 2002;54:561-87.

[76] Friden PM, Walus LR, Musso GF, Taylor MA, Malfroy B, Starzyk RM. Anti-transferrin receptor antibody and antibody-drug conjugates cross the blood-brain barrier. Proceedings of the National Academy of Sciences. 1991;88:4771-5.

[77] Farnaud S, Evans RW. Lactoferrin - a multifunctional protein with antimicrobial properties. Molecular immunology. 2003;40:395-405.

[78] Rodriguez-Franco D, Vazquez-Moreno L, Ramos-Clamont MG. Antimicrobial mechanisms and potential clinical application of lactoferrin. Revista latinoamericana de microbiologia. 2004;47:102-11.

[79] Jiang R, Lopez V, Kelleher SL, Lönnerdal B. Apo- and holo-lactoferrin are both internalized by lactoferrin receptor via clathrin-mediated endocytosis but differentially affect ERK-signaling and cell proliferation in caco-2 cells. Journal of cellular physiology. 2011;226:3022-31.

[80] Huang R, Ke W, Liu Y, Jiang C, Pei Y. The use of lactoferrin as a ligand for targeting the polyamidoamine-based gene delivery system to the brain. Biomaterials. 2008;29:238-46.

[81] Fang JH, Lai YH, Chiu TL, Chen YY, Hu SH, Chen SY. Magnetic core-shell nanocapsules with dual-targeting capabilities and co-delivery of multiple drugs to treat brain gliomas. Advanced healthcare materials. 2014;3:1250-60.

[82] Krishna AD, Mandraju RK, Kishore G, Kondapi AK. An efficient targeted drug delivery through apotransferrin loaded nanoparticles. PloS one. 2009;4:e7240.

[83] Bollimpelli VS, Kumar P, Kumari S, Kondapi AK. Neuroprotective effect of curcumin-loaded lactoferrin nano particles against rotenone induced neurotoxicity. Neurochemistry international. 2016;95:37-45.

[84] Liang CC, Park AY, Guan JL. In vitro scratch assay: a convenient and inexpensive method for analysis of cell migration in vitro. Nature protocols. 2007;2:329-33.

[85] Spitzer N, Sammons GS, Price EM. Autofluorescent cells in rat brain can be convincing impostors in green fluorescent reporter studies. Journal of neuroscience methods. 2011;197:48-55.

[86] Kim SS, Rait A, Rubab F, Rao AK, Kiritsy MC, Pirollo KF, et al. The clinical potential of targeted nanomedicine: delivering to cancer stem-like cells. Molecular therapy. 2014;22:278-91.

[87] Berwick M, Erdei E, Hay J. Melanoma epidemiology and public health. Dermatologic clinics. 2009;27:205-14.

[88] Lens MB, Dawes M. Global perspectives of contemporary epidemiological trends of cutaneous malignant melanoma. The British journal of dermatology. 2004;150:179-85.

[89] Soengas MS, Lowe SW. Apoptosis and melanoma chemoresistance. Oncogene. 2003;22:3138-51.

[90] Longley DB, Harkin DP, Johnston PG. 5-fluorouracil: mechanisms of action and clinical strategies. Nature reviews Cancer. 2003;3:330-8.

[91] Heggie GD, Sommadossi JP, Cross DS, Huster WJ, Diasio RB. Clinical pharmacokinetics of 5-fluorouracil and its metabolites in plasma, urine, and bile. Cancer research. 1987;47:2203-6.

[92] Zhao Z, Meng H, Wang N, Donovan MJ, Fu T, You M, et al. A controlled-release nanocarrier with extracellular pH value driven tumor targeting and translocation for drug delivery. Angewandte Chemie. 2013;52:7487-91.

[93] Wang G, Uludag H. Recent developments in nanoparticle-based drug delivery and targeting systems with emphasis on protein-based nanoparticles. Expert opinion on drug delivery. 2008;5:499-515.

[94] Park K. Albumin: a versatile carrier for drug delivery. Journal of controlled release. 2012;157:3.

[95] Coester CJ, Langer K, van Briesen H, Kreuter J. Gelatin nanoparticles by two step desolvation--a new preparation method, surface modifications and cell uptake. Journal of microencapsulation. 2000;17:187-93.

[96] Bessa PC, Machado R, Nurnberger S, Dopler D, Banerjee A, Cunha AM, et al. Thermoresponsive self-assembled elastin-based nanoparticles for delivery of BMPs. Journal of controlled release. 2010;142:312-8.

[97] Lim LY, Koh PY, Somani S, Al Robaian M, Karim R, Yean YL, et al. Tumor regression following intravenous administration of lactoferrin- and lactoferricin-bearing dendriplexes. Nanomedicine : nanotechnology, biology and medicine. 2015;11:1445-54.

[98] Qiao H, Li J, Wang Y, Ping Q, Wang G, Gu X. Synthesis and characterization of multi-functional linear-dendritic block copolymer for intracellular delivery of antitumor drugs. International journal of pharmaceutics. 2013;452:363-73.

[99] Alexis F, Pridgen E, Molnar LK, Farokhzad OC. Factors affecting the clearance and biodistribution of polymeric nanoparticles. Molecular pharmaceutics. 2008;5:505-15.

[100] Arica B, Calis S, Kas H, Sargon M, Hincal A. 5-Fluorouracil encapsulated alginate beads for the treatment of breast cancer. International journal of pharmaceutics. 2002;242:267-9.

[101] Suzuki YA, Lopez V, Lonnerdal B. Mammalian lactoferrin receptors: structure and function. Cellular and molecular life sciences. 2005;62:2560-75.

[102] Sreedhara A, Flengsrud R, Langsrud T, Kaul P, Prakash V, Vegarud GE. Structural characteristic, pH and thermal stabilities of apo and holo forms of caprine and bovine lactoferrins. Biometals. 2010;23:1159-70.

[103] Taal W, Bromberg JE, van den Bent MJ. Chemotherapy in glioma. CNS oncology. 2015;4:179-92.

[104] Khasraw M, Lassman AB. Advances in the treatment of malignant gliomas. Current oncology reports. 2010;12:26-33.

[105] Young RM, Jamshidi A, Davis G, Sherman JH. Current trends in the surgical management and treatment of adult glioblastoma. Annals of translational medicine. 2015;3:121.

[106] Oberoi RK, Parrish KE, Sio TT, Mittapalli RK, Elmquist WF, Sarkaria JN. Strategies to improve delivery of anticancer drugs across the blood-brain barrier to treat glioblastoma. Neuro-oncology. 2016;18:27-36.

[107] Chamberlain MC. Temozolomide: therapeutic limitations in the treatment of adult high-grade gliomas. Expert review of neurotherapeutics. 2010;10:1537-44.

[108] Fang C, Wang K, Stephen ZR, Mu Q, Kievit FM, Chiu DT, et al. Temozolomide nanoparticles for targeted glioblastoma therapy. ACS applied materials & interfaces. 2015;7:6674-82.

[109] Kang T, Jiang M, Jiang D, Feng X, Yao J, Song Q, et al. Enhancing Glioblastoma-Specific Penetration by Functionalization of Nanoparticles with an Iron-Mimic Peptide Targeting Transferrin/Transferrin Receptor Complex. Molecular pharmaceutics. 2015;12:2947-61.

[110] Bertucci A, Prasetyanto EA, Septiadi D, Manicardi A, Brognara E, Gambari R, et al. Combined Delivery of Temozolomide and Anti-miR221 PNA Using Mesoporous Silica Nanoparticles Induces Apoptosis in Resistant Glioma Cells. Small. 2015;11:5687-95.

[111] Ananta JS, Paulmurugan R, Massoud TF. Temozolomide-loaded PLGA nanoparticles to treat glioblastoma cells: a biophysical and cell culture evaluation. Neurological research. 2016;38:51-9.

[112] Lopez SA, Nonnecke EB, Lönnerdal BL. The lactoferrin receptor is differentially expressed across several human epithelial cell types. The FASEB Journal. 2012;26:644.5-.5.

[113] Elfinger M, Maucksch C, Rudolph C. Characterization of lactoferrin as a targeting ligand for nonviral gene delivery to airway epithelial cells. Biomaterials. 2007;28:3448-55.

[114] Ananta JS, Paulmurugan R, Massoud TF. Nanoparticle-delivered antisense MicroRNA-21 enhances the effects of temozolomide on glioblastoma cells. Molecular pharmaceutics. 2015;12:4509-17.

[115] Fillebeen C, Descamps L, Dehouck MP, Fenart L, Benaissa M, Spik G, et al. Receptor-mediated transcytosis of lactoferrin through the blood-brain barrier. The Journal of biological chemistry. 1999;274:7011-7.

[116] Taverna P, Catapano CV, Citti L, Bonfanti M, D'Incalci M. Influence of O6-methylguanine on DNA damage and cytotoxicity of temozolomide in L1210 mouse leukemia sensitive and resistant to chloroethylnitrosoureas. Anticancer Drugs. 1992;3:401-5.

[117] Gupta V, Su YS, Wang W, Kardosh A, Liebes LF, Hofman FM, et al. Enhancement of glioblastoma cell killing by combination treatment with temozolomide and tamoxifen or hypericin. Neurosurgical focus. 2006;20:E20.

[118] Bocangel DB, Finkelstein S, Schold SC, Bhakat KK, Mitra S, Kokkinakis DM. Multifaceted resistance of gliomas to temozolomide. Clinical Cancer Research. 2002;8:2725-34.

[119] McFarland TJ, Zhang Y, Appukuttan B, Stout JT. Gene therapy for proliferative ocular diseases. Expert opinion on biological therapy. 2004;4:1053-8.

[120] Morrissey DV, Lockridge JA, Shaw L, Blanchard K, Jensen K, Breen W, et al. Potent and persistent in vivo anti-HBV activity of chemically modified siRNAs. Nature biotechnology. 2005;23:1002-7.

[121] Ptasznik A, Nakata Y, Kalota A, Emerson SG, Gewirtz AM. Short interfering RNA (siRNA) targeting the Lyn kinase induces apoptosis in primary, and drug-resistant, BCR-ABL1 (+) leukemia cells. Nature medicine. 2004;10:1187-9.

[122] Akinc A, Zumbuehl A, Goldberg M, Leshchiner ES, Busini V, Hossain N, et al. A combinatorial library of lipid-like materials for delivery of RNAi therapeutics. Nature biotechnology. 2008;26:561-9.

[123] Dar GH, Gopal V, Rao NM. Systemic delivery of stable siRNA-encapsulating lipid vesicles: optimization, biodistribution, and tumor suppression. Molecular pharmaceutics. 2015;12:610-20.

[124] Tatsuka M, Katayama H, Ota T, Tanaka T, Odashima S, Suzuki F, et al. Multinuclearity and increased ploidy caused by overexpression of the aurora-and Ipl1-like midbody-associated protein mitotic kinase in human cancer cells. Cancer research. 1998;58:4811-6.

[125] Fu J, Bian M, Jiang Q, Zhang C. Roles of Aurora kinases in mitosis and tumorigenesis. Molecular Cancer Research. 2007;5:1-10.

[126] Katayama H, Sasai K, Kawai H, Yuan Z-M, Bondaruk J, Suzuki F, et al. Phosphorylation by aurora kinase A induces Mdm2-mediated destabilization and inhibition of p53. Nature genetics. 2004;36:55-62.

[127] Gully CP, Velazquez-Torres G, Shin J-H, Fuentes-Mattei E, Wang E, Carlock C, et al. Aurora B kinase phosphorylates and instigates degradation of p53. Proceedings of the National Academy of Sciences. 2012;109:E1513-E22.

[128] Ota T, Suto S, Katayama H, Han Z-B, Suzuki F, Maeda M, et al. Increased mitotic phosphorylation of histone H3 attributable to AIM-1/Aurora-B overexpression contributes to chromosome number instability. Cancer Research. 2002;62:5168-77.

[129] Tsuno T, Natsume A, Katsumata S, Mizuno M, Fujita M, Osawa H, et al. Inhibition of Aurora-B function increases formation of multinucleated cells in p53 gene deficient cells and enhances anti-tumor effect of temozolomide in human glioma cells. Journal of neuro-oncology. 2007;83:249-58.

[130] Fang B, Guo HY, Zhang M, Jiang L, Ren FZ. The six amino acid antimicrobial peptide bLFcin6 penetrates cells and delivers siRNA. FEBS Journal. 2013;280:1007-17.

[131] Lo SL, Wang S. An endosomolytic Tat peptide produced by incorporation of histidine and cysteine residues as a nonviral vector for DNA transfection. Biomaterials. 2008;29:2408-14.

[132] Ma J, Murphy M, O'Dwyer PJ, Berman E, Reed K, Gallo JM. Biochemical changes associated with a multidrug-resistant phenotype of a human glioma cell line with temozolomide-acquired resistance. Biochemical pharmacology. 2002;63:1219-28.

[133] Bocangel D, Sengupta S, Mitra S, Bhakat KK. p53-Mediated down-regulation of the human DNA repair gene O6-methylguanine-DNA methyltransferase (MGMT) via interaction with Sp1 transcription factor. Anticancer research. 2009;29:3741-50.

[134] Roos WP, Kaina B. DNA damage-induced cell death: from specific DNA lesions to the DNA damage response and apoptosis. Cancer letters. 2013;332:237-48.

[135] Quinn JA, Desjardins A, Weingart J, Brem H, Dolan ME, Delaney SM, et al. Phase I trial of temozolomide plus O 6-benzylguanine for patients with recurrent or progressive malignant glioma. Journal of Clinical Oncology. 2005;23:7178-87.

[136] Srivenugopal KS, Shou J, Mullapudi SR, Lang FF, Rao JS, Ali-Osman F. Enforced expression of wild-type p53 curtails the transcription of the O6-methylguanine-DNA methyltransferase gene in human tumor cells and enhances their sensitivity to alkylating agents. Clinical cancer research. 2001;7:1398-409.

[137] Cerrato JA, Yung WA, Liu T-J. Introduction of mutant p53 into a wild-type p53-expressing glioma cell line confers sensitivity to Ad-p53-induced apoptosis. Neuro-oncology. 2001;3:113-22.

[138] Mao H-Q, Roy K, Troung-Le VL, Janes KA, Lin KY, Wang Y, et al. Chitosan-DNA nanoparticles as gene carriers: synthesis, characterization and transfection efficiency. Journal of controlled release. 2001;70:399-421.

[139] Thierry A, Rabinovich P, Peng B, Mahan L, Bryant J, Gallo R. Characterization of liposome-mediated gene delivery: expression, stability and pharmacokinetics of plasmid DNA. Gene therapy. 1997;4:226-37.

[140] Luo D, Saltzman WM. Synthetic DNA delivery systems. Nature biotechnology. 2000;18:33-7.

[141] Oh S, Rih J, Kwon H, Kim S, Yim J. Lactoferrin as a gene delivery vehicle to hepatocytes. Experimental and Molecular Medicine. 1997;29:111-6.

[142] Yamamoto Y, Nagasaki Y, Kato Y, Sugiyama Y, Kataoka K. Long-circulating poly (ethylene glycol)–poly (d, l-lactide) block copolymer micelles with modulated surface charge. Journal of Controlled Release. 2001;77:27-38.

Publications

List of Publications

Manuscripts published:

1. **Kumari, S**. and A. K. Kondapi (2016). Lactoferrin nanoparticle mediated targeted delivery of 5-fluorouracil for enhanced therapeutic efficacy. **Int J Biol Macromol 95**: 232-237.

2. **Sonali K.**, A. K. Kondapi (2016), Cancer Nanotechnology: Current Status and Glimpse into the future, **International journal of pharmaceutical research (8);3** (ISSN 0975-2366)

3. Bollimpelli, V. S., P. Kumar, **S. Kumari** and A. K. Kondapi (2016). "Neuroprotective effect of curcumin-loaded lactoferrin nano particles against rotenone induced neurotoxicity." **Neurochem Int** 95: 37-45.

Manuscripts communicated:

1. **Sonali Kumari,** saad m ahsan, jerald M kumar,Nalam M Rao & A.K.Kondapi. Overcoming blood brain barrier with a dual purpose Temozolomide loaded Lactoferrin nanoparticles for combating glioma.
   Journal Name: **Scientific reports** Manuscript ID: SREP-17-12433

Manuscripts finalized:

1. **Sonali Kumari**, Nalam M Rao, A.K.Kondapi. A target specific AKB-siRNA loaded Lf nanoparticles, their antitumor effects and chemosensetization against TMZ resistant GBM

2. **Sonali Kumari**, A.K.Kondapi. Lactoferrin nanoparticles for the targeted delivery of plasmid DNA

3. Farhan ahmad, **Sonali Kumari**, A.K.Kondapi. Evaluation of antiprolifeartive activity, saftey and biodistribution of oxaliplatin and 5 flourouracil loaded lactoferrin nanoparticles : an *in vitro and in vivo* study.

International Journal of Biological Macromolecules 95 (2017) 232–237

Contents lists available at ScienceDirect

International Journal of Biological Macromolecules

journal homepage: www.elsevier.com/locate/ijbiomac

Lactoferrin nanoparticle mediated targeted delivery of 5-fluorouracil for enhanced therapeutic efficacy

Sonali Kumari, Anand K. Kondapi*

Department of Biotechnology and Bioinformatics, School of Life Sciences, University of Hyderabad, Prof. C. R. Rao Road, Gachibowli, Hyderabad 500 046, Telangana, India

ARTICLE INFO

Article history:
Received 16 September 2016
Received in revised form 28 October 2016
Accepted 29 October 2016
Available online 15 November 2016

Keywords:
Targeted drug delivery
Lactoferrin nanoparticle
Fluorouracil
Melanoma
pH responsive

ABSTRACT

Malignant melanoma is an aggressive form of skin cancer with high mortality rates. Common treatments for malignant melanoma involve a combination of radiotherapy and chemotherapy with fluorouracil (5-FU). A major challenge with melanoma treatment is active resistance to chemotherapeutic drugs. Superior treatment outcome lies on balance involving optimum therapeutic doses and the side effects associated with dose escalation. The study aimed to efficiently entrap 5-FU in lactoferrin nanoparticles (LfNPs) in an attempt to enhance its therapeutic efficacy. 5-FU loaded lactoferrin nanoparticles (5-FU-LfNPs) were prepared by sol-oil method with a narrow size distribution of 150 ± 20 nm 5-FU-LfNPs exhibits high encapsulation efficiency ($64 \pm 2.3\%$) and increased storage stability at 4 °C. Competitive ligand binding and lysosomal colocalization studies suggested a receptor mediated uptake for LfNPs internalization in B16F10 cells. Moreover, 5-FU-LfNPs show a pH dependent drug release similar to endosomal pH (pH 5 and 6). In addition compared to free 5-FU, 5-FU- LfNPs showed a higher intracellular uptake, prolonged retention and improved cytotoxicity (2.7-fold) in melanoma cells (B16F10). To conclude, LfNPs represent a superior nano-carrier for the targeted delivery of 5-FU in melanoma cells intended for the efficient treatment of melanoma though detailed *in vivo* investigations are warranted.

© 2016 Elsevier B.V. All rights reserved.

1. Introduction

Malignant melanoma is a belligerent form of skin cancer with high mortality rates. There has been a rapid increase in the occurrence of malignant melanoma in the industrialized countries for the last 30 years [1]. As per the American Cancer Society's estimates, around 76,380 new melanoma cases will be diagnosed in 2016, with a predictable mortality of 10,130 people. It's one of the most common cancers in young adults (especially young women). Despite the fact that there is a greater understanding of the risk factors, along with the genetic and epigenetic causes of melanoma, the mortality rate from melanoma is quite predominant compared to any other types of cancer [2]. Risk factors of melanoma take account of gene polymorphism, skin type, many moles on body or unusual moles, family history, a previous melanoma occurrence, sensitivity towards sun, weakened immune system, and excessive ultraviolet (UV) exposure. Common treatments for malignant melanoma involve surgical procedures, chemotherapy and radiotherapy. Despite these stated treatments, at least one third of patients with early-stage melanoma develop metastases, and the prognosis of metastatic melanoma remains dismal. Alarmingly, studies show that the melanoma patients have a median survival of approximately 6–8 months only. Moreover, it has been grimly observed that less than 5% of patients survive for a maximum of five years. Various chemotherapeutic drugs have been ineffective against melanoma cells as these cells become resistance to apoptotic pathways and leads to poor clinical outcome [3]. 5-FU is one of the oldest standard drug used broadly for solid tumors, is a fluorinated analog of pyrimidine base uracil, which gets converted intracellularly to its active form – fluorodeoxyuridine monophophate. This active form inhibits thymidylate synthase (TS) enzyme, required for the synthesis of thymidine, a nucleoside vital for DNA replication. This results in apoptosis of rapidly dividing cancerous cells due to thymine deficiency [4]. Although 5-FU widely used for melanoma, it causes severe systemic toxicity including gastrointestinal, hematological, neural, cardiac, and dermatological origin [5]. 5-FU is sparingly soluble in water and its bioavailability is greatly limited in the blood, liver, and other organs due to rapid metabolism by dihydropyramidine dehydrogenase enzyme. 5-FU has a plasma half-life of only 8–20 min [6]. Complications associated with 5-FU toxicity further limits the effectiveness of the treatment outcome and add detrimental impact on the patient's

* Corresponding author.
E-mail address: akondapi@gmail.com (A.K. Kondapi).

http://dx.doi.org/10.1016/j.ijbiomac.2016.10.110
0141-8130/© 2016 Elsevier B.V. All rights reserved.

quality of life. Therefore, an efficient delivery system is vital to improve the bioavailability and safe delivery of 5-FU.

Nanoparticle based treatments have offered promising clinical outcomes due to their tunable pharmacokinetic properties like prolonged half life, larger surface to volume ratio, enhanced drug solubility, and the likelihood for controlled release [7]. In particular, nanoparticles can be exploited for the targeted delivery of anticancer drugs at the tumor site. Target-specific nanoparticles render a new dimension to the standard conventional chemotherapy. A myriad of biomaterials including lipids, polymers, chatoyant and proteins has been used as matrix for nanoparticles formulation. Amongst which proteins, have garnered a significant interest as biomaterials due to three major associated inherent advantages. Firstly, proteins are biocompatible and show biodegradability [8]. Although some proteins have minor immunogenicity [9], no substance-related toxicity was found as in case of engineered nanoparticles such as carbon annotates, dendrimers and quantum dots [10]. Secondly, drug-binding, imaging or targeting becomes much simpler in case of proteins as it offers numerous moieties for modification. Thirdly, due to the existence of charged groups in proteins they can be a better matrix in which drugs can be physically entrapped. There are many proteins *viz.* albumin [11], gelatin [12], transferrin [13] and elastin [14] which have been used as nanocarriers for several drugs. Nanoparticles can target tumor tissues both actively and passively. The passive targeting is by enhanced permeability and retention effect whereas; active targeting is achieved by functionalization with ligands.

Lactoferrin (Lf), belong to transferrin family with a molecular weight of 80 KDa, is an iron carrying basic protein with numerous physiological roles. Due to its unique antimicrobial, antifungal, anticancer and anti-inflammatiory properties, lactoferrin seems to have great potential in clinical sector. It has been used as a ligand for targeting several nanocarriers [15,16] but none of them utilized Lf as a matrix.

This study aimed to develop and optimize Lf nanoparticles (LfNP) to enhance the therapeutic efficacy of 5-FU in melanoma cells (B16F10) *in vitro.* 5-FU loaded Lf nanoparticles (5-FU-LfNPs) were prepared and characterized by TEM, SEM and DLS. Their loading efficiency, stability and *in vitro* drug release profile were studied. In addition to this, particles uptake mechanism, comparative cytotoxicity of free 5-FU and 5-FU-LfNPs were investigated in B16F10 cells.

2. Materials and methods

2.1. Materials

Lactoferrin and olive oil used for nanoparticles preparation were purchased from Symbiotic (USA) and Leonardo (Italy), respectively. B16F10 melanoma cells were obtained from National Center for Cell Science (NCCS), Pune. 5-Fluorouracil and Rhodamine123 were procured from Sigma (St. Louis, MO). MTT ((3-(4, 5-dimethylthiazol-2-yl)-2, 5-diphenyl tetrazoliumbromide) was purchased from Calbiochem (USA). All other chemicals and reagents were of analytical grade.

2.2. Preparation of 5- FU-LfNPs

5-FU-LfNPs were prepared by sol-oil method as described earlier [13]. Briefly, 5-FU was mixed with Lf in a ratio of 1:2 (w/w) and incubated for 30 min on ice and then slowly added to 15 ml of olive oil at 4 °C with continuous dispersion by vortexing, followed by sonication (Ultrasonic homogenizer 300 V/T, Biologics Inc., Manassas, Virginia, USA) at 4 °C. The resulting mixture was snap frozen and then thawed over ice. The particles were pelleted by centrifugation at 30,000 × *g* for 20 min and the pellet was extensively washed thrice with diethyl ether followed by PBS to remove excess oil and free 5-FU. Finally the pellet was dispersed in phosphate buffered saline (PBS) and either stored at 4 °C or lyophilized as per the experimental constraint. For fluorescent labeling, blank lactoferrin nanoparticles (LfNPs) were prepared by similar procedure as stated above without the addition of 5-FU and then was incubated with 50 μl of 20% Rhodamine123 for overnight at 4 °C to make Rhodamine123 tagged lactoferrin nanoparticles (LfNPs-Rh123).

2.3. Physico-chemical characterization of nanoparticles

Transmission Electron Microscopy (TEM) and Scanning electron microscope (SEM) analysis was carried out to study the morphology and size of nanoparticles. For TEM analysis, LfNPs were then placed on carbon coated copper 300 mesh grids, air dried and stained using 1% aqueous solution of uranyl acetate for 1 min. The samples were examined using Transmission Electron Microscope (JEM-2100, M/S Jeol Limited, Tachikawa, Tokyo, Japan). SEM analysis was carried out by coating nanoparticles onto the glass slides. Afterward slides were sputtered by silver paint. Particles were scanned in (PHILIPS Scanning electron microscope) and data was analyzed according to manufacturer's instruction.

The hydrodynamic diameter, poly dispersity index (PDI) and zeta potential were analyzed by nanoparticles analyzer system (Horiba Scientific, USA). For the *in vitro* storage stability studies, 5-FU-LfNPs were prepared as described earlier, and stored in PBS at 4 °C. At regular time intervals, aliquots were withdrawn and analyzed for their hydrodynamic diameter using a nanoparticle analyzer system (Horiba Scientific, USA) over a period of 5 weeks. Further particle stability is tested in 10% serum at room temperature for several hours using the above mentioned procedure.

2.4. Fourier transform infrared (FT-IR) spectroscopy

The infra-red spectra of free Lf, LfNPs, free 5-FU and 5-FU-LfNPs were obtained at a resolution of 4 cm^{-1} in a FT-IR Spectrometer (Bruker Aplha T, Bruker Optik, Ettingen Germany), equipped with a single reflection diamond attenuated total reflectance accessory. A drop of nanoparticles was air dried on the surface of diamond crystal element by solvent evaporation followed with recording of 64 scans at 200 cm^{-1}/min and averaged.

2.5. Determination of drug encapsulation efficiency and drug loading content

The encapsulation efficiency was determined by resuspending 0.5 mg of 5-FU-LfNPs in 1 ml PBS (0.01 M, pH 5.0) and incubated for 4 h at 37 °C on a rocker. Equal volume of acetonitrile was then added to precipitate the protein, followed by centrifugation at 30,000 × *g* for 15 min. The supernatant was collected and filtered through a 0.2 μm syringe filter and quantified using UV–vis spectrophotometer (JASCO) at 254 nm. All experiments were performed in triplicates. Encapsulation efficiency and drug loading content was calculated by following formula

$$\text{Encapsulation efficiency}\,(\%) = \frac{\text{weight of drug in nanoparticles}}{\text{initial weight of drug used}} X\,100$$

$$\text{Drug loading content}\,(\%) = \frac{\text{weight of drug in nanoparticles}}{\text{weight of the nanoparticles}} X\,100$$

2.6. In vitro *pH release studies*

5-FU-LfNPs (0.5 mg) were resuspended in 1 ml of buffers (ranging from pH 1.0 to 9.0) and incubated for 4 h on rocker at 37 °C. Individual samples were collected by centrifugation at 30,000 × *g* for 15 min 5-FU released from the nanoparticles was quantified using UV–vis spectrophotometer at 254 nm. All assays were done in triplicates.

2.7. *Cell culture*

Mouse melanoma (B16F10) cell line were maintained in a Dulbecco's modified Eagle's growth medium (DMEM, Invitrogen) supplemented with 10% fetal bovine serum (Invitrogen), 5 μg ml^{-1} penicillin, 6 μg ml^{-1} streptomycin, and 10 μg ml^{-1} kanamycin. All cells were grown and maintained in 5% CO_2, 95% humidity at 37 °C.

2.8. *Competitive ligand binding assay*

In order to investigate the receptor specificity of LfNPs, a competitive ligand binding assay with free Lf was performed. Briefly, cells (1×10^6) were incubated simultaneously with increasing amount of free Lf and LfNP-Rh123 (100 μg ml^{-1}) in serum-free medium for 2 h in a 12-well plate. After incubation, cells were harvested and analyzed using a FACSCaliber^{TM} cell analyzer (BD Biosciences). Gating on forward and side scatter was done to exclude cell debris and 10,000 gated events were recorded. Data was analyzed using Cell Quest software (Becton Dickinson).

The effect of competitive ligand binding on 5-FU uptake when delivered through LfNP was also investigated using spectrophotometer. Briefly, cells were incubated with 5-FU-LfNP (equivalent to 60 μg of 5-FU) and simultaneously with free Lf in equal ratio of LfNP. After 2 h incubation, cells were washed thrice with PBS and sonicated in PBST (PBS with 0.1% triton X) for 30 s. The protein in the cell lysate was precipitated by adding equal volumes of 20% silver nitrate ($AgNO_3$) and then incubated overnight at 4 °C. The precipitated protein was separated by centrifugation at 11,000 × *g* for 15 min at 4 °C and 5-FU was estimated using spectrophotometer as mentioned earlier.

2.9. *Lysosome co-localization assay*

The sub-cellular localization of LfNPs was investigated to provide further evidence on the receptor mediated endocytotic uptake mechanism. B16F10 cells were incubated with LfNPs-Rh123 for 2 h followed by addition of lysosome tracking dye (Lysosensor) for another 30 min. Cells were washed thrice with PBS and analyzed for co-localization using confocal laser scanning microscopy (Carl Zeiss NLO710, Germany) using Zen 2010 software at Ex = 505 nm, Em = 530 nm for LfNPs-Rh123 (green) and Ex = 384 nm, Em = 540 nm for LysoSensor (yellow).

2.10. *Cell uptake assay*

2.10.1. *Quantitative determination of 5-FU*

Cells were seeded in a 12-well plate and upon 70% confluence, free 5-FU and 5-FU-LfNPs (equivalent to 100 μg of 5-FU) were added. After 2 h cells were washed thrice with PBS and further incubated for indicated time points (30 min to 24 h). At the end of experiments, cells were harvested and equal number of cells was processed for 5-FU estimation using a UV–vis spectrophotometer as described earlier.

2.10.2. *Confocal microscopy*

Cells grown on cover slips to 70% confluence, were treated with 100 μg ml^{-1} of free Rhoda mine (Rh123) and equivalent amount of LfNPs-Rh123 for indicated time points (0.5, 1, 2 and 4 h). After indicated time points cells were washed thrice in PBS and fixed with 4% formaldehyde solution. Cells were counterstained with DAPI and mounted in VECTASHIELD mounting medium and analyzed by confocal laser scanning microscopy (Lexica TCS-SP8) under 63× oil immersion objective lens.

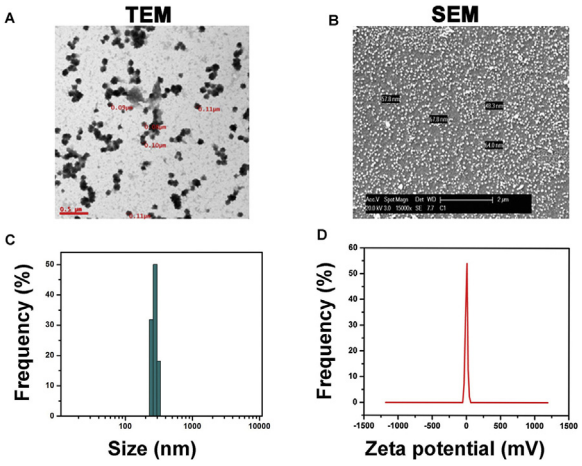

Fig. 1. Characterization of 5-FU-LfNPs. (**A**) TEM and (**B**) SEM analysis of particles. (**C**) Hydrodynamic diameter and (**D**) Zeta-potential of LfNPs at pH 7.4.

2.11. *Toxicity studies*

The cytotoxicity of 5-FU-LfNPs in B16F10 cells, was measured by MTT assay and compared with free 5-FU. Briefly, cells were seeded in a 96-well plate at a density of 5000 cells per well and incubated at 37 °C with 5% CO_2 and 95% humidity. After obtaining the desired confluency, cells were incubated with increasing concentrations of either free 5-FU or 5-FU-LfNPs (ranging from 5 to 50 μg ml^{-1}). Cells were then incubated for another 24 h and the % cell inhibition was calculated using the following formula.

$$\text{Inhibition}\,(\%) = \text{Inhibition}\quad(\%) = \frac{\text{A570nm of control cells} - \text{A570nm of treated cells}}{\text{A570nm of control cells}}$$

In order to determine the toxicity of the drug carrier (i.e. blank LfNPs without 5-FU), cells were cultured in 12-well plate and incubated with increasing concentrations (5–1000 μg ml^{-1}) of blank LfNPs for 48 h. The cells were scraped, washed and fixed in 70% ethanol followed with addition of presidium iodide (PI) at a final concentration of 0.5 μg ml^{-1}. The samples were analyzed using flow cytometry as described above.

3. Results and discussion

3.1. *Physico-chemical characterization of nanoparticles*

The 5-FU-LfNPs were prepared by our previously reported patented protocol sol-oil chemistry [13]. The structure and morphology of the nanoparticles were characterized by TEM and SEM suggests that particles are spherical in shape with the size range of 90–110 nm (Fig. 1**A & B**). As expected the hydrodynamic diameter of the particles, as determined by DLS, was found to be 150 ± 20 nm (Fig. 1**C**). DLS analysis account solvent shell around the particle, thus measures hydrodynamic radii of particles, in case of proteins due to their surface hydrophobic and hydrophilic projections facilitate an interactive solvent environment thus the apparent hydrody-

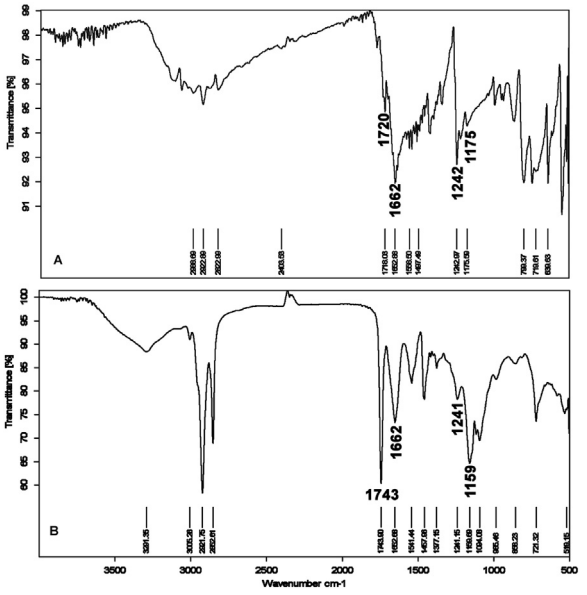

Fig. 2. FT-IR spectra of **(A)** free 5-FU **(B)** 5-FU-LfNP. It reveals that 5-FU is physically entrapped/adsorbed in LfNP.

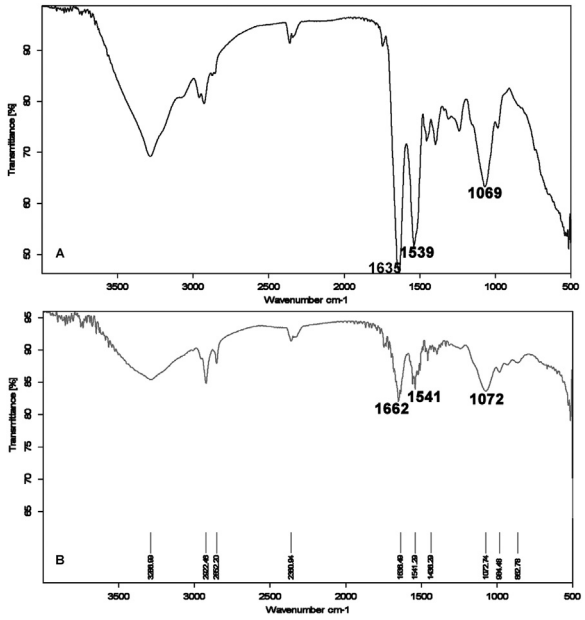

Fig. 3. FT-IR spectra of **(A)** Lf **(B)** LfNP. Lf maintain its structural integrity in the nanoparticlulate form as there was no major changes in the stretching frequency.

namic radii will be higher in DLS measurements, which was absent when analyzed in a dry state using TEM or SEM which is also in agreement with other report [17,18]. The polydispersity index (PDI) value and zeta potential of the particles was found to be 0.332 ± 0.1 and -2.5 ± 1 mV respectively, an indicative of a narrow size distribution with near neutral surface charge on the nanoparticles suggesting a stable dispersion of nanoparticles in aqueous media. Particles size and surface charge play a major role in cell uptake. The small size of the particles and a near neutral surface charge (ζ potential) of the LfNPs may help in evading their phagocytic uptake by macrophages, resulting in prolonged *in vivo* circulation and improved pharmacokinetics of 5-FU [19,20].

The encapsulation efficiency (EE) of 5-FU in LfNPs was found to be $64 \pm 3.60\%$ with a drug loading content (DLC) of $31.21 \pm 2.5\%$. The high encapsulation efficiency and DLC, suggest significantly high 5-FU encapsulation in the nanoparticles, which is much higher than the reports available [21]. Such high encapsulation efficiency of 5-FU in LfNPs could be attributed to the strong hydrophobic interactions between Lf and 5-FU. Taken together, the high drug encapsulation efficiency of LfNPs along with an optimum size and surface charge provides an increased advantage under *in vivo* conditions. The LfNPs may thus carry large amounts of drug to the site of action and increases the plasma half life of 5-FU.

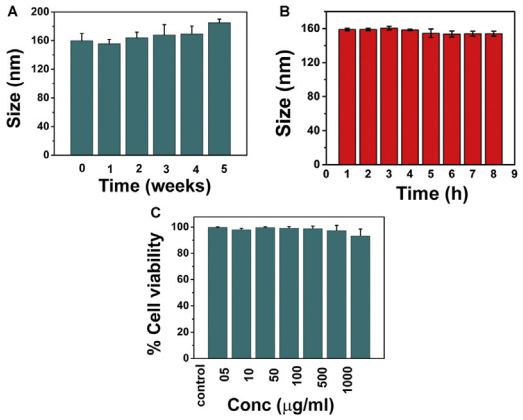

Fig. 4. Stability and biocompatibity of LfNPs. **(A)** Size of 5-FU-LfNPs recorded for a period of 5 weeks at 4 °C in PBS pH 7.4. **(B)** Size of 5-FU-LfNPs recorded for a several hours at RT in DMEM with 10% serum. **(C)** Assessment of biocompatibility of LfNPs. B16F10 cells were treated with LfNPs at the indicated doses followed by assessing the PI uptake using Flow cytometry 48 h post treatment. Cells treated with PBS were considered as controls having 100% viability. Graph represents data from three independent experiments (n = 3) and presented as mean ± SD.

3.2. FT-IR spectroscopy

To confirm the entrapment of 5-FU in the LfNPs, FT-IR was performed. It has been observed in FT-IR spectrum, the amide bonds in Lf which makes the backbone has major characteristic stretching and bending vibrations as amide I (1636 cm), amide II (1539 cm), and C—O—C stretch (1069 cm). Almost similar pattern of stretching frequencies for amide I (1662), amide II (1541) and C—O—C stretch (1072) were observed in LfNPs (Fig. 2**A & B**). The characteristic peak positions of free 5-FU in FTIR for C=O stretch, C—N stretch, C—H in plane and C—O was 1720, 1662, 1242 and 1175 respectively (Fig. 3**A**) likewise the characteristic peaks of 5-FU in 5-FU-LfNP were in 1718, 1662, 1241, and 1159.69 respectively (Fig. 3**B**). Overlay spectra of all four components (Supplementary Fig. S1 can be found, in the online version, at doi:10.1016/j.ijbiomac.2016.10.110) suggest that there was no loss or major shift in stretching frequency between free 5-FU and 5-FU-LfNPs. In addition 5-FU-LfNPs exhibited characteristic, peaks of both lactoferrin and 5-FU, suggesting successful encapsulation of 5-FU without any instability.

3.3. Stability and biocompatibility of lf nanoparticles

Long shelf-life is pre-requisite to increase the translational potential of any formulation. Therefore, the storage stability of LfNPs was monitored by measuring their size over a period of 5 weeks. As shown in (Fig. 4**A**), the nanoparticles showed no significant size change when stored under refrigerated conditions in PBS (pH 7.4), suggesting the high stability of LfNPs. Further particles were also remained constant in size when tested at physiological conditions (Fig. 4**B**) which suggest that particles are indeed stable for several hours in serum as well and possibly that will facilitate in their increased *in vivo* half life.

The *in vitro* toxicity of the nanoparticles was assessed in B16F10 cells. Cells were treated with increasing amount of LfNPs (without

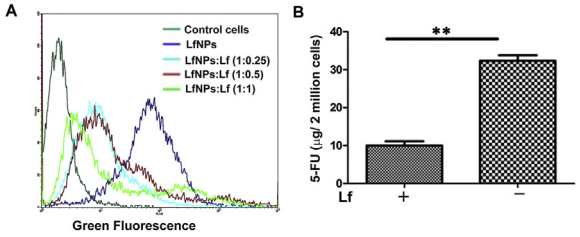

Fig. 5. **(A)** Competitive ligand binding assay. B16F10 cells were treated with LfNPs-Rh123 and simultaneously with increasing doses of free Lf. Cellular uptake of LfNP-Rh123 in presence of free Lf was studied by flow cytometry. **(B)** Quantification of intracellular 5-FU concentration in B16F10 cells treated with 5-FU-LfNPs in the presence and absence of Lf. 5-FU concentration was estimated in cell lysates using spectrophotometry. Graph represents data from three independent experiments (n = 3) and presented as mean ± SD.

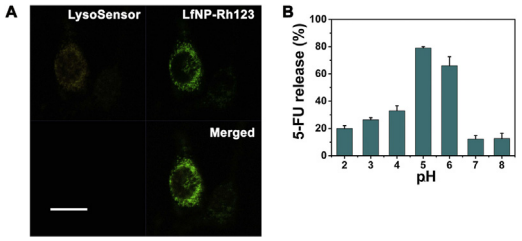

Fig. 6. **(A)** Colocalization study. Colocalization of LfNP-Rh123 (green) with LysoSensor (yellow) suggests receptor mediated endocytosis of LfNPs **(B)** Release of 5-FU from LfNPs studied at different pH values. Maximum 5-FU release was observed at pH 5 and 6. Data represent from three independent experiments (n = 3) and presented as mean ± SD. (For interpretation of the references to colour in this figure legend, the reader is referred to the web version of this article.)

5-FU) and cell death was analyzed by PI uptake and subsequent flow cytometry analysis. The nanoparticles were found to be safe at each tested concentration (Fig. 4**C**).

3.4. Receptor mediated endocytotic

Ligand functionalized nanoparticle is a regular trend in active targeting, facilitate the drug accumulation particularly at the tumor site and prevent off-target effects. Using Lf as a matrix for preparation of nanoparticles and targeted delivery of 5-FU in melanoma cells is a novel approach in the present study. It has been reported that cellular uptake of Lf is mediated by the Lf receptors (LfRs) [22]. We therefore carried out a competitive ligand binding assay to confirm the lactoferrin receptor mediated uptake of lactoferrin nanoparticles in B16F10 cells. Flow cytometry results (Fig. 5**A)** suggest a gradual decrease in the uptake of LfNPs (labeled with Rh123) by B16F10 cells in the presence of increasing amount of free Lf. The results were further validated by a spectrophotometric estimation of the intracellular 5-FU concentration delivered through LfNPs in the presence and absence of Lf (Fig. 5**B)**. A significantly reduced uptake of 5-FU when delivered through LfNPs in the presence of free Lf, suggesting a competitive inhibition of LfNP uptake by Lf. Our results corroborate with our previous reports of LfR mediated uptake of LfNPs, suggesting that the targeting ability of Lf is preserved even in the nanoparticlulate formulation. However some fraction of LfNP uptake has been observed even after blocking the receptor, this could be due to some alternative pathways of entry due to nanoparticle nature and size.

3.5. Lysosome co-localization and 5-FU release studies

Having confirmed the LfR mediated uptake of LfNPs, we further investigated the sub cellular localization of the particles. The co-localization of LfNP-Rh123 with lysosome (LysoSensor) was studied in B16F10 cells using confocal fluorescence microscopy. The merged fluorescence signals from LfNP-Rh123 (green) and lysosome (yellow) as observed in confocal microscopy images (Fig. 6**A)** confirms the co-localization of LfNPs with the lysosome.

To understand the release mechanism of 5-FU from 5-FU-LfNPs, a pH-dependent release study was carried out. Interestingly, it was found that approximately 60–80% of the entrapped 5-FU was released at a pH of 5.0–6.0 which is similar to endo-lysosomal pH (Fig. 6**B)**. The ability of LfNPs to release 5-FU even at a mildly acidic pH as compared to neutral pH may facilitate a triggered release of 5-FU in response to low pH encountered in the tumor environment and inside the endosomes. The low pH release of 5-FU from 5-FU-LfNPs may be attributed to structural changes in the Lf protein molecules constituting the nanoparticles. It has been reported by Sreedhara et al., that lactoferrin undergoes a structural transition with an increase in α-helical content (by 30%) and decrease in β-sheet and random coil content (by 12%) as the pH is lowered from 7.4 to 5 [23]. The pH triggered release of 5-FU may provide an advantage in enhancing the pharmacological effects of 5-FU by increasing its release specifically at the tumor site.

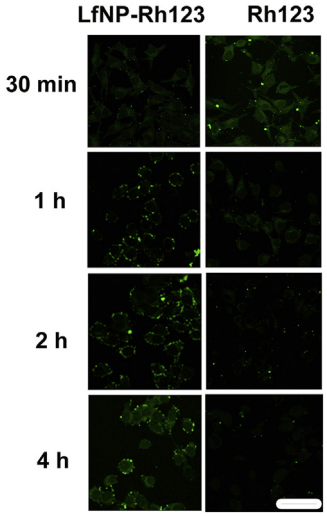

Fig. 7. Comparative 5-FU uptake and clearance by B16F10 cells when delivered through LfNPs (square) and free 5-FU (circle), quantified using spectrophotometry. Graph represents data from three independent experiments (n = 3) and presented as mean ± SD. Scale bar = 25 μm.

3.6. Cellular uptake assay

3.6.1. Quantitative determination of intracellular 5-FU

The cellular uptake and the comparative intracellular concentration of the 5-FU-LfNPs was carried out using spectrophotometric estimation of 5-FU. Our results (Fig. 7), indicate that the intracellular concentration of free 5-FU was high at 30 min followed with a constant decrease thereafter up to 24 h. However, the intracellular concentration of 5-FU, delivered through LfNPs, significantly increased from 30 min to 4 h in a linear fashion and remained constant thereafter up to 24 h.

3.6.2. Cellular uptake by confocal microscopy

The prolonged retention of LfNPs was further confirmed by comparative uptake of free Rh123 and LfNP-Rh123 through confocal studies (Fig. 8**)**. It has been observed that although free Rh123 enters cells quickly (within 30 min), however they get cleared rapidly (within 1 h). Whereas the uptake of LfNP-Rh123 was found to be low at 30 min but increases gradually with time and retained up to 4 h.

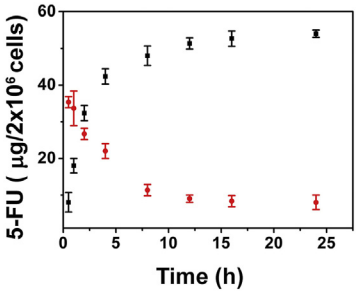

Fig. 8. Time based cellular uptake of LfNP-Rh123 compared with free Rh-123 in B16F10 cells. Time course experiment shows that nanoparticles are retained for longer time in cells as compared to free Rh-123 that penetrate cells promptly nevertheless gets clear very rapidly within 30 min.

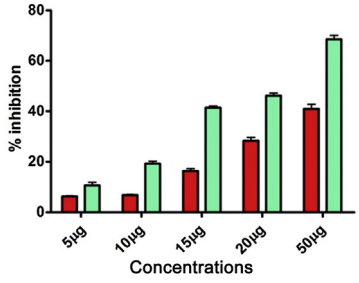

Fig. 9. Enhanced cytotoxicity of 5-FU-LfNPs. B16F10 cells treated with various equivalent doses of 5-FU (red) and 5-FU-LfNPs (cyan). Graph shows an enhanced cytotoxicity of 5-FU-LfNPs compared to free 5-FU. Graph represents data from three independent experiments (n = 3) and presented as mean + SD. (For interpretation of the references to colour in this figure legend, the reader is referred to the web version of this article.)

3.7. *Enhanced antiproliferative activity of 5-FU-LfNPs*

5-FU, the standard drug widely used for melanoma treatment is not effective because of the inability to achieve therapeutic doses at the target site due to its non-specificity. In addition, associated systemic toxicity greatly limits their therapeutic index which in due course leads to poor prognosis. A delivery system that can enhance the potency of drug by reducing its IC_{50} value would be desirable. The cytotoxic effect of 5-FU-LfNPs was measured using MTT assay. The results suggest that 5-FU-LfNPs exhibited more cytotoxic effect over all the experimental concentrations (Fig. 9). Also, there was a significant decrease (3-fold) in IC_{50} value of 5-FU-LfNPs ($21.5 \pm 2.56\ \mu g\ ml^{-1}$) as compared to free 5-FU ($59 \pm 3.0\ \mu g\ ml^{-1}$). The enhanced cytotoxicity of 5-FU delivered through LfNPs may be attributed to the higher intracellular concentration and prolonged retention of the drug achieved through delivery with LfNPs.

4. Conclusion

The present work deals with development of a nano delivery system using lactoferrin protein for pharmaceutical use. The LfNPs developed in the study demonstrate a highly efficient delivery of 5-FU specifically to melanoma cells. The 5-FU-LfNPs is featured with high drug loading capacity, modest particle size (150 ± 20 nm) and narrow size distribution. A high 5-FU release at mild acidic pH values, as observed in our studies might be favourable for targeting tumor cells and reducing toxicity to normal cells. Moreover, 5-FU-LfNPs exhibited receptor mediated cellular uptake, prolonged retention and enhanced cytotoxicity in melanoma cells. Thus our results suggest LfNPs might be used as potential delivery vehicle to elevate the anticancer effects of chemotherapeutic drugs such as 5-FU.

Acknowledgements

The work presented here was supported by grants from Department of Science and Technology, Government of India. SK acknowledges the fellowship received from CSIR, India during her doctoral research. Authors would like to gratefully acknowledge the technical assistance obtained from Ms. Nalini. We would also like to thank Dr. Farhan Ahmad for helping in obtaining SEM images and Dr. Saad M. Ahsan for assisting in FACS studies.

References

[1] M. Berwick, E. Erdei, J. Hay, Melanoma epidemiology and public health, Dermatol. Clin. 27 (2) (2009) 205–214, viii.
[2] M.B. Lens, M. Dawes, Global perspectives of contemporary epidemiological trends of cutaneous malignant melanoma, Br. J. Dermatol. 150 (2) (2004) 179–185.
[3] M.S. Soengas, S.W. Lowe, Apoptosis and melanoma chemoresistance, Oncogene 22 (20) (2003) 3138–3151.
[4] D.B. Longley, D.P. Harkin, P.G. Johnston, 5-Fluorouracil: mechanisms of action and clinical strategies, Nat. Rev. Cancer 3 (5) (2003) 330–338.
[5] A. Di Paolo, R. Danesi, A. Falcone, L. Cionini, F. Vannozzi, G. Masi, G. Allegrini, E. Mini, G. Bocci, P.F. Conte, M. Del Tacca, Relationship between 5-fluorouracil disposition, toxicity and dihydropyrimidine dehydrogenase activity in cancer patients, Ann. Oncol. 12 (9) (2001) 1301–1306.
[6] G.D. Heggie, J.P. Sommadossi, D.S. Cross, W.J. Huster, R.B. Diasio, Clinical pharmacokinetics of 5-fluorouracil and its metabolites in plasma, urine, and bile, Cancer Res. 47 (8) (1987) 2203–2206.
[7] Z. Zhao, H. Meng, N. Wang, M.J. Donovan, T. Fu, M. You, Z. Chen, X. Zhang, W. Tan, A controlled-release nanocarrier with extracellular pH value driven tumor targeting and translocation for drug delivery, Angew. Chem. Int. Ed. Engl. 52 (29) (2013) 7487–7491.
[8] G. Wang, H. Uludag, Recent developments in nanoparticle-based drug delivery and targeting systems with emphasis on protein-based nanoparticles, Expert Opin. Drug Deliv. 5 (5) (2008) 499–515.
[9] K.A. Grafe, H. Hoffmann, Development and validation of an indirect enzyme-linked immunosorbent assay (ELISA) for the nonsteroidal anti-inflammatory drug S-ibuprofen, Pharmazie 55 (4) (2000) 286–292.
[10] W.H. De Jong, P.J. Borm, Drug delivery and nanoparticles:applications and hazards, Int. J. Nanomed. 3 (2) (2008) 133–149.
[11] K. Park, Albumin: a versatile carrier for drug delivery, J. Control. Release 157 (1) (2012) 3.
[12] C.J. Coester, K. Langer, H. van Briesen, J. Kreuter, Gelatin nanoparticles by two step desolvation-a new preparation method, surface modifications and cell uptake, J. Microencapsul. 17 (2) (2000) 187–193.
[13] A.D. Krishna, R.K. Mandraju, G. Kishore, A.K. Kondapi, An efficient targeted drug delivery through apotransferrin loaded nanoparticles, PLoS One 4 (10) (2009) e7240.
[14] P.C. Bessa, R. Machado, S. Nurnberger, D. Dopler, A. Banerjee, A.M. Cunha, J.C. Rodriguez-Cabello, H. Redl, M. van Griensven, R.L. Reis, M. Casal, Thermoresponsive self-assembled elastin-based nanoparticles for delivery of BMPs, J. Control. Release 142 (3) (2010) 312–318.
[15] Z. Su, L. Xing, Y. Chen, Y. Xu, F. Yang, C. Zhang, Q. Ping, Y. Xiao, Lactoferrin-modified poly(ethylene glycol)-grafted BSA nanoparticles as a dual-targeting carrier for treating brain gliomas, Mol. Pharm. 11 (6) (2014) 1823–1834.
[16] L.Y. Lim, P.Y. Koh, S. Somani, M. Al Robaian, R. Karim, Y.L. Yean, J. Mitchell, R.J. Tate, R. Edrada-Ebel, D.R. Blatchford, M. Mullin, C. Dufes, Tumor regression following intravenous administration of lactoferrin- and lactoferricin-bearing dendriplexes, Nanomedicine 11 (6) (2015) 1445–1454.
[17] F. Ahmed, M.J. Ali, A.K. Kondapi, Carboplatin loaded protein nanoparticles exhibit improve anti-proliferative activity in retinoblastoma cells, Int. J. Biol. Macromol. 70 (2014) 572–582.
[18] V.S. Bollimpelli, P. Kumar, S. Kumari, A.K. Kondapi, Neuroprotective effect of curcumin-loaded lactoferrin nano particles against rotenone induced neurotoxicity, Neurochem. Int. 95 (2016) 37–45.
[19] H. Qiao, J. Li, Y. Wang, Q. Ping, G. Wang, X. Gu, Synthesis and characterization of multi-functional linear-dendritic block copolymer for intracellular delivery of antitumor drugs, Int. J. Pharm. 452 (1–2) (2013) 363–373.
[20] F. Alexis, E. Pridgen, L.K. Molnar, O.C. Farokhzad, Factors affecting the clearance and biodistribution of polymeric nanoparticles, Mol. Pharm. 5 (4) (2008) 505–515.
[21] B. Arica, S. Calis, H. Kas, M. Sargon, A. Hincal, 5-Fluorouracil encapsulated alginate beads for the treatment of breast cancer, Int. J. Pharm. 242 (1–2) (2002) 267–269.
[22] Y.A. Suzuki, V. Lopez, B. Lonnerdal, Mammalian lactoferrin receptors: structure and function, Cell. Mol. Life Sci. 62 (22) (2005) 2560–2575.
[23] A. Sreedhara, R. Flengsrud, T. Langsrud, P. Kaul, V. Prakash, G.E. Vegarud, Structural characteristic, pH and thermal stabilities of apo and holo forms of caprine and bovine lactoferrins, Biometals 23 (6) (2010) 1159–1170.

LACTOFERRIN NANOPARTICLES FOR TARGETED TUMOR THERAPY : IMPLICATIONS IN GLIOBLASTOMA AND MELANOMA MANAGEMENT

ORIGINALITY REPORT

%13	%8	%10	%2
SIMILARITY INDEX	INTERNET SOURCES	PUBLICATIONS	STUDENT PAPERS

PRIMARY SOURCES

1	www.readcube.com Internet Source	%2
2	clok.uclan.ac.uk Internet Source	%2
3	"Encyclopedia of Cancer", Springer Nature, 2011 Publication	%2
4	Aihui MaHam. "Protein-Based Nanomedicine Platforms for Drug Delivery", Small, 08/03/2009 Publication	%1
5	Advances in Delivery Science and Technology, 2014. Publication	%1
6	pharmaceuticalintelligence.com Internet Source	%1
7	en.wikipedia.org Internet Source	%1
8	clincancerres.aacrjournals.org	